

American University in Cairo

## AUC Knowledge Fountain

---

Theses and Dissertations

Student Research

---

Winter 1-31-2022

# Impact of Rapid Urbanization, Climate Change, and Drainage Design on Urban Flash Floods in New Cairo, Egypt

Bassma Taher Hassan

The American University in Cairo AUC, [bassma@aucegypt.edu](mailto:bassma@aucegypt.edu)

Follow this and additional works at: <https://fount.aucegypt.edu/etds>



Part of the [Environmental Engineering Commons](#)

---

## Recommended Citation

### APA Citation

Hassan, B. T. (2022). *Impact of Rapid Urbanization, Climate Change, and Drainage Design on Urban Flash Floods in New Cairo, Egypt* [Master's Thesis, the American University in Cairo]. AUC Knowledge Fountain. <https://fount.aucegypt.edu/etds/1935>

### MLA Citation

Hassan, Bassma Taher. *Impact of Rapid Urbanization, Climate Change, and Drainage Design on Urban Flash Floods in New Cairo, Egypt*. 2022. American University in Cairo, Master's Thesis. *AUC Knowledge Fountain*. <https://fount.aucegypt.edu/etds/1935>

This Master's Thesis is brought to you for free and open access by the Student Research at AUC Knowledge Fountain. It has been accepted for inclusion in Theses and Dissertations by an authorized administrator of AUC Knowledge Fountain. For more information, please contact [thesisadmin@aucegypt.edu](mailto:thesisadmin@aucegypt.edu).

**The American University in Cairo**  
**School of Sciences and Engineering**

**Impact of Rapid Urbanization, Climate Change, and Drainage Design on  
Urban Flash Floods in New Cairo, Egypt**

By

**Bassma Taher Mohamed Hassan**

A Thesis submitted in a partial fulfillment of the requirements for the degree of  
**Master of Science in Environmental Engineering**

Under Supervision of:

**Dr. Mohamad Yassine**

Assistant Professor of Environmental Engineering  
The American University in Cairo

**Dr. Doaa Amin**

Associate Professor  
Water Resources Research Institute

**Fall 2021**

# Abstract

Urban flooding is considered one of the most hazardous disasters in metropolitan areas, which causes growing risk on people's lives, infrastructure and environment. Egypt witnessed an unprecedented extreme rainfall event in 2020 that caused more than four hundred injuries and major damage in properties and infrastructures affecting the economic and social aspects adversely. This was not the first extreme rainfall event causing catastrophic implications, over the past 5 years, New Cairo have been experiencing intense rainfall events almost every year that put the community in jeopardy. This research intends to investigate the main drivers prompting urban flash floods in New Cairo; particularly, the effects of rapid urbanization, climate change and drainage design on the surface runoff. The rainfall analysis is conducted over the period of 2000 to 2020 using Global Precipitation Measurement (GPM), which had the best rainfall measurements within six satellite rainfall products and ground rainfall data. The spatial urban sprawl is assessed through runoff simulations of seven land use maps between 1990 to 2020. Watershed Management System (WMS) simulation indicated that the rapid urban expansion in the area led to an increase in the total runoff of about 180%. On the other hand, the potential effect of climate change on urban flash floods was investigated through comparing ground observed storm data with six bias corrected climate change scenarios. Storm intensities in New Cairo seemed to reasonably agree with climate change precipitation scenario CNRM4.5. Finally, an actual drainage load-capacity balance during storm events was evaluated for seventeen neighborhoods in New Cairo. The analysis suggested that poor drainage capacities might have caused a significant increase in the surface runoff during storm events causing the flash floods. The research suggests that upgrading the current pump stations and planning emergency pumping strategies during storm events may effectively mitigate New Cairo's flooding problem.

# Dedication

This research dedicated to my family. My supportive and loving husband, Hesham Bassiouny, who is constantly a source of encouragement during the challenges of graduate school and life. I am truly thankful for having you in my life and pushing me to keep going even if tasks seemed so hard or impossible and for holding so much burden off my shoulder. This research is for my dad, Dr. Taher Hassan, and mom, Eng. Nahed Faisal, for incurring my absence through those years and who have always been and forever my backbone, supporters, motivators and endless guiders all through life and academic studies; their presence and overwhelming love never failed me, their many sacrifices are the reason for who I am now. For my dear brothers, Mohamed and Mo'men, for constantly supporting me and helping me throughout life. Finally, full gratitude and appreciation goes back to my daughter, Julia, I truly owe you a lot of time, I wish to make you proud. Finally, I want to extend my gratitude to Dr. Ahmed El-Gendy who has helped me to reveal new potentials in myself since my undergraduate years and guiding me in my overall academic challenges, he is like a father to me.

# Acknowledgments

First and foremost, thank you dear Allah for the countless blessings granted to me all through my thesis study, research and in my life.

I want to thank my supervisors, firstly Dr. Mohamad Yassine, for always freeing up time to track my work even during the pandemic times, he has always provided support and guidance and helped me a in managing my efforts to stay on track and follow the research plan. Dr. Doaa Amin. for her constant support, encouragement and taking a great deal of time and effort to support and guide me and for reviewing my work meticulously but at the same time very rapidly to push me graduate faster.

On the other hand, I want to thank the “USAID graduate scholarship for professionals” for funding my studies at AUC and giving me this great opportunity to quality education. I want to thank all the professors and staff in the Water Resources Research Institute (WRRI) for constantly providing me with support, guidance, data and equipment.

Finally, I want to thank my university AUC for granting me funding to buy the needed data and tools to complete my research and giving me an extra credit to overcome the delay occurred due to the COVID pandemic.

This research would not be completed without each and every one of you..

# Table of Content

Chapter 1. Introduction .....	1
1.1 Background .....	1
1.2 Objectives.....	3
1.3 Thesis organization.....	4
Chapter 2. Literature Review .....	5
2.1 Hazards of Flashfloods on Urban Areas.....	5
2.2 Role of Urbanization in Increasing Surface Runoff .....	7
2.3 The Effect of Climate Change on Urban Flash Floods .....	9
2.4 Role of Drainage Design in Mitigating Urban Floods .....	11
2.5 Summary .....	12
Chapter 3. Materials and Methods .....	14
3.1 Case Study – New Cairo .....	15
3.2 Rainfall Data Collection and Validation .....	17
3.2.1. Ground Observed Rainfall Data .....	17
3.2.2. Satellite Rainfall Data .....	18
3.2.3. Validation of Satellite Rainfall Data with Ground Observation .....	20
3.3 Comparing Climate Change Scenarios to Ground Observed Rainfall Data .....	24
3.4 Evaluating the Effect of Urban Sprawl on the Surface Runoff.....	25

3.4.1. Analysis of Urbanization Growth Rate .....	25
3.4.2. Calculating Surface Runoff Using WMS Hydrological Model .....	26
3.5 Impact of Drainage Design on Surface Runoff .....	26
3.5.1. Drainage Network Load-Capacity Balance During Storm Events.....	27
3.5.2. Validation using SewerGEMS .....	29
Chapter 4. Results and Discussion.....	30
4.1 Satellite Rainfall Products Evaluation Using Gauge Observation and The Extraction of Actual Storm Distribution .....	30
4.1.1. Comparison between Gridded Rainfall Products and Ground Observed Rainfall	30
4.1.2. Bias Correction of Gridded Rainfall Products .....	32
4.1.3. Extracting Design Storm Distribution from Actual Storms Captured by GPM....	37
4.2 Climate Change Scenarios Analysis and Projections.....	39
4.2.1. Validating that Historical Rainfall Events Following Climate Change Scheme...	39
4.2.2. Analyzing the Climate Change Effect of Rainfall Patterns on Cairo.....	40
4.3 Effect of Urbanization on Surface Runoff .....	43
4.3.1. Analysis of Urbanization Growth Rate .....	43
4.3.2. Results of Rainfall-Runoff Model.....	45
4.4 Drainage Design Effect on Surface Runoff.....	47
4.4.1. Drainage Network Evaluation using Load-Capacity Balance.....	49
4.4.2. Pump Stations Evaluation using Load-Capacity Balance .....	52

4.4.3. Validation of the General Evaluation using SewerGEMS .....	56
4.5 Discussion .....	61
Chapter 5. Conclusion and Recommendation.....	65
5.1 Summary .....	65
5.2 Conclusion.....	67
5.3 Recommendation.....	69
Chapter 6. References .....	73



# List of Appendices

Appendix A.	Identify the Nearest Ground Station to the Study Area Using TPM Method ...	A-1
Appendix B.	Satellite Rainfall Data-Sets Detailed Description and Analysis Equations .....	B-3
Appendix C.	Rainfall Runoff Model Detailed Inputs.....	C-15
Appendix D.	SewerGEMS Model Structure and Details and Results .....	D-24

# List of Tables

Table 3.1: Summary of the Satelites Rainfall Data used in this Research (Resolution, Time Range and Data availibility).....	20
Table 3.2: Summary of Statistical Indicators Equations and Ranges .....	22
Table 3.3: Summary of Statistical Criteria limits .....	22
Table 3.4: Rational Method Run off Coefficient Values (ECP , 2010).....	28
Table 4.1: The Results of Six Satellite Rainfall products in Six Statistical Indicators for the Total Monthly Rainfall Data .....	31
Table 4.2: The Results of Six Satellite Rainfall products in Six Statistical Indicators for the Maximum Rainy Day per Month.....	31
Table 4.3: Comparison of Monthly Data Variance ( $R^2$ ) from scatter plots before and after LS ..	34
Table 4.4: Statistical Analysis of Biased Correction of Monthly Data.....	35
Table 4.5: Comparison of GPM Performance Before and After Bias Correction .....	36
Table 4.6: Satellite Daily Data Performance After the Bias Correction .....	36
Table 4.7: Results of the statistical analysis for the climate change models .....	39
Table 4.8: Comparison of Return Period Intensities between the period of (1976 -1999) and (2000 – 2020) .....	42
Table 4.9: Urbanization Growth Rate with time from 1990 to 2020, showing area covered by each category and total percentage of urbanized areas vs. rural areas in each year.....	45
Table 4.12: Runoff Values for New Cairo at each year correspond to six return period storms..	46
Table 4.13: The change in runoff corresponding to the increase of urbanized area from 1990 to 2020 for the whole New Cairo Watershed.....	47

Table 4.14: Percentage used of the Drainage Network at Different Scenarios .....	51
Table 4.15: Percentage Used of the Pump Stations with different scenarios .....	53
Table 4.16: Evaluation Summary for Drainage Network and Pump stations for seventeen Neighborhoods in New Cairo .....	54
Table 4.17: Summary of the SewerGEMS Simulation Results .....	60

# List of Appendix Tables

Table C-1: Morphological Properties of Watersheds Upstream New Cairo .....	C-17
Table C-2: Morphological Properties of Watersheds Upstream New Cairo .....	C-18
Table C-3: Detailed Description of Each Basin Affecting New Cairo .....	C-21
Table C-4: Summary of the geological soil types in New Cairo Watershed and their percentage area and the final CN Value for Rural Areas.....	C-21
Table C-5: CN for Urban land use and cover used in this research.....	C-22
Table C-6: Rainfall corresponds to each return period for the rainfall runoff model .....	C-23
Table D-1: Calculated Runoff Corresponds to 2-Year Storm .....	D-25
Table D-2: Calculated Runoff Corresponds to 5-Year Storm .....	D-25
Table D-3: Calculated Runoff Corresponds to 10-Year Storm .....	D-26
Table D-4: Calculated Runoff Corresponds to 20-Year Storm .....	D-27
Table D-5: Calculated Runoff Corresponds to 50-Year Storm .....	D-28
Table D-6: Calculated Runoff Corresponds to 100-Year Storm .....	D-28
Table D-7: Calculated Runoff Corresponds to Maximum Predicted Storm.....	D-29
Table D-8: Pump Stations Evaluation for Base Scenario (Wastewater Only).....	D-30
Table D-9: Pump Stations Evaluation for Wastewater Combined with 2-year scenario.....	D-30
Table D-10: Pump Stations Evaluation for Wastewater Combined with 5-year scenario.....	D-31
Table D-11: Pump Stations Evaluation for Wastewater Combined with 10-year scenario.....	D-32
Table D-12: Pump Stations Evaluation for Wastewater Combined with 20-year scenario.....	D-33
Table D-13: Pump Stations Evaluation for Wastewater Combined with 50-year scenario.....	D-33
Table D-14: Pump Stations Evaluation for Wastewater Combined with 100-year scenario.....	D-34

## List of Figures

Figure 1.1: Urban Flooding at New Cairo in 2018 and 2020 .....	2
Figure 2.1: Storm hydrograph for a watershed showing the relation between lag time and time of concentration.....	9
Figure 3.1: New Cairo's 17 Neighborhoods included in the Study showing their locations and areas (km <sup>2</sup> ).....	16
Figure 3.2: Part A: Shows Monthly Rainfall Data for Cairo Station. Part B: Statistical Features (Mean, Median, Minimum, Maximum and Extreme values as outliers) for Monthly and Maximum Daily Rainfall Data of Cairo Station.....	18
Figure 3.3: Illustration of ground rainfall station shortfalls. Section (2,3&4) represent storms occurred on the study area that was not measured by ground stations. Section (1) represent rainfall measured from ground stations but did not occur over the study area .....	19
Figure 3.4: Summary of Climate Change Data Used .....	24
Figure 3.5: Drainage Network of Academy El Fareeya, showing red rectangles that indicates inundation areas during past rainfall storms (New Urban Communities Authority, 2018) .....	29
Figure 4.1: Scatter plot showing correlation between six gridded rainfall products and ground observed data for monthly precipitation .....	30
Figure 4.2: Bias Correction of Mean Monthly Values .....	33
Figure 4.3: Bias Correction of Total Monthly Values .....	34
Figure 4.4: Distribution of Eight Main Rainfall Events from 2015 to 2020 acquired from GPM	37

Figure 4.5: Cumulative Half Hourly Distribution for all eight storm events.....	38
Figure 4.6: Nested Hyetograph after applying block method.....	38
Figure 4.7: Final Unit Hyetograph to be used in the Rainfall-Runoff Simulation .....	39
Figure 4.8: Total Rainfall Every Year (mm/year) For the period of 1981 to 2020 .....	40
Figure 4.9: Maximum Rainfall Event in each Year (mm/day) For the period of 1981 to 2020 ...	41
Figure 4.10: CNRM 4.5 Total Annual Projected Precipitation from 2006 to 2050.....	43
Figure 4.11: Urbanization stages from the year 1990 to 2020 showing rural area (beige), green areas (green), urban areas (red) and urban under construction (yellow) .....	44
Figure 4.12: Digital Elevation Model Map showing Names and shapes of basins affecting New Cairo with their names, areas and lengths .....	46
Figure 4.13: Pumping Stations Network Plan for New Cairo's Districts.....	48
Figure 4.14: Elevation Map of New Cairo Neighborhoods.....	49
Figure 4.15: Land use percentages of 17 Neighborhoods in New Cairo for four main categories (Impervious Areas, Gardens, unurbanized areas and industrial areas). Map was obtained from (USGS, 2021).....	50
Figure 4.16: Al Academy El-Fareeya Pipes Layout and Diameters .....	57
Figure 4.17: Sections that will be assessed for water levels during the simulation.....	57
Figure 4.18: 2-Year Return Period Inundation Areas.....	59
Figure 4.19: 2-year Return Period Rainfall Pumping Operation within 24 Hours .....	59
Figure 4.20: Validation of Inundation areas caused by March 2020 Storm against Actual Inundation Areas from site.....	60
Figure 5.1: Example of simple French drainage to be used on the side of the main roads .....	70

# List of Appendix Figures

Figure A-1: Thiessen Polygon Method (Jamal, 2017).....	A-1
Figure A-2: Rainfall Stations Around New Cairo .....	A-2
Figure A-3: Theissen Polygon for stations around New Cairo.....	A-2
Figure B-1:Daily and Monthly GPCC Rainfall Data Statistical Features (Mean, Median, Minimum, Maximum and Extreme values as outliers).....	B-4
Figure B-2: Daily and Monthly GPCP Rainfall Data Statistical Features (Mean, Median, Minimum, Maximum and Extreme values as outliers).....	B-5
Figure B-3: Daily and Monthly TRMM Rainfall Data Statistical Features (Mean, Median, Minimum, Maximum and Extreme values as outliers).....	B-6
Figure B-4: Daily and Monthly GPM Rainfall Data Statistical Features (Mean, Median, Minimum, Maximum and Extreme values as outliers).....	B-7
Figure B-5: Daily and Monthly PERSIANN Rainfall Data Statistical Features (Mean, Median, Minimum, Maximum and Extreme values as outliers).....	B-8
Figure B-6: Daily and Monthly CHIRPS Rainfall Data Statistical Features (Mean, Median, Minimum, Maximum and Extreme values as outliers).....	B-9
Figure B-7: Graphical comparison of monthly rainfall data for ground observed data vs. gridded rainfall products showing (Mean, Median, Minimum, Maximum and Extreme values as outliers) .....	B-12
Figure B-8: Graphical comparison of daily rainfall data for ground observed data vs. grided rainfall products showing (Mean, Median, Minimum, Maximum and Extreme values as outliers).....	B-12

Figure B-9: Scatter plot showing correlation between six gridded rainfall products and ground observed data for monthly precipitation .....	B-13
Figure B-10: Scatter plot showing correlation between six gridded rainfall products and ground station data for daily precipitation .....	B-14
Figure C-1: Satellite image from 1990 showing New Cairo area before urbanization and some streamlines appear to exist .....	C-15
Figure C-2: Boundaries of seven watersheds affecting the area of New Cairo, modified according to the topographic map.....	C-16
Figure C-3: Names and shapes of basins affecting New Cairo with their names, basins areas and lengths .....	C-17
Figure C-4: Geological Map of the watershed affecting New Cairo, showing the soil types ..	C-19
Figure C-5: Probability Distribution fit for Cairo Station .....	C-23
Figure C-6: Probability Distribution Fit for GPM .....	C-23
Figure D-1: Water Consumption Pattern in Egypt (ECP, 1998) .....	D-24



# List of Equations

Equation 1: Bias Correction (LS) .....	23
Equation 2: Rational Method .....	28
Equation 3: Mean Absolute Error (MAE) .....	B-9
Equation 4: Root Mean Square Error (RMSE) .....	B-10
Equation 5: Coefficient of Determination ( $R^2$ ) .....	B-10
Equation 6: Percent Bias (PBias) .....	B-10
Equation 7: RMSE-Observation Standard Deviation (RSR) .....	B-11
Equation 8: Nash Sutcliffe Efficiency (NSE) .....	B-11
Equation 9: Excess Rainfall .....	C-19
Equation 10: Initial Abstraction .....	C-19
Equation 11: Potential Maximum Soil Retention .....	C-19

# Acronyms

<b>CC</b>	Climate Change
<b>CHIRPS</b>	Climate Hazards Group InfraRed Precipitation with Station data
<b>CN</b>	Curve Number
<b>CORDEX</b>	Coordinated Regional Climate Downscaling Experiment
<b>DEM</b>	Digital Elevation Model
<b>ECP</b>	Egyptian Code of Practice
<b>EMA</b>	Egyptian Meteorological Authority
<b>GCM</b>	Global Climate Model
<b>GIS</b>	Geographic Information System
<b>GPCC</b>	Global Precipitation Climatology Center
<b>GPCP</b>	Global Precipitation Climatology Project
<b>GPM</b>	The Global Precipitation Measurement
<b>IMERG</b>	Integrated Multi-Satellite Retrievals for GPM
<b>IPCC</b>	Intergovernmental Panel on Climate Change
<b>LS</b>	Linear Scaling
<b>LID</b>	Low Impact Development
<b>MAE</b>	Mean Average Error
<b>MENA</b>	Middle East and North Africa
<b>MoSS</b>	Ministry of Social Solidarity
<b>NCCA</b>	New Cairo City Authority
<b>NSE</b>	Nash Sutcliffe Efficiency
<b>PBIAS</b>	Percent Bias
<b>PERSIAN</b>	Precipitation Estimation from Remotely Sensed Information using Artificial
<b>NN</b>	Neural Networks
<b>PM</b>	Passive Microwave
<b>PS</b>	Pump Station
<b>RCM</b>	Regional Climate Model
<b>RCP</b>	Representative Concentration Pathway
<b>RICCAR</b>	The Regional Initiative for the Assessment of Climate Change Impacts on Water Resources and Socio-Economic Vulnerability in the Arab Region
<b>RMSE</b>	Root Mean Square Error
<b>RSR</b>	The RMSE-observations standard deviation ratio
<b>SCS</b>	Soil Conservation Services
<b>TIR</b>	Thermal Infrared
<b>T<sub>c</sub></b>	Time of Concentration
<b>T<sub>L</sub></b>	Lag Time
<b>TP</b>	Topmix Permeable
<b>TPM</b>	Theissen Polygon Method
<b>TRMM</b>	Tropical Rainfall Measuring Mission
<b>WMS</b>	Watershed Modelling System

# Chapter 1. Introduction

## 1.1 Background

Egypt has an arid weather with hot dry summers and moderate winters and a few rainfall events except on the Mediterranean coastline (Saber M., Abdrabo, Habiba, Kantosh, & Sumi, 2020). The large population and their dense residence in the Nile delta make Egypt vulnerable to floods resulting from extreme rain events (ElGanzori, 2012). Gradually over time, rainfall events became more intense and frequent and occurring at a wider range of temperatures (Egypt's Cabinet Information and Decision Support Centre, 2011). The frequency of flash flood events increased across the Arab region especially the medium scale events with 30 years return period (The World Bank, 2011). Over the past 5 years, Greater Cairo experienced rainfall events every year that caused major damage in properties and infrastructures and caused traffic obstruction affecting the economic and social aspects adversely. After these dramatic effects of flash floods on Cairo, several concerns were raised by the public opinion and the scientific society regarding the forthcoming winter periods and how to better prepare to face them properly; therefore, accurate models are required to examine the drivers behind urban flash floods occurring in Cairo. Urbanization, climate change and drainage design are three main factors found to promote urban flashfloods (Caradot, Granger, Chapgier, Cherqui, & Chocat, 2011; Saber M., Abdrabo, Habiba, Kantosh, & Sumi, 2020; Douglas, et al., 2008; Huang, Wang, Li, Fei, & Dong, 2017).

The study takes place in New Cairo, which is an extension to Cairo. It was established in the year 2000. On April-24-2018 and Mar-12-2020, New Cairo was affected by heavy rainfall events that turned the city roads into lakes of flooded water as the combined sewer network in New Cairo drains both surface runoff and sewage flows in the same conduit. As a result, tens of basements,

low-level houses, and cars were entirely covered with water (Mabrouk & Sharnouby, 2018). The flood caused a complete power outage and manholes in the streets exploded with backflow water, therefore, drainage during storms relied heavily on mobile pumping units as a backup of the drainage system as shown in Figure 1.1.



Figure 1.1: Urban Flooding at New Cairo in 2018 and 2020

In order to study the drivers behind urban flashfloods in Cairo, it is vital to have accurate spatial and temporal rainfall measurements over New Cairo. Although the gauge measurement is accurate and dependable, its spatial distribution is very weak that makes the rainfall data dispersed and cannot represent dense urban areas (Salem, Shahid, Dewan, Ismail, & Alias, 2020). Currently, satellite-based precipitation became exceedingly popular to be used in hydrological studies (Abdelmoneim, Soliman, & Moghazy, 2020; Peng, et al., 2021; Salem & El-Sayed, 2017) as it is

freely available with high resolution that can reach  $0.05^\circ$  and a time scale with a minimum of 30 minutes (Funk, et al., 2015). Having small temporal resolution is particularly useful in calculating the actual storm duration, distribution and peak discharge of a single rainfall event (Bertini, Buonora, Ridolfi, Russo, & Napolitano, 2020; Zhu, Wang, Ren, & L., 2020), which is not available in ground rainfall measurements in Egypt. On the other hand, the accuracy of using satellite measured precipitation products can be questionable and needs to be verified and validated against ground rain gauges data (Ebert , 2007).

## **1.2 Objectives**

The objectives of this research are to:

- 1) Reaching accurate rainfall measurements over the study area using satellite-captured rainfall data.
- 2) Analyze the effect of rapid urbanization on urban flash floods in New Cairo through rainfall-runoff simulations at different urbanization levels and with several storm return periods.
- 3) Investigate whether the current intensities of major storm events occurred in New Cairo are connected to Climate Change or are mere recurrence of the normal historical trends.
- 4) Investigate the effect of drainage network design on flash floods in New Cairo by analyzing as-built sewer design drawings and water inundation data of previous storms' records.
- 5) Recommendations of best practices for the alleviation of urban flooding based on the findings of this work.

### 1.3 Thesis organization

The research is divided into five chapters.

**Chapter one** is the current chapter, it provides description regarding the current urban flashflood problem, and it gives an overview for the research objectives and organization.

**Chapter two** is a comprehensive summary for the literature review showing the main effects of urbanization, climate change and drainage design on urban flash floods from previous studies.

**Chapter three** includes the description of the followed methodology to fulfill the research objectives and it contains all the used equations and assumptions.

**Chapter four** is designated to show the results of the described methodology and it concludes with a discussion that connects between the results of all factors affecting urban flashfloods in New Cairo.

**Chapter five** this chapter concludes the research, it provides a brief summary for the work and the reached conclusion and presents some solutions for the current situation as well as the recommendations for the mitigation of urban flooding based on the findings of this research.

# Chapter 2. Literature Review

## 2.1 Hazards of Flashfloods on Urban Areas

Flood is a natural disaster that can cost loss of lives and damages to the economy. It is important to provide sufficient protection for people and properties. Due to climate change and urbanization, flooding is likely to occur more frequently (Zhou, Leng, Su, & Ren, 2018). In order to cope with the future flooding, sufficient planning and new strategies are required.

Over the past 5 years, Egypt has been witnessing extreme rainfall events causing major destruction not only in rural or underdeveloped areas, but also in major cities with fully established drainage systems. On 11<sup>th</sup> of March in 2020, Egypt witnessed an unprecedented extreme weather event that included heavy rainfall, thunderstorms and fierce winds. The flash floods occurred on many areas in Egypt causing more than 430 injuries, 400 of which occurred in Cairo alone and it killed more than 40 citizens (IFRC, 2020; MoSS, 2020). A rapid assessment by the Ministry of Social Solidarity (MoSS), showed that number of people affected by the floods estimated to be 20,000 people, moreover, several essential highways and public infrastructure, including international airports as a well as seaports were shut down. Furthermore, due to the extreme events all schools and public and private workplaces were closed (MoSS, 2020), all of which caused economic and social losses. Urban floods can be one of the most hazardous disasters in metropolitan areas (Galloway, et al., 2018), which can cause a growing risk on damaging infrastructure and environment; moreover, floods disrupt the daily services of individuals like transportation, electricity and water supply (Dawson, et al., 2008; Zhou, Leng, Su, & Ren, 2018).

Globally, countless floodplains and streams were designated to accommodate urban settlements, which poses a great flood risk on those metropolises. On the other hand, floodplains are natural management system for stormwater, which -unfortunately- not considered during the fast urban expansion in developing countries (ASFPM, 2020; WMO; Cap-Net, 2007; Parkinson, 2003). For example, Saber, et. al (2020) concluded that most of the new urban areas in Egypt are planned within flood hazardous area.

The only mitigation measure to flood risks within the rapidly developed urban areas is the drainage system, which should be built to compensate for blocking the natural floodplain and accommodate for the storm water runoff. However, increased runoff that was introduced due to the new impervious surfaces was not accounted nor controlled. Hence, causing an increase in flood-prone locations within the urban cities and induce a great pressure on the drainage systems (ASFPM, 2020; Parkinson, 2003; Zhou, Leng, Su, & Ren, 2018; Caradot, Granger, Chapgier, Cherqui, & Chocat, 2011).

Flooding is expected to increase in many regions worldwide, especially in densely populated metropolitan areas (Larsen, Gergersen, Christensen, Linde, & Mikkelsen, 2009; Zhou, Leng, Su, & Ren, 2018). Among many factors that contribute to flood hazards increasing, rapid urbanization, climate change and under sized drainage networks are three of the most influential factors that affect urban runoff greatly and challenge the future flood management strategies (Arnone, Pumo, Francipane, La Loggia, & Noto, 2018; Huong & Pathirana, 2013; Jung, Kim, Mallari, Pak, & Yoon, 2015; Zhou, Leng, Su, & Ren, 2018; Kleidorfer, et al., 2014; IPCC, 2014).

Urbanization is one of the most common causes of increasing impervious surfaces, which makes urban areas very vulnerable to floods and increase of surface runoff (Zhou, Leng, Su, & Ren, 2018; Huong & Pathirana, 2013). On the other hand, climate change has substantial impact



on water cycles causing extreme precipitation, hence, directly increase surface runoff and affects the magnitude of floods (Salem & El-Sayed, 2017; USEPA, 2021). Urban drainage is a critical component in the infrastructure as it is meant to transfer wastewater as well as surplus water away from urban areas in order to keep floods to a manageable level (Zhou, 2014). Therefore, urbanization and climate change can have an impact not only on surface floods, but also on the drainage systems. For example, the constant changes surface flooding can lead to change in drainage system and sometimes land use upgrades to avoid flood implications (Mahmood, Alagib, Horn, & Saad, 2017). Therefore, it is important to incorporate the evaluation of the drainage system while assessing the urban floods changes under the effect of urbanization and climate change.

## **2.2 Role of Urbanization in Increasing Surface Runoff**

Rapid urbanization is one of the main important drivers for urban flooding in Egypt that increases the vulnerability of cities and puts people and assets at risk. Spanning over the past two decades, urban development in Egypt has increased drastically (Verner , 2012). Saber, et al. (2020) concluded that urbanization growth is a key factor that contributed to the increase or decrease of flood events based on the size and direction of the new developments. However, in Egypt the high frequency of urban flooding depends on poor planning of new developments (Saber M. , Abdrabo, Habiba, Kanotsh, & Sumi, 2020).

Many new cities are built on what was a desert; consequently, the permeable natural surface is converted into thousands of kilometers of impervious areas such as roads, buildings and parking lots. Unfortunately, these surfaces prevented rainwater to infiltrate into the ground causing great stress on sewer systems during the heavy rainstorm events and sometimes it causes system failure (Arnone, Pumo, Francipane, La Loggia, & Noto, 2018; Miller, et al., 2014).

Zhou, et al. (2018) investigated the effect of land use change on flood volumes and surface runoff by observing the urban levels over a period of time. Mahmoud & Gan (2018) studied the effect of urbanization as a main factor in increasing flood risk, where the curve number (i.e., change in land use) was used to analyze the change in runoff from 1948 to 2014 (Mahmoud & Gan, 2018). Both studies suggested that urbanization led to higher surface runoff compared to rural areas.

As Saber, et. al (2020) highlighted the importance of identifying the watersheds before the construction of new urban area. This is done in Egypt by analyzing the topographic maps that show any floodplains and water streams used to be in the area before urbanization. Using modeling software along with digital elevation models (DEM), the watersheds are defined and modified according to the topographic maps (Morad, Youssef, & Ibrahim, 2020). The watershed delineation results in important morphological characteristics of the basins, which will be used beside the historical rainfall data in the calculation of runoff quantities. For example, Abdein & Stephen (2019) used a spatiotemporal framework for flood modeling and mapping in urban watersheds; the main factors used to simulate and validate flood models were the rainfall quantity, drainage capacity of the inlets and land cover (Abedin & Stephen, 2019). The important morphological attributes are the area and length of the basin, the time of concentration ( $T_C$ ) and lag time ( $T_L$ ) (Kent, Woodward, Hoeft, Humpal, & Cerrelli, 2010).  $T_C$  &  $T_L$  are particularly important as they are used to identify the final runoff hydrograph as shown in Figure 2.1.

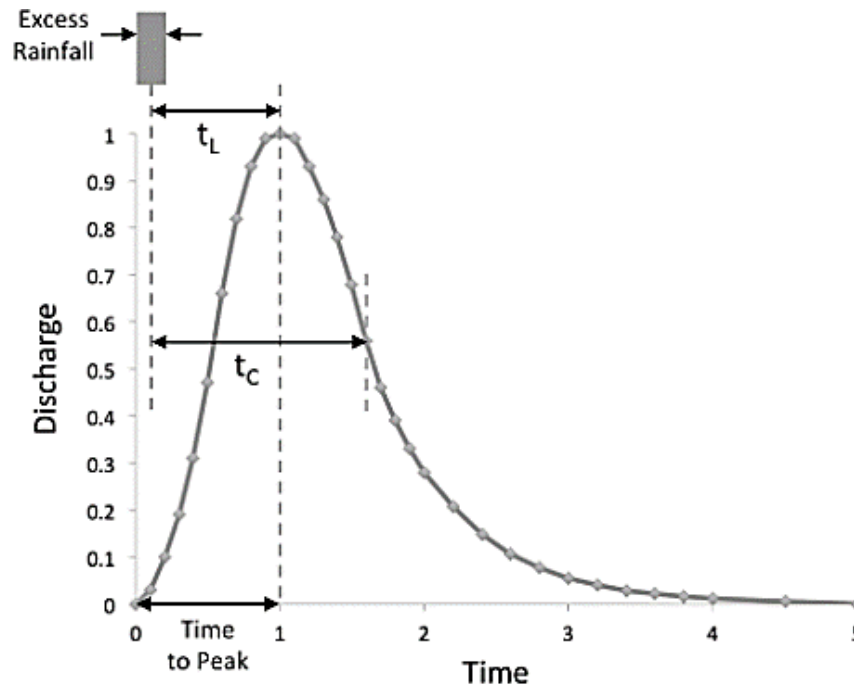


Figure 2.1: Storm hydrograph for a watershed showing the relation between lag time and time of concentration

## 2.3 The Effect of Climate Change on Urban Flash Floods

Climate change (CC) has been widely acknowledged as a natural climatic phenomenon that can be indicated with several meteorological factors including the increase in precipitation (IPCC, 2014; USEPA, 2021); heavy precipitation does not mean the increase of the number of rainfall events, rather than the increase of the magnitude of a single rainfall event that has become more extreme (Larsen, Gergersen, Christensen, Linde, & Mikkelsen, 2009). According to the US-EPA, since the 1980's the percentage of a single rainfall events with intense rainfall magnitude has increased as an alternative of having few rainfall events distributed over the span of a year (USEPA, 2021). Therefore, this raises a question on whether the recent extreme rainfall events on Cairo follows a climate change trend.

The climate change data are data produced by a Global Climate Models (GCM). The GCMs are set of equations that are designed to replicate past and present climate components like

precipitation and temperature, upon their successfulness they are used to predict the future that can detect the climatic changes. However, the resolution of GCM is very course it ranges between 100 to 300 km (NOAA, 2020). Therefore, an initiative called CORDEX aimed to downscale the climate information model to a smaller scale that covers regions i.e., MENA region. The finer scale models are called Regional Climate Model (RCM) and their resolution is 50 km and, in some regions, it can reach 25 km (AMS, 2013). On the other hand, the projection of any climatic change in the future is not based on one assumption, due to the natural variability in factors affecting the climate conditions, therefore, there are few scenarios established to capture future climatic trends through changing the concentrations of greenhouse gases as a result of future human activities up to the year 2100. The climate change emission scenarios are called Representative Concentration Pathway (RCP), and they are RCP2.6, RCP4.5, RCP6.0 and RCP8.5, however, the most popular to be used in research are RCP4.5 and RCP8.5 as per the recommendation of IPCC ( Intergovernmental Panel on Climate Change) since they used RCP4.5 and RCP8.5 in their fifth Climate Change assessment report (Spinoni, et al., 2020; van Vuuren, et al., 2011; IPCC, 2014).

Several studies have demonstrated the effects of climate change on the increase in precipitation and urban runoff. Larsen et al. (2009) anticipated that future 1-hr storm events will increase by 20–60% within the period of 2071–2100 compared to storm events before 1990. Zhou, et al. (2019) used climate change projection acquired from five bias-corrected climate scenarios GCM models and each is analyzed by using two different representative concentrations pathways (RCPs 2.6 and 8.5). He quantified the Total Flood Volume (TFV) for different climate scenarios and found that in all climate scenarios the TFV is expected to increase although the total summation of rainfall intensities is decreasing. Michael, et al. (2009) studied the effect of climate

change and land use over the runoff and found that the climate change has a higher effect on increasing surface runoff than change of land use by 1.1% within a period of 9 years.

On the other hand, numerous studies investigated the role of mitigation and adaptation in reducing urban flood damages due to climate change. Zhou, et.al. (2018) showed that although the urban flood volume in the period 2020-2040 is projected to increase by 52 %, it can be reduced significantly through reducing the Green House Gases (GHG) emissions. Zahmatkesh, et al. (2015) tested the use of Low Impact Development (LID) as a mitigation measure for climate change increase in runoff; the LID includes using green rooftops, rain gardens and permeable pavements. The results showed that the annual runoff volume under climate change scenarios projected to increase by 48%. However, LID provided about 28% reduction in annual runoff volume and an average of 8 to 13% reduction in peak flow rates correspond to 2-years storm. As for 50-years storm it provided 14% reduction in runoff volumes. From literature, despite using climate change models come with uncertainty the increase in surface runoff under CC scenarios has a great likelihood.

## **2.4 Role of Drainage Design in Mitigating Urban Floods**

Drainage Design has a significant role in either mitigating or increasing the risk of urban flash floods. In order for the capacity of the sewer system to be adequate, the probability and intensity of past rainfall events should be considered. (Caradot, Granger, Chapgier, Cherqui, & Chocat, 2011; Notaro, Liuzzo, Freni, & La Loggia, 2015). Egypt's sewerage system is combined sewers, where both wastewater and stormwater are collected in the same conduit and transported to wastewater treatment plants (Awadallah, Magdy, Helmy, & Rashed, 2017). This system has

adequate capacity to manage the daily sewage but fails during extreme storms, due to their unpredictability.

Notaro, et al. (2015) suggested that the drainage design is becoming a significant concern as it is based on frequency analysis of past rainfall intensities, however, under the influence of CC, where climate models project an increase in rainfall severity, the drainage systems are becoming ineffective and insufficient to drain the increased runoff volumes. Therefore, the drainage design should be re-evaluated to account for not only the past trends but also the future rainfall projections. According to Willems, et al. (2012), for return periods from 2 to 100 years, the design intensities are expected to rise by 10% to 50% in Denmark, due to climate change.

In addition to climate change, the urbanization also adds stress to the drainage network. Kleidorfer, et al. (2009) show that the urban sprawl is putting pressure on the current drainage systems, where new urban areas are connected to existing networks along with the increase in surface runoff due to using impervious surfaces. Zhou, et al. (2019) found that the urbanization resulted in more intense changes in the surface runoff and flood volumes than runoff quantities induced by CC.

Therefore, the performance of combined sewer system needs to be assessed under various scenarios as a factor that potentially increase the risk of urban flooding, to achieve better adaptations strategies.

## **2.5 Summary**

According to the findings of the literature review, studying the drivers that influence the increase of urban runoff is crucial to aid in the development of flood mitigation and adaptation measures. From previous research the change in land use due to urbanization and the projected

increase of extreme events due to climate change have the most significant effect on the increase of urban flood volumes. Nevertheless, the drainage systems have a key role in resisting urban floods under the effect of urbanization and climate change according to their design.

Studying flash floods' runoff and flood volumes inside an urban area did not draw the needed attention from the scientific society in Egypt where most of the research work done within the domain was to study climate change and floods in an arid System, which touched upon urbanization through satellite images but without studying the drainage effectiveness. Therefore, this research provides a state of art framework to analyzing the factors affecting urban flooding, which is important for Egypt as well as developing regions in the world, which are anticipated to undergo rapid urbanization with large-scale land use changes.

## Chapter 3. Materials and Methods

To study the main factors affecting urban flashfloods in New Cairo, the research starts by compensating the shortfalls in the ground measured rainfall data through comparing six satellite precipitation data against observed rainfall from Cairo Station verifying the most accurate satellite to provide the missing information. The analysis includes graphical and statistical comparisons, followed by bias correction for the selected rainfall product and it is finalized by validating the assessment through applying the final product in a hydrological model setup to evaluate its performance.

The rapid urbanization effect is studied through analyzing the seepage capability of the soil in New Cairo before and after urbanization. Following, a rainfall-runoff simulates at different urbanization levels from 0% to 100% and with several storm return periods (2, 5, 10, 20, 50 and 100 years) to fully understanding the urbanization effect on runoff. On the other hand, the validation of whether the storms occurred in New Cairo is following Climate Change scheme or just recurrence of the normal historical trends, is done through comparing ground observed data with six climate change projections using statistical analysis.

Finally, the sewer network assessment of New Cairo is conducted to understand the role of drainage design in mitigating flashfloods through validating its accommodation for the normal drainage operation, followed by an actual drainage load-capacity balance during storms to evaluation of the performance of the drainage network with various rainfall frequencies. Lastly, simulation of an extreme rainfall event previously occurred to indicate the inundation areas and validate it with flood-prone areas recorded by local authorities.



### **3.1 Case Study – New Cairo**

New Cairo was established in the year 2000. The total area of the city is about three hundred and fifty square kilometers. The freshwater reaches the city through three pumping stations with six hundred thousand m<sup>3</sup>/d. There are currently four treatment plants to process sewage water with a capacity of four hundred thousand m<sup>3</sup>/d and there is a treatment plant with a capacity of one million m<sup>3</sup>/d under construction (New Urban Communities Authority, 2018). The difference between water supply and treated water is according to the Egyptian code of practice where it assumes that the wastewater is eighty percent of the water supply (ECP , 2010).

In this research, the drainage network of seventeen neighborhoods in New Cairo will be evaluated, the location and area of each district are shown in Figure 3.1. All neighborhoods have pumping stations that drains wastewater to either another neighborhood or treatment plant.

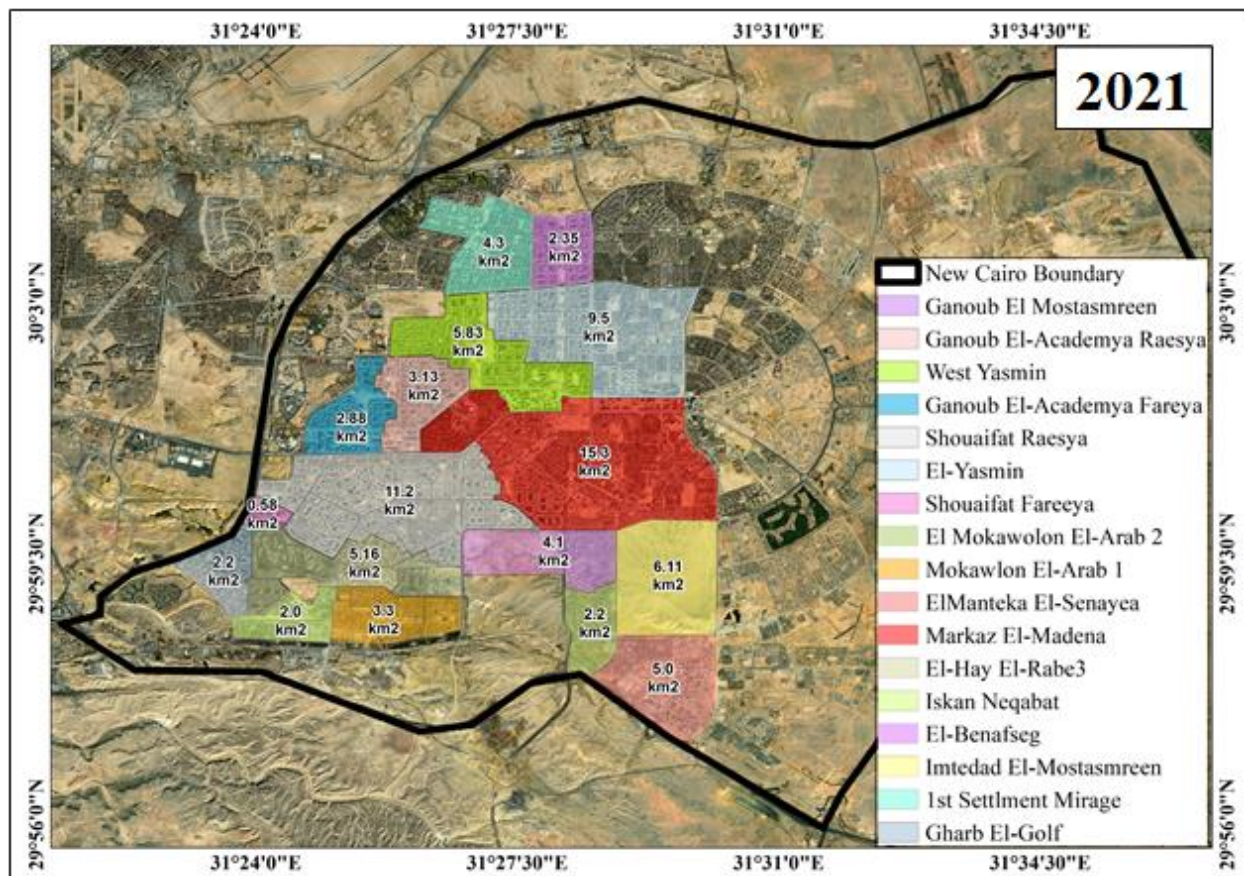


Figure 3.1: New Cairo's 17 Neighborhoods included in the Study showing their locations and areas (km<sup>2</sup>)

## **3.2 Rainfall Data Collection and Validation**

### **3.2.1. Ground Observed Rainfall Data**

Collecting historical rainfall data from ground gauges is necessary to determine the quantities of rainfall that occurred, which is used for rainfall analysis and projections. The Egyptian Meteorological Authority (EMA) is the main governmental organization responsible for the collection and distribution of ground measured rainfall data from meteorological stations located all over Egypt (EMA, 2021). EMA claims that the measured rainfall data taken from a ground station is applicable for a perimeter of 50 km around the station, which makes the data resolution very coarse and weakly distributed (Salem, Shahid, Dewan, Ismail, & Alias, 2020). Accordingly, the closest station to the study area is Cairo Station, which is identified using Thiessen Polygon Method (TPM); details regarding the TPM method and how Cairo station was chosen are shown in Appendix A.

Cairo Station is located 15 km away from the center of New Cairo. The rainfall data is available for total 45 years from 1976 to 2020 and it is given in terms of the maximum rainfall occurred in 24 hours per year and total monthly rainfall. Figure 3.2 shows monthly rainfall data of Cairo Station in part (A), while part (B) shows the statistical features of the monthly and daily rainfall data as a Box plot showing the mean, median, minimum and maximum monthly rainfall and the extreme events in the form of outliers.

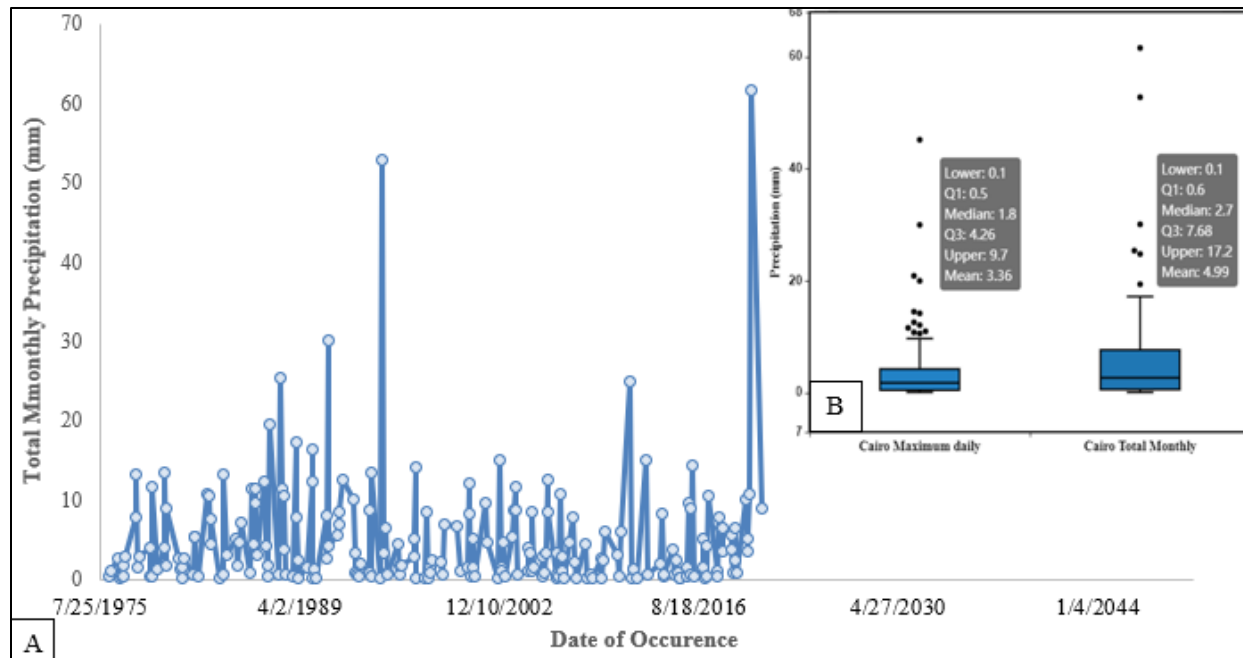


Figure 3.2: Part A: Shows Monthly Rainfall Data for Cairo Station. Part B: Statistical Features (Mean, Median, Minimum, Maximum and Extreme values as outliers) for Monthly and Maximum Daily Rainfall Data of Cairo Station

### 3.2.2. Satellite Rainfall Data

The satellite rainfall data (gridded rainfall products) are useful in addressing ground observed data shortfalls by strengthen the spatial and temporal resolution of rainfall measurements. It can also be used in areas that has few rain gages or poor coverages. Figure 3.3 illustrates some of the shortfalls of ground rainfall data, divisions 2, 3 and 4 show the spatial distribution of some storm events occurred over New Cairo but was not captured by the surrounding rainfall station. On the other hand, division 1 shows rainfall fell over the ground stations but did not pass over the entire study area. Therefore, due to the far distance between the study area and the surrounding ground station, the later readings can be miss-representing rainfall information over the study area. Moreover, the figure shows that the values red by the ground stations might not equal to the actual rainfall fell over the study area.

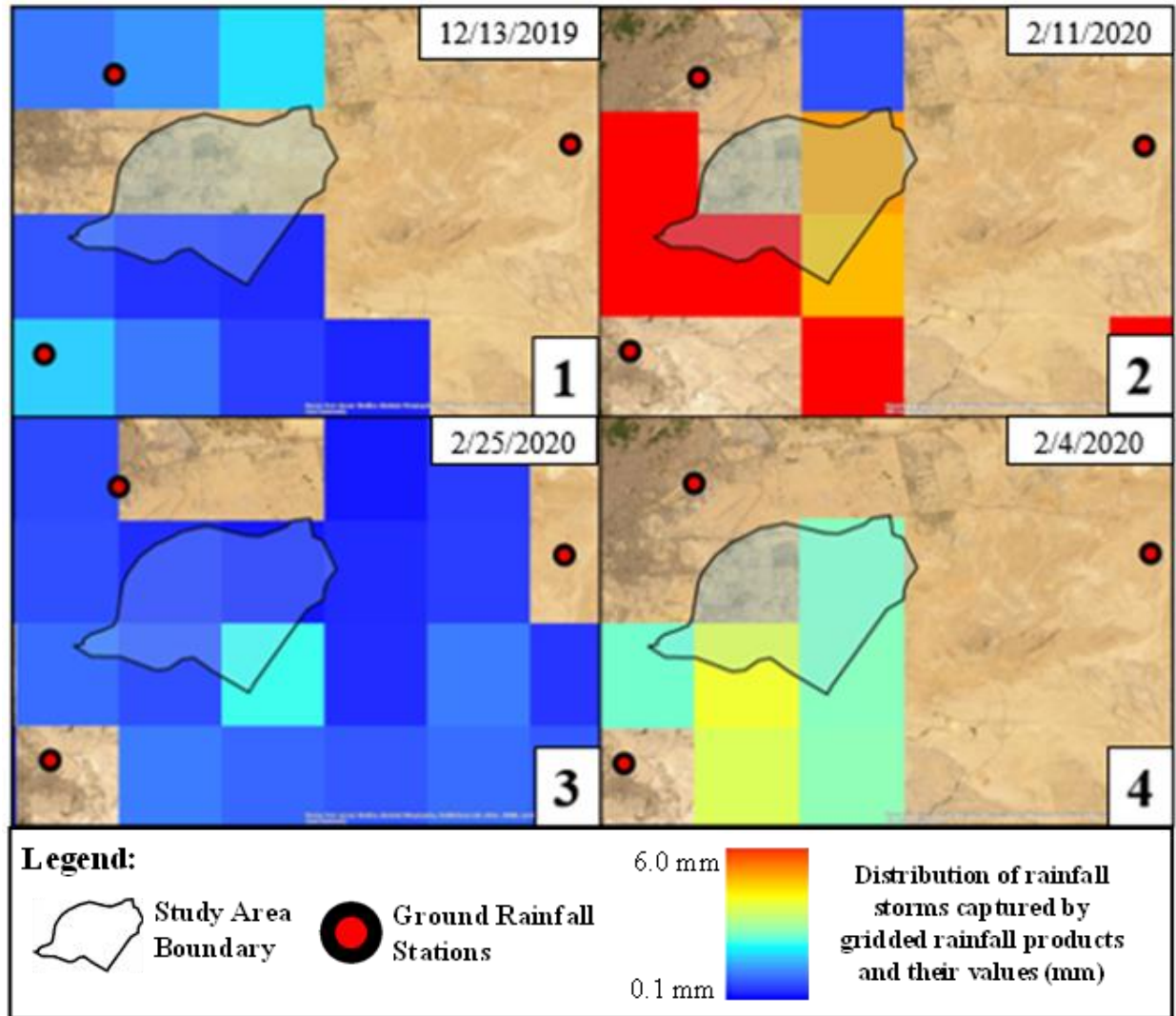


Figure 3.3: Illustration of ground rainfall station shortfalls. Section (2,3&4) represent storms occurred on the study area that was not measured by ground stations. Section (1) represent rainfall measured from ground stations but did not occur over the study area

In this study the ground measured rainfall data from Cairo Station is compared to six satellite rainfall products; that will enable the verification of which product(s) is/are more accurate to capture the rainfall events occurred over Cairo Airport station, consequently, dependable to extract storm distribution over the study area. The used satellite rainfall products are mentioned in Table 3.1 and their detailed description is mentioned in Appendix B.

Table 3.1: Summary of the Satelites Rainfall Data used in this Research (Resolution, Time Range and Data availability)

Data Set	Resolution	Time Range	Data Availability	Refrence
PERSIANN <sup>1</sup>	0.25°	March 2000 - Present	Hourly, 3hrs, 6-hrs, daily, monthly, yearly	(Nguyen, et al., 2019)
GPCC <sup>2</sup>	0.5°	1891 - 2019	Monthly	(NCAR, 2020)
	1°	1982 - 2019	Daily	
GPCP <sup>3</sup>	2.5°	1979 - Present	Monthly	(Pendergrass, Wang, &
	1°	October 1996 - Present	Daily	NCAR, 2020)
CHIRPS <sup>4</sup>	0.05°	1981 - Present	Daily, Monthly	(USAID & UCSB, 2021)
GPM <sup>5</sup>	0.1°	June 2000- Present	30 minutes, Daily, Monthly	(NCAR, 2017)
TRMM <sup>6</sup>	0.25°	1998 to 2019	3 hours, Daily, Monthly	(Huffman & Pendergrass, 2021)

### 3.2.3. Validation of Satellite Rainfall Data with Ground Observation

As shown in Table 3.1 the satellite rainfall products have different resolutions and temporal variability. However, the primary focus when using satellite rainfall data is to validate and bias correct it with ground measured data before usage to evaluate its effectiveness over the study area (Shrestha & Dangol, 2020). Therefore, the comparison between the ground measured rainfall and the rainfall aims to ascertain which product can describe the rainfall events occurred over the study area and use it in extracting data that are not provided by the ground measured rainfall like, measuring precipitation hourly. The validation is done through three main steps, firstly, comparing gridded rainfall data graphically and statistically with ground measured data; secondly, calibrate

<sup>1</sup> Precipitation Estimation from Remotely Sensed Information using Artificial Neural Networks

<sup>2</sup> Global Precipitation Climatology Center

<sup>3</sup> Global Precipitation Climatology Project

<sup>4</sup> Climate Hazards group InfraRed Precipitation with Station data

<sup>5</sup> The Global Precipitation Measurement

<sup>6</sup> Tropical Rainfall Measuring Mission

rainfall products through bias correction technique and finally evaluate the final chosen gridded product through a hydrological model.

#### 3.2.3.1. Comparison of Rainfall Products through Graphical Representation and Statistical Equations

The comparison is conducted on the monthly rainfall data; the monthly data are the most suitable temporal resolution that could evaluate the correlation between gridded rainfall products and rain gauge data (Dembélé & Zwart, 2016), where the monthly accumulation reduces the noise in the data. However, the daily data are also included as a check as it is important in the analysis of extreme rainfall events. The data extraction and analysis are done through Arc-GIS (ESRI, 2012). The comparison of all data should be during the same time period, accordingly, the common period between all rainfall data is from March 2000 to 2019 (19 years).

The visual comparison offers an initial overview of the expected outcome (Moriassi, et al., 2007). However, the validation through statistical analysis is crucial to verify the accuracy of the satellite rainfall data numerically. Six statistical methods are used to evaluate the rainfall data, where each shows a part of the error in the data set. The statistical methods are Mean Absolute Error (MAE), Root Mean Square Error (RMSE), The coefficient of determination ( $R^2$ ), Percent Bias (PBIAS), The RMSE-observations standard deviation ratio (RSR) and Nash Sutcliffe Efficiency (NSE). A summary of the equations and general range are shown in Table 3.2, while the detailed limits of all statistical criteria are shown in Table 3.3 (Moriassi, et al., 2007; Moore, Notz, & Flinger, 2013).

Table 3.2: Summary of Statistical Indicators Equations and Ranges

Statistical Indicator	Equation	Range	Ideal Value
Mean Absolute Error	$MAE = \frac{1}{n} \sum_{i=1}^n  P_i - O_i $	0 to $\infty$	0
Root Mean Square Error	$(RMSE) = \sqrt{\frac{\sum_{i=1}^n (P_i - O_i)^2}{n}}$	0 to $\infty$	0
Coefficient of Determination	$R^2 = \left[ \frac{\sum_{i=1}^n (O_i - \bar{O})(P_i - \bar{P})}{\sqrt{\sum_{i=1}^n (O_i - \bar{O})^2} \sqrt{\sum_{i=1}^n (P_i - \bar{P})^2}} \right]^2$	0 to 1	1
Percent Bias	$PBIAS = \left[ \frac{\sum_{i=1}^n (O_i - P_i) * 100}{O_i} \right]$	$-\infty$ to $\infty$	0
RMSE-Observation Standard Deviation	$RSR = \frac{RMSE}{STDEV_{Obs}}$	0 to $\infty$	0
Nash Sutcliffe Efficiency	$NSE = 1 - \left[ \frac{\sum_{i=1}^n (O_i - P_i)^2}{\sum_{i=1}^n (O_i - \bar{O})^2} \right]$	$-\infty$ to 1	1

Table 3.3: Summary of Statistical Criteria limits

Assesment	PBIAS	NSE	RSR	R <sup>2</sup>	RMSE	MAE
Very Good	$\leq \pm 10$	0.75 to 1	0 to 0.5	$> 0.7$	The value can range from 0 to $\infty$ , generally the lower the better	
Good	$\pm 10$ to $\pm 15$	0.65 to 0.75	0.5 to 0.6	0.5 to 0.7		
Satisfactory	$\pm 15$ to $\pm 25$	0.50 to 0.65	0.6 to 0.7	0.3 to 0.5		
Unsatisfactory	$\geq \pm 25$	$\leq 0.5$	$> 0.7$	$< 0.3$		

### 3.2.3.2. Bias Correction of Gridded Rainfall Products

The rainfall product could perform better if they calibrated using bias correction. There are several techniques to correct the bias and remove errors; one of these methods is the Linear Scaling (LS). It is a quite simple, yet effective method that is useful to this day (Shrestha, Acharyaa, & Shrestha, 2017; Soriano, Mediero, & Garijo, 2019). The LS method is based on calculating a correction factor for each calendar month through the difference between the monthly mean of observed ground measured data and the rainfall product (Luo, et al., 2018). Then, the monthly



rainfall product value is adjusted through multiplying it to the factor that corresponds to the month the value occurred in. Equation 1 shows the LS bias correction formulas for the monthly data.

$$P(m)^* = P(m) \cdot \left[ \frac{\mu_{m_i} \text{ Observed}}{\mu_{m_i} \text{ Satellite}} \right] \quad \text{Equation 1: Bias Correction (LS)}$$

Where, P stands for the rainfall product data.  $\mu_{m_i}$  is the mean monthly of the  $i^{\text{th}}$  month, m denotes for monthly data.

The statistical indicators and graphical representation of the data are reapplied after the bias correction in order to see its effect on the individual monthly data points and to check if the correction enhanced the performance of the satellite products, accordingly this enables choosing the satellite that represents the ground measured data best.

### 3.2.3.3. Extracting Design Storm Distribution from Actual Storms Captured by the Satellite Rainfall Data

The hydrological calculations are based on the design storm, which is a storm distribution that typically represents a rainfall event occurred in 24 hours over the study area. The design storm is represented in a form of a hyetograph, which is a graphical representation of the rainfall intensity distribution over time. On the other hand, the magnitude of the total rainfall intensity changes according to the return period. A hyetograph progressively increases until reaching the maximum intensity and then regularly decrease.

The calculation of the hyetograph was based on the cumulative value of eight major rainfall storms occurred since 2015, then by using block method (Chow, Maidment, & Mays, 1988) the hyetograph was derived. The block method formulated through calculating the incremental rainfall value between each time step, then placing the maximum incremental depth in the middle of the

hyetograph, the remaining blocks are positioned in descending order by alternating the blocks before and after the center to create a bell shape. Afterward, the hyetograph is linearized by converting it into a unit hyetograph to be multiplied by the rainfall value according to the different return periods.

### 3.3 Comparing Climate Change Scenarios to Ground Observed Rainfall Data

The climate change (CC) data used in this thesis are acquired from RICCAR (The Regional Initiative for the Assessment of Climate Change Impacts on Water Resources and Socio-Economic Vulnerability in the Arab Region), which is a program that aims to evaluate the potential impacts of climate change on the Arab Region in terms of water availability and its effect on the social, economic and environmental aspects in the MENA region (RICCAR, 2020).

The scenarios are acquired from three Global Climate Models (GCMs), which are EC-Earth, GFDL-ESM2M and CNRM-CM5. They are downscaled and bias corrected against ground measured rainfall data from the year 1986 to 2005 by one Regional Climate Model (RCM) to a resolution of  $0.44^\circ$ . The climate change data used from two emission scenarios, which are RCP4.5 that represents a moderate emission scenario and RCP8.5 that represents a high emission scenario. The CC projected data are available from the year 2006 to 2100. Figure 3.4 shows a summary of the six scenarios used of the climate change data.

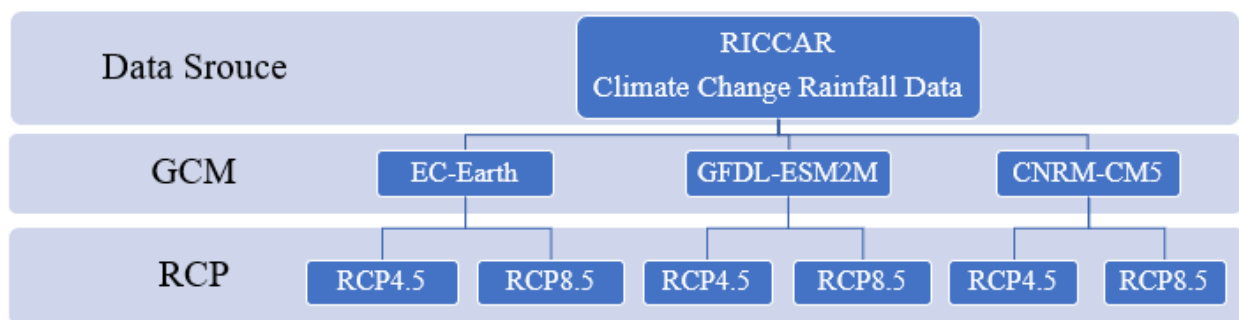


Figure 3.4: Summary of Climate Change Data Used

The evaluation between the ground measured rainfall and the CC data is conducted on the monthly temporal resolution. The statistical criteria summarized in Table 3.2 will be used to evaluate the climate change ensembles. The evaluation of the ground measured data against the CC prediction models is conducted for the common period from 2006 to 2020 (15 years). After the comparison, the rainfall trends are analyzed to understand the effect of climate change on rainfall intensities.

### **3.4 Evaluating the Effect of Urban Sprawl on the Surface Runoff**

The impact of urbanization on surface runoff was investigated through simulating surface runoff during six return periods using Watershed Modeling System (WMS) software at different urbanization levels. The urbanization expansion adopted in this research are from 1990 to 2020 extracted through satellite images for the study area at five years interval. The analysis will be conducted through two main steps, first, analyzing satellite images to detect urbanization growth rate through time. Second, developing a rainfall-runoff model to calculate the surface runoff resulted at different urbanization levels.

#### **3.4.1. Analysis of Urbanization Growth Rate**

The identification of the urbanization growth rate is done through land use data extracted from remote sensing images (USGS, 2021) showing urbanization stages of New Cairo each five years for a total of seven years (1990, 1995, 2000, 2005, 2010, 2015 and 2020). The urbanization growth evaluation is achieved through the quantification of land use categories; the categorization will aid in the calculation of the runoff coefficient, as each type of land use has a different infiltration ability. There are two main groups in land use urbanized and unurbanized areas. The urbanized areas include areas under construction, fully urbanized areas and urban areas that has more than

50% green space. On the other hand, the unurbanized areas are rural areas that does not have any human interventions.

### **3.4.2. Calculating Surface Runoff Using WMS Hydrological Model**

Rainfall-runoff models aims to study the effect of urbanization on the surface runoff. In this research, rainfall corresponds to six return periods (2, 5, 10, 20, 50, and 100) is used to calculated surface runoff corresponds to eight urbanization levels from 1990 to 2020 and a 100% urbanization level. The model is conducted through Watershed Modelling System (WMS) (Aquaveo, 2021), which requires two main inputs, design storm and soil data to calculate infiltration values as well as excess rainfall water that will be converted to runoff. Detailed description of the model inputs is provided in Appendix C.

## **3.5 Impact of Drainage Design on Surface Runoff**

The drainage system in urban areas has a significant role in mitigating urban flashfloods; the investigation of the performance of New Cairo's drainage system is done through analyzing sewer network efficiency under different conditions, to assess whether the previously occurred urban flashfloods were due to the effect of climatic changes and urbanization solely, or the drainage system contributed to the increase of flooded areas as well.

The sewer network in new Cairo is combined, where it drains both wastewater and storm loads in one pipe (New Urban Communities Authority, 2018). According to the Egyptian Code of Practice for designing drainage network (ECP, 2010), the design of the combined sewer network has a predictive methodology, where the designer should include rainfall quantities according to the desired return period; however, the return period is identified according to the risk probability of the project's location to face flashfloods and according to the required degree of conservativity

in the network design. In this research, there are no information regarding the return period or the exact storm intensity that the sewer network was designed for, therefore it is important to simulate different return periods in order to evaluate the current drainage system and identify its capacity. The analysis is done through actual drainage load-capacity balance during storm events conducted for seventeen districts in New Cairo, in addition, to results' validation through SewerGEMS (Bentley, 2021) simulation for one district.

### **3.5.1. Drainage Network Load-Capacity Balance During Storm Events**

The assessment of the drainage network starts by evaluating the capacity of the seventeen neighborhoods' networks for the base scenario in order to ensure that the system is sufficient for the wastewater flows they usually manage. Moreover, drainage load-capacity balance during storm events correspond to different return periods (2, 5, 10, 20, 50 and 100 years) will be simulated to identify the maximum storm the current sewer network can handle, for each district. Finally, the evaluation will be conducted during the maximum projected storm according to the climate change scenario. The assessment will be done on the pipelines and the pumping station separately. The daily domestic discharge corresponds to 2016 and it is assumed to still represent drainage loads in 2020, furthermore, it is averaged at steady state and loaded into the discharge network. Finally, the storm events are assumed to be uniform over the catchment area throughout a 24-hours period and simulated through hyetograph derived from satellite captured rainfall data.

The rainfall is calculated by the rational method, which is a popular equation used to design storm sewer networks (Chow, Maidment, & Mays, 1988; ECP , 2010), the equation is as follows:

$$Q = CIA$$

Equation 2: Rational Method

Where, Q, is the total rainfall load (m<sup>3</sup>/d)

i, is the rainfall intensity (m<sup>3</sup>/d)

C, is the rational coefficient (no units)

A, is the catchment area (m<sup>3</sup>)

The rational coefficient depends on the land use type as shown in Table 3.4.

Table 3.4: Rational Method Run off Coefficient Values (ECP , 2010)

Land Use	C
Paved Roads and Building Surfaces	0.70 – 0.95
Exposed Soil, Undeveloped Roads	0.10 – 0.20
Residential Areas (Flat)	0.50 – 0.30
Residential Areas (Mountainous)	0.50 – 0.70
Industrial Areas (Light)	0.55 – 0.65
Industrial Areas (Heavy)	0.60 - 0.80

### 3.5.2. Validation using SewerGEMS

SewerGEMS simulates the drainage network during storms and evaluate the system's hydrologic and hydraulic performances. The evaluation is conducted for one neighborhood called Al Academya El-Fareeya. The aim of this simulation is to validate the findings of the load-capacity balance analysis, in addition, to identifying the inundated locations during storms and validate them with water accumulation areas recorded from previous storms as shown in Figure 3.5.



Figure 3.5: Drainage Network of Academya El Fareeya, showing red rectangles that indicates inundation areas during past rainfall storms (New Urban Communities Authority, 2018)

The simulation will be conducted for the base scenario with only wastewater discharge first, then simulating a 2-year storm to check if the network accommodates the smallest return period rainfall along with the wastewater it usually manages. Finally, a simulation of an extreme rainfall event that may correspond to return period of 100-years, which is the maximum daily storm occurred in 12<sup>th</sup> of March 2020 with intensity of 45.2 mm/d to validate the resulted inundation areas. The total discharge of the area is assumed to be equally distributed over all manholes. Moreover, the rainfall is assumed to occur over the entire neighborhood equally, with a duration of 24-hours. The Detailed SewerGEMS model inputs are mentioned in Appendix D.

# Chapter 4. Results and Discussion

## 4.1 Satellite Rainfall Products Evaluation Using Gauge Observation and The Extraction of Actual Storm Distribution

### 4.1.1. Comparison between Gridded Rainfall Products and Ground Observed Rainfall

The total monthly and maximum daily precipitation from six gridded rainfall products were evaluated against Cairo ground station graphically and statistically. The total comparison points were one hundred months for total 19 years from September 2000 to December 2019. The initial overview of the rainfall products through scatter plot of monthly data (Figure 4.1) shows that GPCC has the closest correlation to ground measured data with  $R^2=0.41$  followed closely by GPM with  $R^2=0.40$ . However, the  $R^2$  value should exceed 0.5 to be accepted.

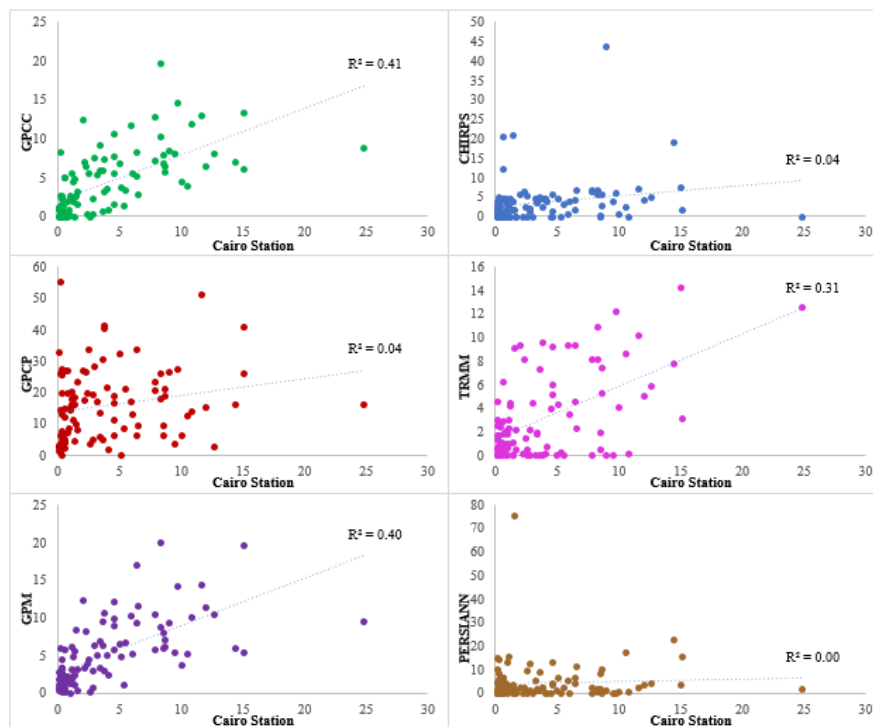


Figure 4.1: Scatter plot showing correlation between six gridded rainfall products and ground observed data for monthly precipitation



On the other hand, the validation through statistical indicators (Table 3.2) is crucial to verify the accuracy of the satellite rainfall data numerically. The results of the statistical evaluation for the monthly and daily rainfall data are shown in Table 4.1 and Table 4.2 simultaneously. It should be emphasized that the monthly comparison is more dependable than the daily comparison as it has higher precision since it includes all rainy days and shows the seasonal effect. However, the daily data sets were included for general overview of the data.

Table 4.1: The Results of Six Satellite Rainfall products in Six Statistical Indicators for the Total Monthly Rainfall Data

Satellite Indicator	TRMM	GPM	PERSIANN	GPCC	GPCP	CHIRPS
RMSE	3.78	4.1	6.22	3.73	16.46	15.92
RSR	0.81	0.57	1.33	0.83	3.72	2.22
% Bias	-7.04	29.79	12.04	10.59	304.54	13.09
NSE	0.34	0.67	-0.76	0.30	-12.81	-3.93
R <sup>2</sup>	0.61	0.87	0.15	0.63	0.20	0.12
MAE	0.28	1.37	0.50	0.43	11.89	0.60



Strong Correlation  Weak Correlation

Table 4.2: The Results of Six Satellite Rainfall products in Six Statistical Indicators for the Maximum Rainy Day per Month

Satellite Indicator	TRMM	GPM	PERSIANN	GPCC	GPCP	CHIRPS
RMSE	3.52	2.98	4.41	2.68	5.64	4.68
RSR	1.00	0.57	1.24	0.81	1.72	0.89
% Bias	45.48	16.36	52.03	11.80	5.20	67.24
NSE	-0.01	0.68	-0.54	0.34	-1.96	0.21
R <sup>2</sup>	0.45	0.84	0.15	0.62	0.10	0.66
MAE	1.31	0.52	1.54	0.33	0.14	2.15

Strong Correlation  Weak Correlation

For the monthly data, GPM showed the best correlation with Cairo station as R<sup>2</sup> was larger than 0.70 with a value of 0.87, likewise it has the highest value for NSE of 0.67. On the other hand, CHIRPS data showed the smallest R<sup>2</sup> value of 0.12 and the weakest NSE -3.93, which is

unsatisfactory. As for the RSR, GPM showed the best performance with value of 0.57, while the least performed was GPCP with value of 3.72. TRMM had the least bias of -7%, where the negative value indicates overestimation, and the best MAE of 0.28 (mm/month); whereas GPCP presented largest Bias of 304% and the worst MAE with a value of 11.89 (mm/month); Furthermore, the best RMSE value is 3.73 for GPCC followed closely by TRMM with a value of 3.78 and the worst value is 16.46 belongs to GPCP. As a result, the statistical indicator for the monthly precipitation data shows that GPM and TRMM have acceptable correlation and prediction capabilities for the ground measured data followed by GPCC. Nevertheless, the least suitable satellite to represent precipitation data over Cairo station are GPCP and CHIRPS. As for the daily data, GPM showed a good agreement with the rain-gauge data in most of the statistical criteria, followed by GPCC. On the other hand, PERSIANN and GPCP demonstrated the worst performance in most of the numerical criteria.

Generally, GPM stood out in both the daily and monthly comparisons, but it was followed closely by GPCC in the monthly comparison and TRMM for the daily comparison; However, this is not the final conclusion as the data calibration using bias correction method will improve the performance of most of the satellites.

#### **4.1.2. Bias Correction of Gridded Rainfall Products**

The calibration results done by LS method are shown in Figure 4.2 and Figure 4.3, which represent the effect of bias correction on the mean monthly values and total monthly values simultaneously; the monthly values are used as they include rain values of all days within the given month. As demonstrated in the charts, the bias correction improves the mean monthly and total monthly values of the gridded rainfall products data to be almost equal to the ground measured data. The effect of the bias correction on individual data are represented with a comparison of the

scatter plot results before and after the bias correction as shown in Table 4.3 and a recalculation of the statistical indicators is shown in Table 4.4.

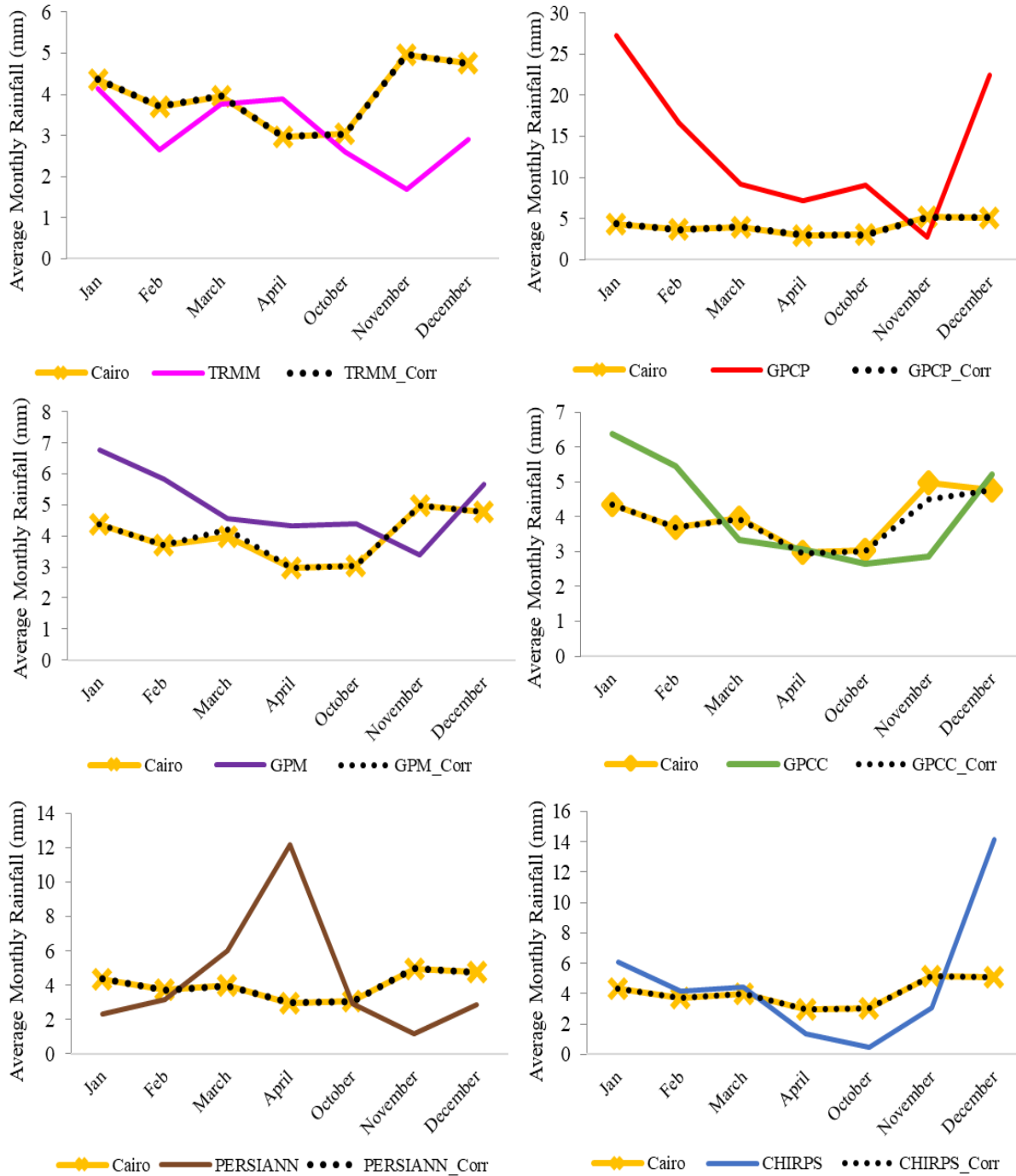


Figure 4.2: Bias Correction of Mean Monthly Values

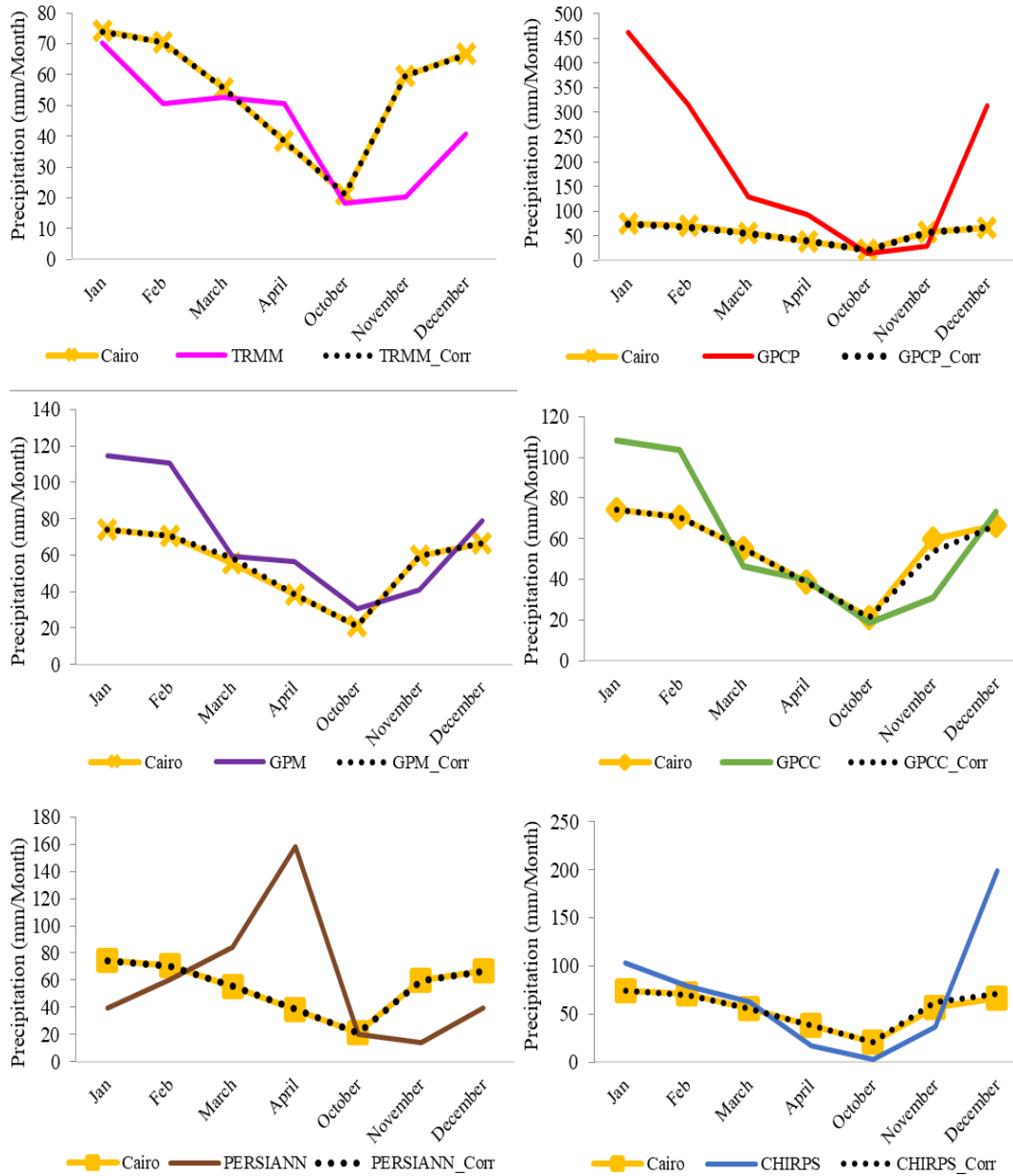


Figure 4.3: Bias Correction of Total Monthly Values


Table 4.3: Comparison of Monthly Data Variance ( $R^2$ ) from scatter plots before and after LS

Satellite	$R^2$		Difference
	Before Bias	After Bias	
TRMM	0.31	0.42	0.11
GPM	0.40	0.50	0.1
PERSIANN	0.00	0.06	0.06
GPCC	0.41	0.55	0.14
GPCP	0.04	0.02	-0.02
CHIRPS	0.04	0.02	-0.02

The scatter plot results after the bias correction showed a significant improvement where the values of  $R^2$  for GPM and GPCC were in the acceptable range, which is  $\geq 0.5$ . On the other hand, the results of the statistical analysis after the bias correction shows an outstanding performance for GPM, as it is within the upper acceptable range in all statistical criteria. Followed by GPCC, which also has acceptable values that are satisfactory. On the other hand, GPCP was rejected, it underperformed in all criteria with unacceptable values for the bias percentage, RSR and Nash-Sutcliff. CHIRPS and PERSIANN improved in most of the statistical criteria however they had unacceptable values for NSE. Finally, TRMM performed moderately in all criteria, however, its NSE value is exceptionally low. Worth noting that NSE is an important indicator for the ability of the data to predict rainfall.

Table 4.4: Statistical Analysis of Biased Correction of Monthly Data

Satellite Indicator	TRMM	GPM	PERSIANN	GPCC	GPCP	CHIRPS
RMSE	4.25	3.18	5.77	2.99	11.12	6.35
RSR	0.96	0.46	1.30	0.67	2.51	1.43
% Bias	0.02	0.03	0.03	1.49	73.51	0.61
NSE	0.08	0.79	-0.70	0.55	-5.31	-1.03
$R^2$	0.65	0.89	0.25	0.74	0.15	0.16
MAE	0.00	0.00	0.00	0.06	2.87	0.02

Strong Correlation  Weak Correlation

The Global Precipitation Model (GPM) showed a strong correlation with the observed data from Cairo Stations with a slight underestimation but with a great ability in rainfall detection. Table 4.5 shows a comparison of the performance of GPM before and after bias correction, where GPM met the upper range criteria of all statistical indicators.


Table 4.5: Comparison of GPM Performance Before and After Bias Correction

Statistical Indicator	GPM		Test Acceptable Range
	Before Bias	After Bias	
RMSE	4.1	3.18	Ideal Value is 0, generally, the lower the better
MAE	1.37	0.00	
RSR	0.57	0.46	0 to 0.5
% Bias	29.79	0.03	$\leq \pm 10$
NSE	0.67	0.79	0.75 to 1
R <sup>2</sup>	0.87	0.89	> 0.7

Table 4.6 shows the effect of the bias correction on the maximum daily data. The table shows that the bias correction improved the performance of the daily data as well; GPM performance is very good and has a good correlation with the ground station as well and the statistical indicators results are within the acceptable range in all criteria.

Table 4.6: Satellite Daily Data Performance After the Bias Correction

Satellite Indicator	TRMM	GPM	PERSIANN	GPCC	GPCP
RMSE	3.72	2.72	4.25	3.02	4.05
RSR	1.14	0.52	1.30	0.92	1.22
% Bias	-34.52	-3.81	-61.83	-11.83	-63.44
NSE	-0.29	0.73	-0.68	0.15	-0.48
R <sup>2</sup>	0.59	0.88	0.17	0.61	0.11
MAE	0.94	0.12	1.69	0.32	1.81

Strong Correlation  Weak Correlation

In conclusion, GPM effectively can represent ground measured rainfall data at Cairo Station with a small acceptable percentage of underestimation. Therefore, it is a dependable source for the extraction of storm distribution over New Cairo.

### 4.1.3. Extracting Design Storm Distribution from Actual Storms Captured by GPM

The calculation of the design storm (hyetograph) was based on the cumulative value of eight major rainfall storms occurred since 2015. Figure 4.4 shows the exact storms distribution during each rainfall event, which were acquired from GPM Satellite and their corresponding dates.

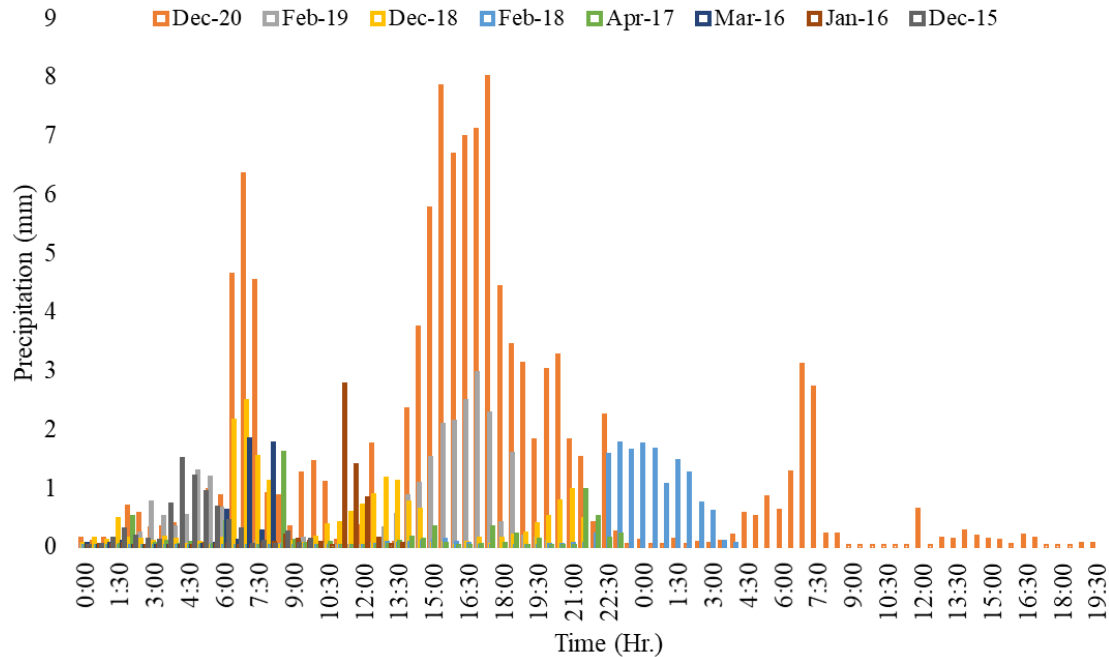


Figure 4.4: Distribution of Eight Main Rainfall Events from 2015 to 2020 acquired from GPM

The block method was then used to derive the hyetograph that will be applied in the rainfall simulation; the first step was to add all storm events at each incremental value as illustrated in Figure 4.5.

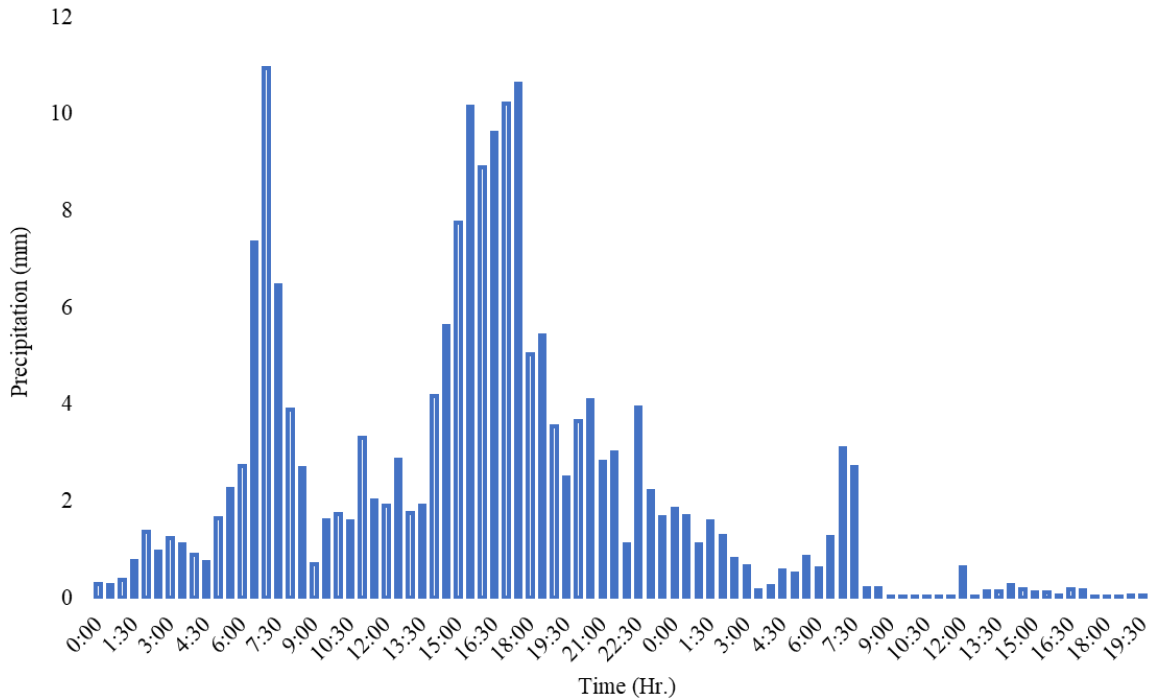


Figure 4.5: Cumulative Half Hourly Distribution for all eight storm events

Secondly, the maximum incremental depth is placed in the middle of the hyetograph and the remaining blocks are positioned in descending order by alternating the blocks before and after the center to create a bell shape as shown in Figure 4.6.

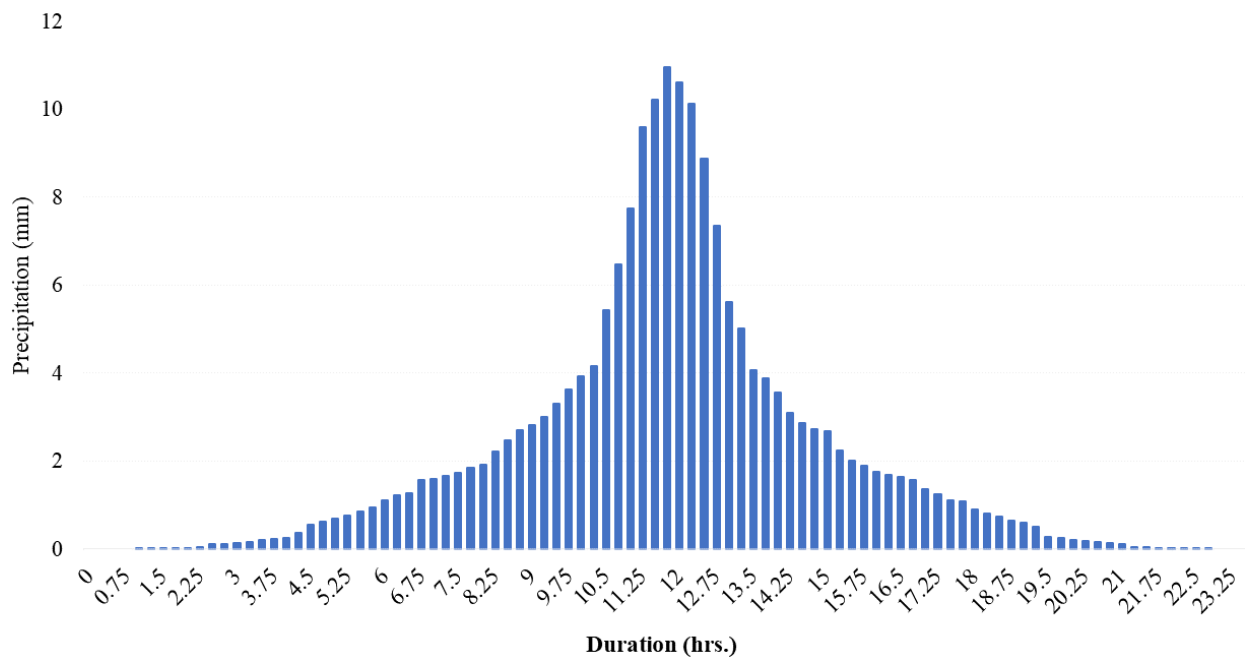


Figure 4.6: Nested Hyetograph after applying block method



Finally, the hyetograph is linearized through converting it into a unit value to be multiplied by the rainfall data according to the different return periods (Figure 4.7).

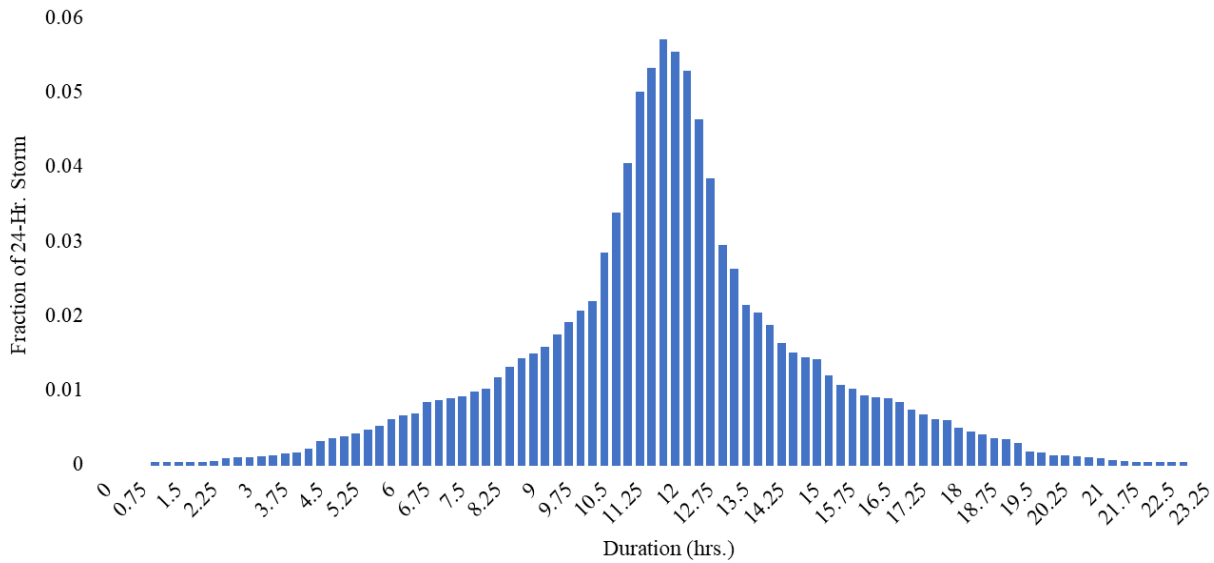


Figure 4.7: Final Unit Hyetograph to be used in the Rainfall-Runoff Simulation

## 4.2 Climate Change Scenarios Analysis and Projections

### 4.2.1. Validating that Historical Rainfall Events Following Climate Change Scheme

The six ensembles were evaluated against the Cairo ground station using the statistical indicators, which are summarized in Table 3.2. The total comparison points were seventy-nine months that had rainfall events occurred for total fourteen years from 2006 to 2020. The results of the statistical analysis of climate change scenarios are shown in Table 4.7.

Table 4.7: Results of the statistical analysis for the climate change models

Indicator	RCP4.5			RCP8.5		
	CNRM	EC-Earth	GFDL	CNRM	EC-Earth	GFDL
RMSE	6.70	9.18	10.04	10.35	8.34	5.60
RSR	0.68	1.06	1.15	1.20	1.03	1.32
% Bias	-6.12	64.43	-42.60	-20.33	-31.27	-36.54
R <sup>2</sup>	0.64	0.09	-0.13	-0.04	0.20	-0.16
MAE	0.29	1.90	2.04	0.97	1.48	1.21

Strong Correlation  Weak Correlation

The statistical indicators for the climate change ensembles showed that CNRM 4.5 have overall acceptable correlation for the ground measured data, moreover, it was the only climate model that projected high precipitation value for Cairo in March 2020, it predicted a total monthly precipitation of 46.5 mm/month, while the actual monthly rainfall occurred was 61 mm/month.

#### 4.2.2. Analyzing the Climate Change Effect of Rainfall Patterns in Cairo

Figure 4.8 shows the total rainfall yearly (mm/year) from the year 1976 to 2020, while Figure 4.9 shows the maximum rainfall event (mm/d) occurred in a single day in each year. From the figures, the precipitation trends on New Cairo, shows that extreme rainfall events' frequency has an increasing trend (Figure 4.9), although the total annual precipitation values have a decreasing trend (Figure 4.8). This observation is consistent with the reports of the Intergovernmental Panel on Climate Change (IPCC) (S. I., et al., 2012) that the climate change is likely to increase the frequency of single day extreme rainfall event in the 21<sup>st</sup> century despite the decrease in the total annual rainfall. Moreover, it is also consistent with CNRM4.5 rainfall projection as shown in Figure 4.11.

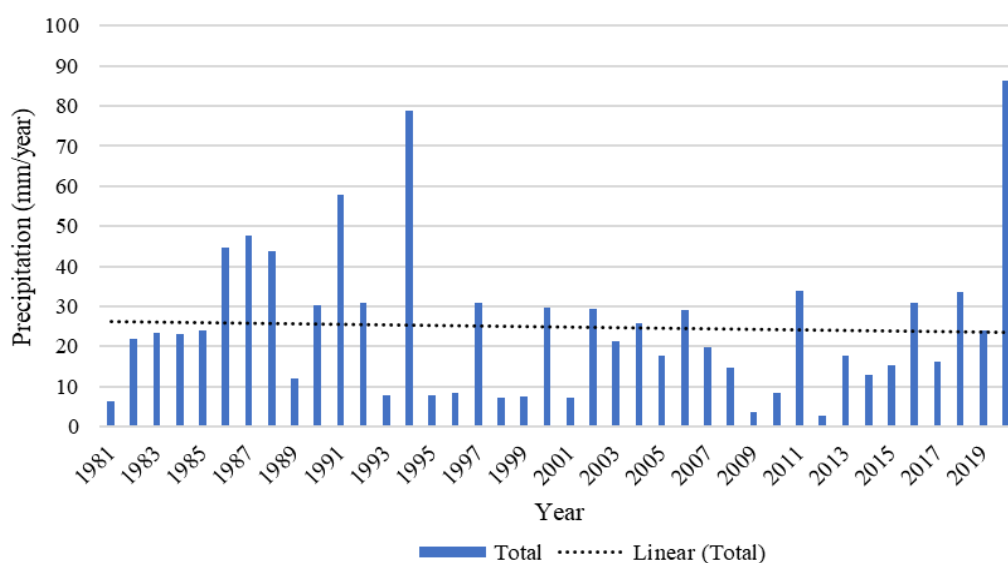


Figure 4.8: Total Rainfall Every Year (mm/year) For the period of 1976 to 2020

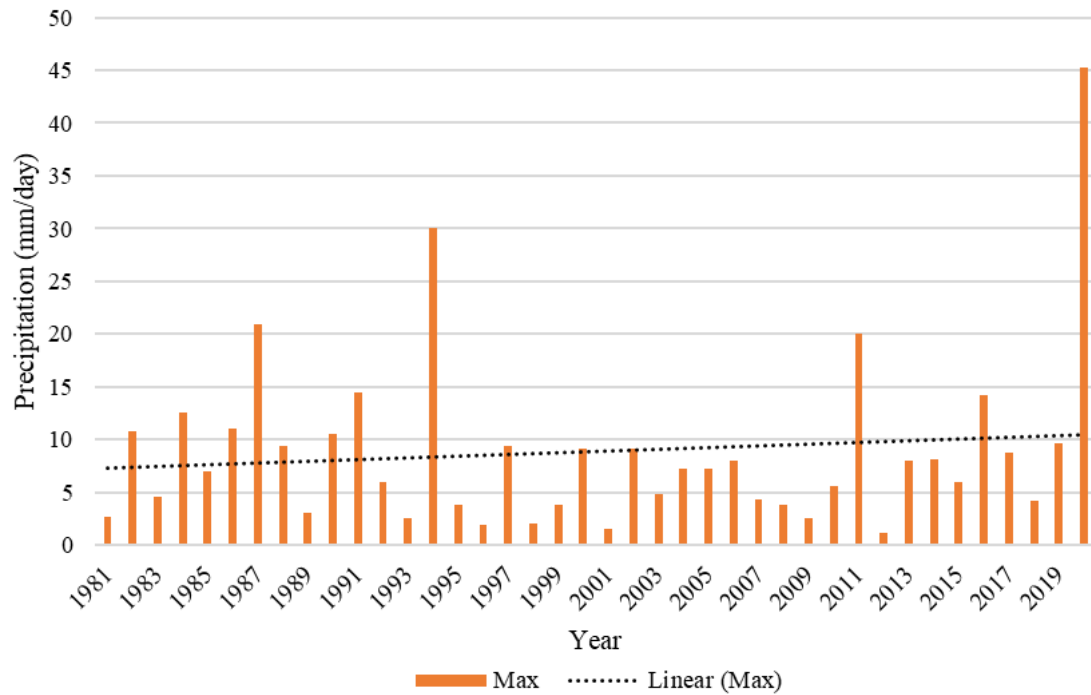


Figure 4.9: Maximum Rainfall Event in each Year (mm/day) For the period of 1976 to 2020

Additionally, the climate change affected the value of rainfall intensity for different return periods as well.

Table 4.8 shows the return period intensities threshold with data adopted from the period of 1976 to 1999 (24 years) compared with return period intensities calculated by rainfall data recorded from 2000 to 2020 (21 years). As illustrated, there is an increase of the rainfall intensities for all return periods, however, the most affected was the 100-year storm it increased by 17% followed by the 50-year storm, which increased by 12%, where both represent the extreme rainfall events. On the other hand, the normal return period used for design increased with smaller percentages, for example the 2-year storm increased by 6%, while the 5- year storm increased by 1%. Therefore, this table shows another indicator that climate change increased the intensities of the extreme rainfall events.

Table 4.8: Comparison of Return Period Intensities between the period of (1976 -1999) and (2000 – 2020)

Time Range Return Period	1976-1999		2000-2020		Percent of Increase
	Rainfall (mm/d)	Confidence Interval	Rainfall (mm/d)	Confidence Interval	
100	33.1	20.3 - 45.8	38.8	14.3 - 63.3	17%
50	28.3	17.5 - 39.1	31.6	13.4 - 49.9	12%
20	22.1	13.8 - 30.3	23.3	11.6 - 34.9	5%
10	17.3	11.0 - 23.7	17.7	9.93 - 25.5	2%
5	12.6	8.19 - 17.0	12.7	7.92 - 17.5	1%
2	6.35	4.45 - 8.25	6.75	4.58 - 8.92	6%

Additionally, looking at the number of events occurred for each return period in two time periods before the year 2000 and after as shown in Figure 4.10, the 2-year and 5-year events decreased by 30% between the two time periods. Moreover, the period between 1976 to 1999 shows that a 50-year event occurred, however in the following period a 100-year event occurred, which struck before its time. This might be due to the effect of climate change.

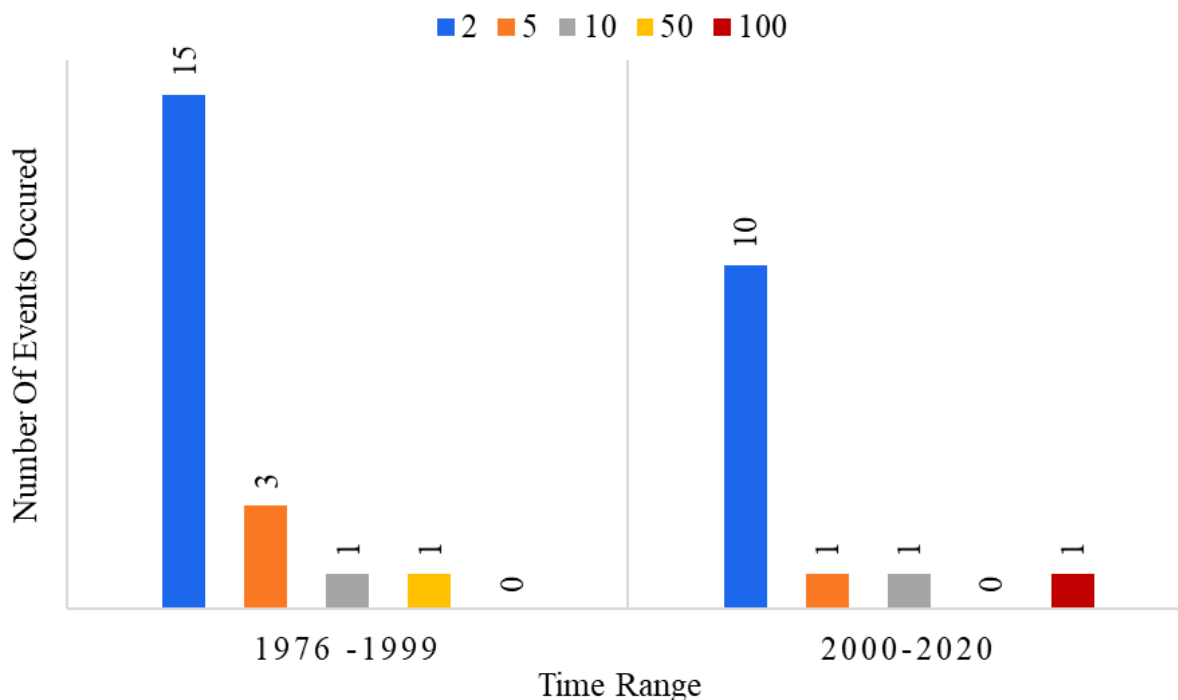


Figure 4.10: Number of Rainfall Events Occurred for each Return Period for Two Time Periods (1976 to 1999) and (2000 to 2020)

According to the CNRM4.5, the storm occurred in March 2020 over New Cairo could be considered an extreme event due to climatic changes. Figure 4.11 shows the CNRM4.5 annual projection of rainfall from 2006 to 2050, illustrates that the year 2048 might experience an extreme rainfall event larger than or equal March 2020.

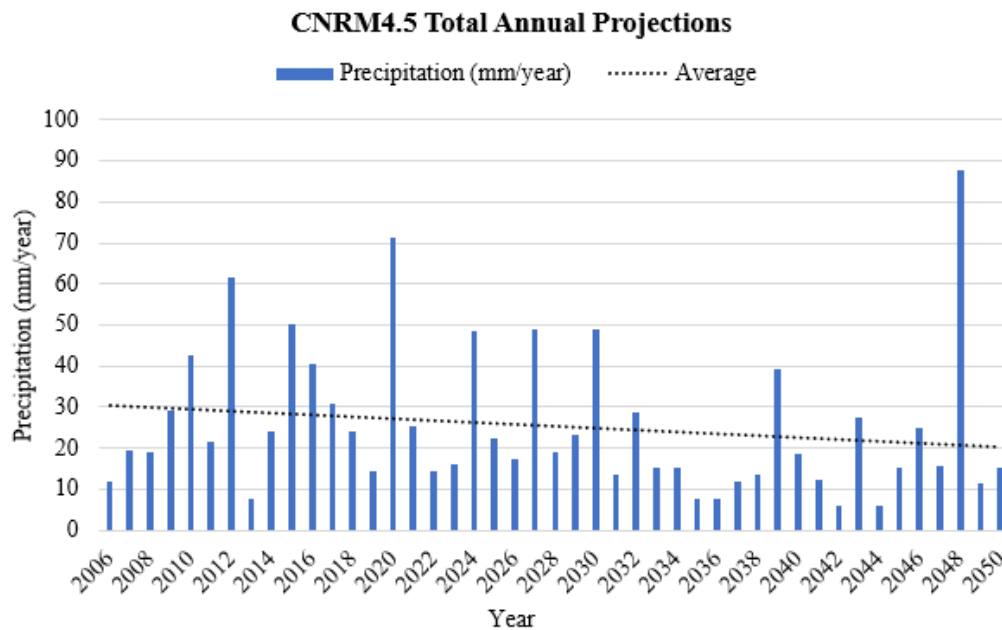


Figure 4.11: CNRM 4.5 Total Annual Projected Precipitation from 2006 to 2050

## 4.3 Effect of Urbanization on Surface Runoff

### 4.3.1. Analysis of Urbanization Growth Rate

The urbanization stages are observed through satellite-captured images for seven years as follows 1990, 1995, 2000, 2005, 2010, 2015 and 2020. Figure 4.12 shows the urbanization stages during the mentioned periods; where areas under construction are denoted by yellow, fully urbanized areas are denoted by red and urban areas that has more than 50% green space are denoted by green. In addition, the unurbanized areas are denoted by beige. Table 4.9 shows the area covered by each category and total percentage of urbanized versus rural areas in each year.



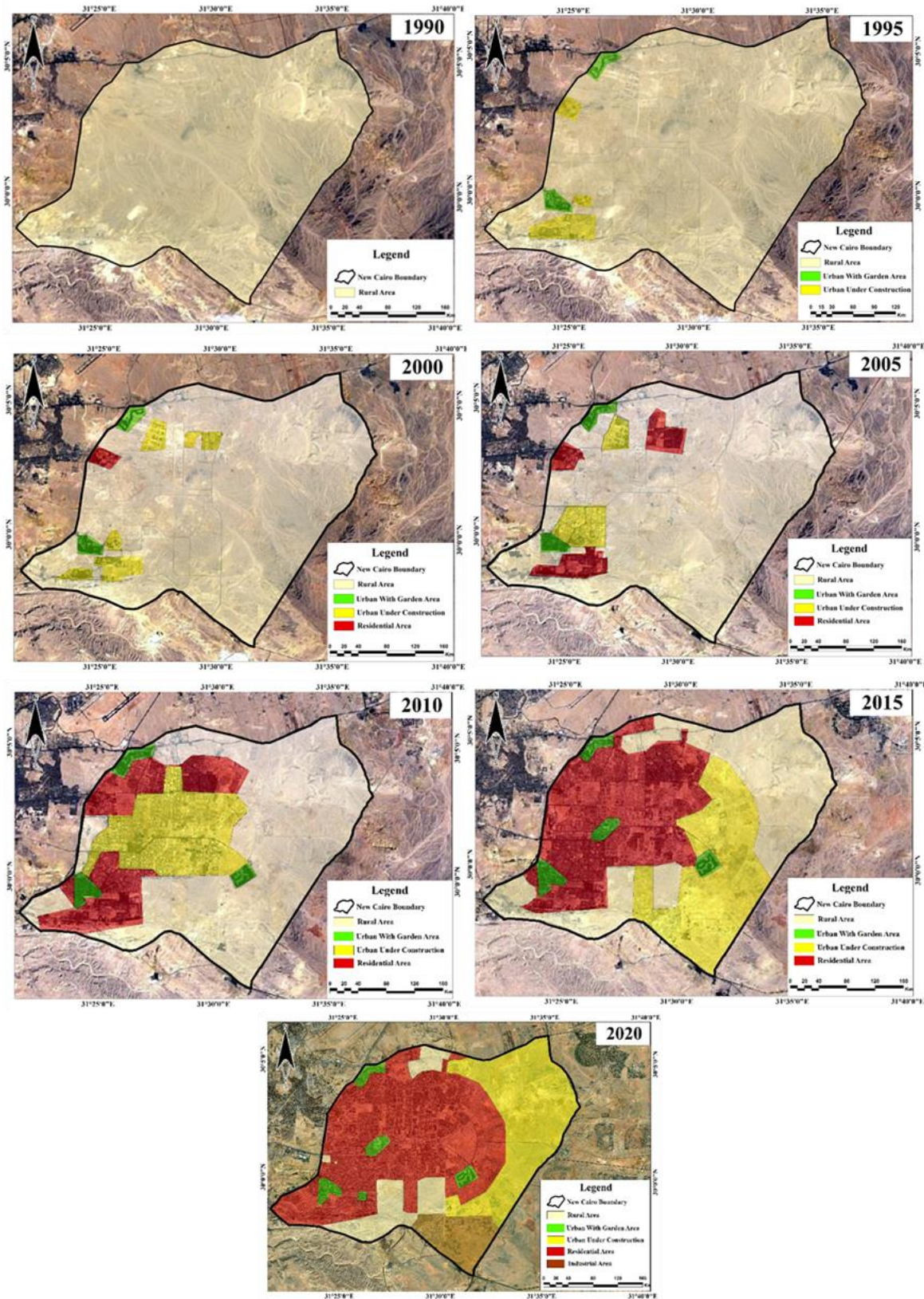


Figure 4.12: Urbanization stages from the year 1990 to 2020 showing rural area (beige), green areas (green), urban areas (red) and urban under construction (yellow)

Table 4.9: Urbanization Growth Rate with time from 1990 to 2020, showing area covered by each category and total percentage of urbanized areas vs. rural areas in each year

Year	Land use Distribution (km <sup>2</sup> )				Result	
	Rural	Urban			Rural	Urban
		Garden	Under Construction	Fully Urbanized		
1990	246.19	0.00	0.00	0.00	100%	0%
1995	235.90	7.70	2.60	0.00	96%	4%
2000	224.13	7.50	11.70	2.86	91%	9%
2005	211.97	8.45	12.43	13.34	86%	14%
2010	145.58	8.45	49.29	42.88	59%	41%
2015	85.57	9.98	47.50	103.14	35%	65%
2020	23.28	16.39	98.57	107.95	9%	91%

#### 4.3.2. Results of Rainfall-Runoff Model

The rainfall runoff model results in the runoff quantities correspond to each urbanization stage, which enables to understand the actual effect of the increase in urban areas on runoff quantities. The first output of the model is the identification of the watersheds affecting New Cairo; according to the topographical maps and the digital elevation models there are seven watersheds affecting New Cairo, their names and characteristics are shown in Figure 4.13. The second output is the peak discharge (m<sup>3</sup>/s), time to the peak (min) and the runoff volume (m<sup>3</sup>) calculated for each basin for all return periods and at different urbanization levels. The simulation was initiated for eight urbanization percentages from 0% to 100%; each urbanization stage has six values of runoff corresponds to different return periods of 2, 5, 10, 20, 50 and 100.



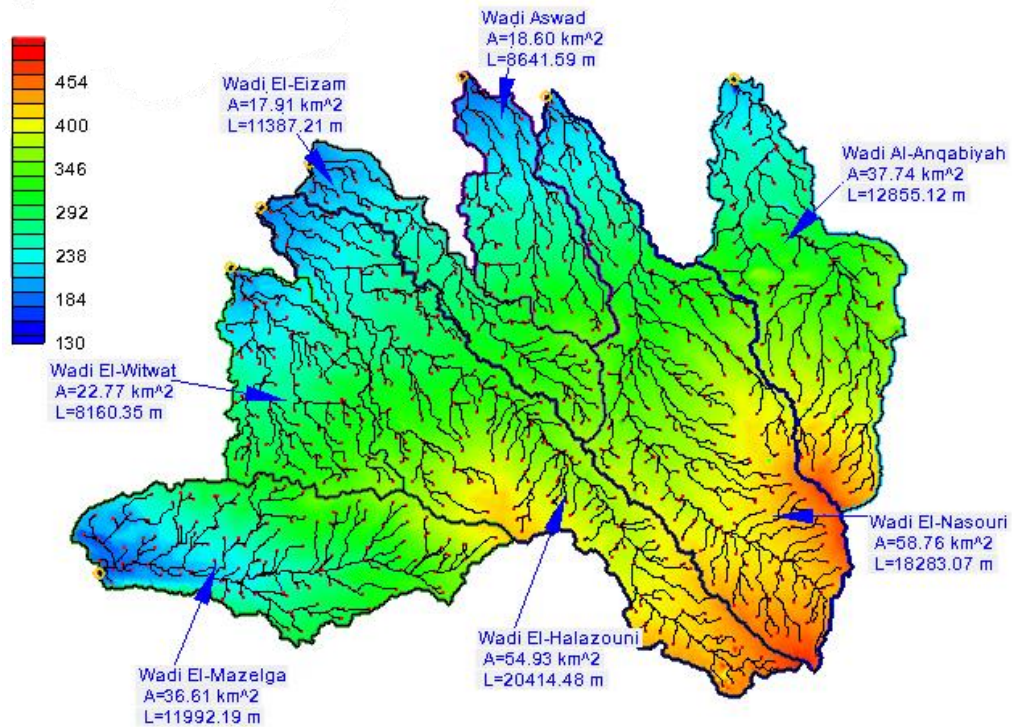


Figure 4.13: Digital Elevation Model Map showing Names and shapes of basins affecting New Cairo with their names, areas and lengths

The total New Cairo's runoff values for all return periods at different urbanization percentages are illustrated in Table 4.10 and summarized in Table 4.11. As demonstrated in the tables the runoff values are amplified with the increase of urbanization, in 30 years 91% of the total area of New Cairo was urbanized, which corresponded to a significant increase in surface runoff by 135%. For a 100% urbanization level in New Cairo the runoff increases by a 185%. Moreover, the increase in urban areas shortens the time the peak runoff flow takes to occur.

Table 4.10: Runoff Values for New Cairo at each year correspond to six return period storms

Year	Urbanization Stage	Runoff Value for Each Return Period (Mm <sup>3</sup> )					
		2	5	10	20	50	100
1990	0%	-	0.33	1.06	2.21	4.40	6.60
1995	4%	0.16 x 10 <sup>-3</sup>	0.35	1.09	2.27	4.48	6.70
2000	10%	529 x 10 <sup>-3</sup>	0.37	1.14	2.34	4.61	6.85
2005	15%	0.005	0.43	1.25	2.50	4.81	7.10

Year	Urbanization Stage	Runoff Value for Each Return Period (Mm <sup>3</sup> )					
		2	5	10	20	50	100
2010	40%	0.075	0.79	1.83	3.32	5.90	8.40
2015	65%	0.179	1.13	2.36	4.02	6.80	9.43
2020	90%	0.355	1.72	3.25	5.21	8.35	11.23
-	100%	0.636	2.37	4.16	6.33	9.86	12.74

Table 4.11: The change in runoff corresponding to the increase of urbanized area from 1990 to 2020 for the whole New Cairo Watershed

Year	Urban Area Change	Surface Runoff Change
1990	0	0%
1995	4%	2%
2000	6%	6%
2005	12%	13%
2010	37%	49%
2015	65%	81%
2020	91%	135%
-	100%	185%

Therefore, the urbanization has a direct impact on increasing surface runoff due to changing the natural land use to impervious surfaces that prevent the rainwater to seep into the ground. Moreover, as illustrated in Figure 4.12 due to the rapid urban expansion the planning is poor as the natural streams and flood plains were not preserved nor integrated within the design, which could have prevented the increasing volumes of runoff as they are natural management systems for flashfloods.

#### 4.4 Drainage Design Effect on Surface Runoff

The results of the drainage network revealed that each neighborhood has a pumping station as an outfall because it pumps the wastewater to a higher elevation destination. Figure 4.14 shows a schematic drainage network plan for all the districts, where it shows that the pumping network

starts at El-Mirage and El-Banafseg areas and the final destination is Imtidad El-Mostasmreen, on the other hand, Figure 4.15 shows the elevation map for the neighborhoods. It illustrates that Imtidad El-Mostasmreen has the highest elevation of about 400 m asl and El-Mirage and El-Banafseg has the lowest elevation of 200 m asl. The problem with the design is that the system is reversed. The drainage system should have drained wastewater from the highest neighborhood, which is Imtidad El-Mostasmreen to drain all the way to the lowest neighborhood, which is El-Mirag and then send the wastewater to the final treatment plant destination, which would have decreased the number of pump stations used.

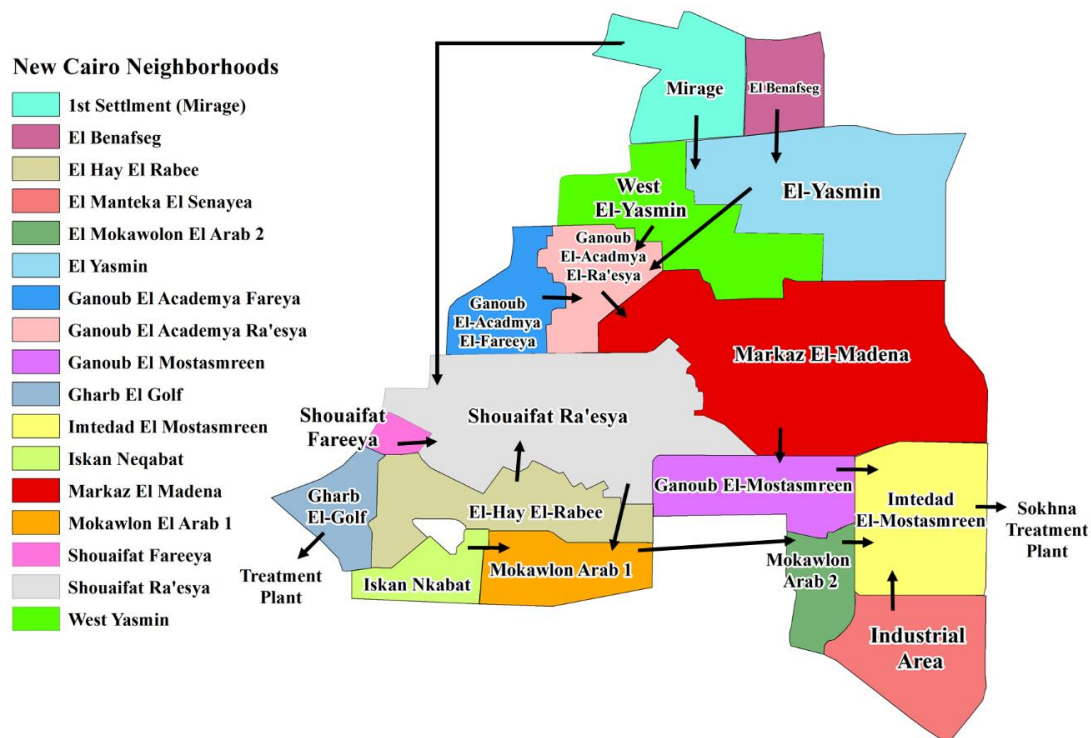


Figure 4.14: Pumping Stations Network Plan for New Cairo's Districts

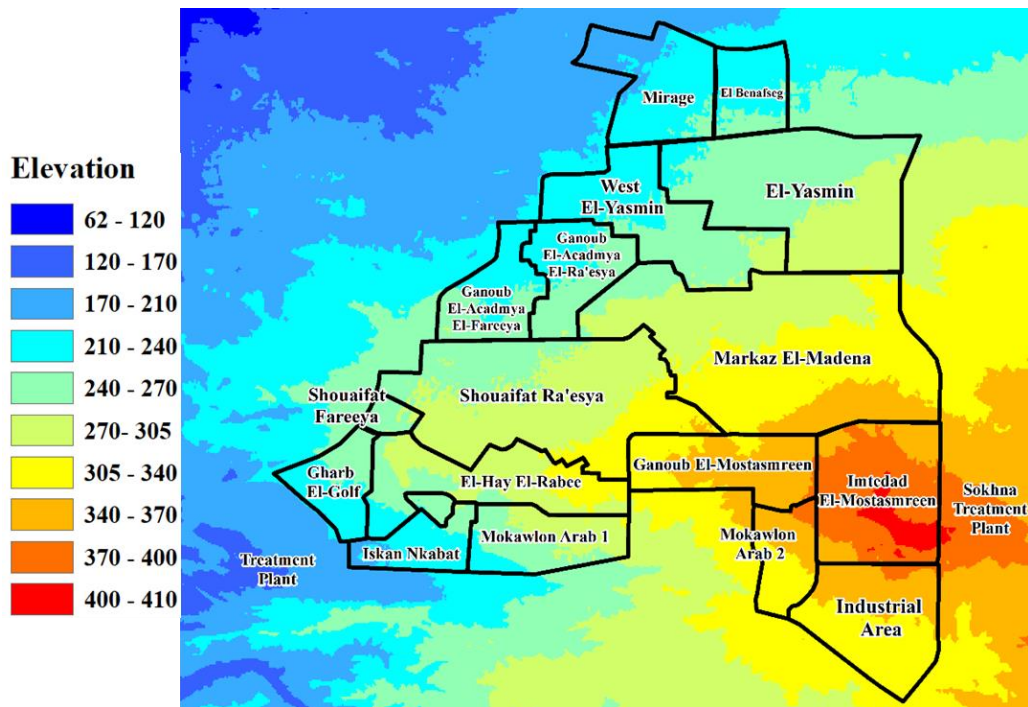


Figure 4.15: Elevation Map of New Cairo Neighborhoods

Therefore, with 200 m difference in elevation between the upstream and downstream, where the downstream at 400 asl and the upstream is at 200 asl, the drainage network is venerable to any power outage during the storms, where it leads to backing up water withing the neighborhoods that can cause flooding specially in districts with low elevations.

#### 4.4.1. Drainage Network Evaluation using Load-Capacity Balance

As mentioned in the methodology the evaluation is conducted over three scenarios, the base scenario without rainfall and the evaluation during rainfall storms corresponds to six return periods and maximum storm occurred in March 2020, which may correspond to 100-year return period. The drainage network evaluation is based on assessing its capacity for the base scenario by discharging wastewater only.

In order to calculate the runoff quantities in each district, the land use is identified by using satellite images acquired from USGS (USGS, 2021). The land use for the seventeen districts is

shown in Figure 4.16. Consequently, the total rainfall volumes were calculated using the rational method.

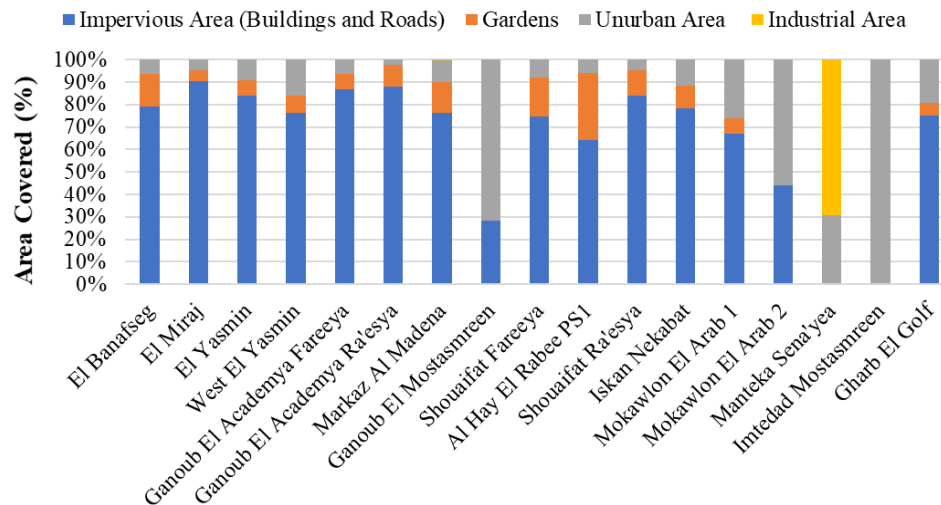


Figure 4.16: Land use percentages of 17 Neighborhoods in New Cairo for four main categories (Impervious Areas, Gardens, unurbanized areas and industrial areas). Map was obtained from (USGS, 2021)

The results of the analysis are shown in Appendix D and summarized in Table 4.12. According to the runoff calculations and pipelines' capacities, seven neighborhoods may not be able to afford the minimum rainfall event that correspond to 2-years storm; therefore, they are in a critical condition and need an urgent upgrade. Moreover, eight neighborhoods cannot afford 5-year storm beside the wastewater discharges they normally manage. Generally, the stress on the sewer network increase with the increase of rainfall intensity according to the return period. On the other hand, eight neighborhoods out of seventeen can accommodate for 5-years storm, six neighborhoods accommodate for 10-years storm and five accommodate for 20-years storm. Finally, two districts were able to accommodate the maximum climate change projected storm, which are Imtedad Mostasmreen and Ganoub El Mostasmreen, assuming that the wastewater flows remain the same.

Table 4.12: Percentage used of the Drainage Network at Different Scenarios

Color Coding of Percent filled of the total Drainage Network

< 90%	90.1% to 99.1%	100% <
-------	----------------	--------

District Name	No Rain	2	5	10	20	50	100	Max CC Storm	No. of inundated areas
El Banafseg	55%	78%	97%	114%	132%	160%	183%	253%	6
El Miraj	56%	87%	114%	137%	163%	201%	234%	331%	4
El Yasmin	80%	137%	188%	230%	278%	348%	409%	590%	27
West El Yasmin	39%	159%	265%	354%	454%	602%	731%	1108%	23
Ganoub El Academya Fareeya	53%	118%	175%	223%	277%	356%	426%	629%	17
Ganoub El Academya Ra'esya*	80%	92%	56%	60%	66%	73%	80%	100%	18
Markaz Al Madena*	66%	95%	97%	114%	133%	162%	187%	260%	40
Ganoub El Mostasmreen*	85%	91%	96%	99%	53%	56%	59%	68%	0
Shouaifat Fareeya	46%	111%	168%	216%	269%	348%	417%	620%	5
Al Hay El Rabee PS1	77%	198%	304%	394%	494%	643%	772%	1152%	27
Shouaifat Ra'esya	56%	125%	186%	238%	295%	381%	455%	673%	122
Iskan Nekabat	24%	40%	54%	65%	78%	98%	114%	163%	14
Mokawlon El Arab 1	69%	79%	87%	93%	101%	112%	122%	150%	4
Mokawlon El Arab 2	66%	70%	75%	78%	82%	88%	93%	108%	0
Manteka Sena'yea	43%	83%	118%	147%	181%	230%	272%	398%	2
Imtedad Mostasmreen	49%	51%	53%	55%	57%	60%	63%	70%	0
Gharb El-Golf	42%	131%	209%	275%	349%	458%	552%	831%	5

\*These areas had planned upgrade for the drainage system, the extra capacity was starting storm with 5-year return period.

#### **4.4.2. Pump Stations Evaluation using Load-Capacity Balance**

The pump stations were separated from the drainage network, as most of the pump stations collect sewage from the local district in addition to sewage from other pump stations as well. The evaluation scenarios are the same as the drainage network assessment.

The detailed results are shown in Appendix D and summarized in Table 4.13. The pump stations are in a critical condition. Four stations cannot handle the wastewater discharge in the base scenario. During the minimum rainfall of 2-years return period, six pump stations cannot drain the combined sewer, which can cause flooding and water shortages. Furthermore, one pump station can afford up to 10-years storm and three were able to accommodate more than 20 years storm. Finally, none of the districts were able to accommodate the maximum climate change projected storm. A summary for the evaluation of both the pipelines and pump stations for the seventeen districts of New Cairo is provided in Table 4.14, which contains conclusions regarding the performance of the drainage system for each district.

On Friday 3<sup>rd</sup> of September 2021, local newspapers reported on wastewater flooding occurrence at Ganoub El-Academya El-Fareeya pump station. According to Amin Ghoneim the head of New Cairo City Authority, this area suffered from frequent water outages and flooding due to the underperformance of this pump station especially with every rainfall event (Saleh, 2021). This is a validation for the evaluation done in this research, as it concluded that the pump station of Ganoub El-Academya El-Fareeya should be urgently upgraded as well as the drainage network of this area because they cannot afford 2-years storm and with the increase of population the situation will become more critical.



Table 4.13: Percentage Used of the Pump Stations with different scenarios

Color Coding of Percent filled of the total Drainage Network

&lt; 90%

90.1% to 99.1%

100% &lt;

District Name	No Rain	2	5	10	20	50	100	Max CC Storm
El Banafseg	28%	37%	46%	54%	62%	75%	87%	125%
El Miraj	35%	51%	67%	81%	96%	119%	139%	206%
El Yasmin	68%	103%	138%	167%	199%	249%	293%	437%
West El Yasmin	39%	136%	236%	318%	411%	552%	676%	1086%
Ganoub El Academya Fareeya	53%	106%	160%	205%	255%	332%	400%	623%
Ganoub El Academya Ra'esya*	98%	140%	183%	219%	258%	319%	373%	550%
Markaz Al Madena*	98%	137%	178%	211%	248%	305%	355%	520%
Ganoub El Mostasmreen*	107%	139%	173%	200%	231%	277%	319%	455%
Shouaifat Fareeya	35%	74%	114%	147%	184%	241%	291%	456%
Al Hay El Rabee PS1	27%	60%	95%	123%	155%	203%	246%	387%
Shouaifat Ra'esya	37%	78%	119%	153%	191%	250%	301%	471%
Iskan Nekabat	21%	32%	43%	53%	63%	79%	93%	140%
Mokawlon El Arab 1*	51%	74%	98%	118%	140%	174%	203%	302%
Mokawlon El Arab 2*	68%	90%	112%	131%	151%	183%	210%	301%
Manteka Sena'yea	43%	72%	102%	127%	155%	198%	236%	360%
Imtedad Mostasmreen*	135%	170%	207%	237%	271%	322%	367%	517%
Gharb El-Golf	5%	15%	24%	32%	41%	54%	66%	105%

\*These areas had planned upgrade for the pump stations, the extra capacity was added in the calculations



Table 4.14: Evaluation Summary for Drainage Network and Pump stations for seventeen Neighborhoods in New Cairo

Name	Drainage Network	Pumping Station	Conclusion
<b>El Banafseg</b>	Up to 5-Years Storm	More than 10 Year Storm	For current loads the drainage network is effective up to 5-years storm, and the pump station is sufficient
<b>El Miraj</b>	Up to 2-Years Storm	More than 10 Year Storm	The Pump station is sufficient but the drainage network can't afford more than 2-years storm and needs upgrade
<b>El Yasmin</b>	Cannot afford 2-years Storm	Cannot afford 2-years Storm	Both the drainage system and the pump station need urgent upgrade as they can't afford 2-years storm
<b>West El Yasmin</b>	Cannot afford 2-years Storm	Cannot afford 2-years Storm	The drainage system need and the pump station need an urgent upgrade as they can't afford 2-year storm
<b>Ganoub El Academya Fareeya</b>	Cannot afford 2-years Storm	Cannot afford 2-years Storm	The drainage system need and the pump station need an urgent upgrade as they can't afford 2-year storm
<b>Ganoub El Academya Ra'esya</b>	More than 10-Year Storm	<b>Not sufficient for the base scenario</b>	The Pump Station Need Urgent Upgrade
<b>Markaz Al Madena</b>	Up to 5-Years Storm	Cannot afford 2-years Storm	The Pump Station Need Urgent Upgrade
<b>Ganoub El Mostasmreen</b>	More than 10-Year Storm	<b>Not sufficient for the base scenario</b>	The Pump Station Need Urgent Upgrade
<b>Shouaifat Fareeya</b>	Cannot afford 2-years Storm	Up to 2-Years Storm	The drainage network needs urgent upgrade and the pump station will need aid for storm more than 2-year
<b>Al Hay El Rabee PS1</b>	Cannot afford 2-years Storm	Up to 5-Years Storm	The drainage network needs urgent upgrade and the pump station will need aid for storm more than 5-year

Name	Drainage Network	Pumping Station	Conclusion
<b>Shouaifat Ra'esya</b>	Cannot afford 2-years Storm	Up to 2-Years Storm	The drainage network needs urgent upgrade and the pump station will need aid for storm more than 2-year
<b>Iskan Nekabat</b>	More than 10-Year Storm	More than 10-Year Storm	No upgrade needed
<b>Mokawlon El Arab 1</b>	More than 10-Year Storm	Up to 5-Years Storm	Pump station needs aid for storms more than 5 years
<b>Mokawlon El Arab 2</b>	More than 10-Year Storm	Up to 2-years storm	Pump station needs aid for storms more than 2-years
<b>Manteka Sena'yea</b>	Up to 2 years storm	Up to 2-years storm	The drainage network and the pump station can't afford storm more than 2-years
<b>Imtedad Mostasmreen</b>	More than 10-Year Storm	<b>Not sufficient for the base scenario</b>	The pump station needs urgent upgrade
<b>Gharb El Golf</b>	Cannot afford 2-years Storm	More than 10-Year Storm	The drainage network needs urgent upgrade

#### **4.4.3. Validation of the General Evaluation using SewerGEMS**

The evaluation of the drainage network is conducted on Al Academya El-Fareeya, as it is one of the critical neighborhoods. The model is performed as a transient analysis, where the storm is entered as a hyetograph (Figure 4.7) and the wastewater discharge is also distributed according to the ECP's consumption pattern (ECP, 1998).

SewerGEMS (Bentley, 2021) was used to evaluate the drainage network and pump station. The model was imported and edited according to the as built pipelines drawings for the area and the wastewater loads were distributed equally over the manholes. The system consists of 912 manholes, 912 pipes and a pump that provides a maximum pumping rate of 220 l/s to simulate the actual pump station. Sewer network layout and the pipes' diameters are shown in Figure 4.17.

For the three main tested scenarios, three sections in the drainage network are checked in terms of water levels inside the pipelines, the sections are shown in Figure 4.18. Section 1 represent the pump station section; section 2 represents the east side collection pipe and finally section 3 represents the southern collection pipe that collects from the rest of the neighborhood.

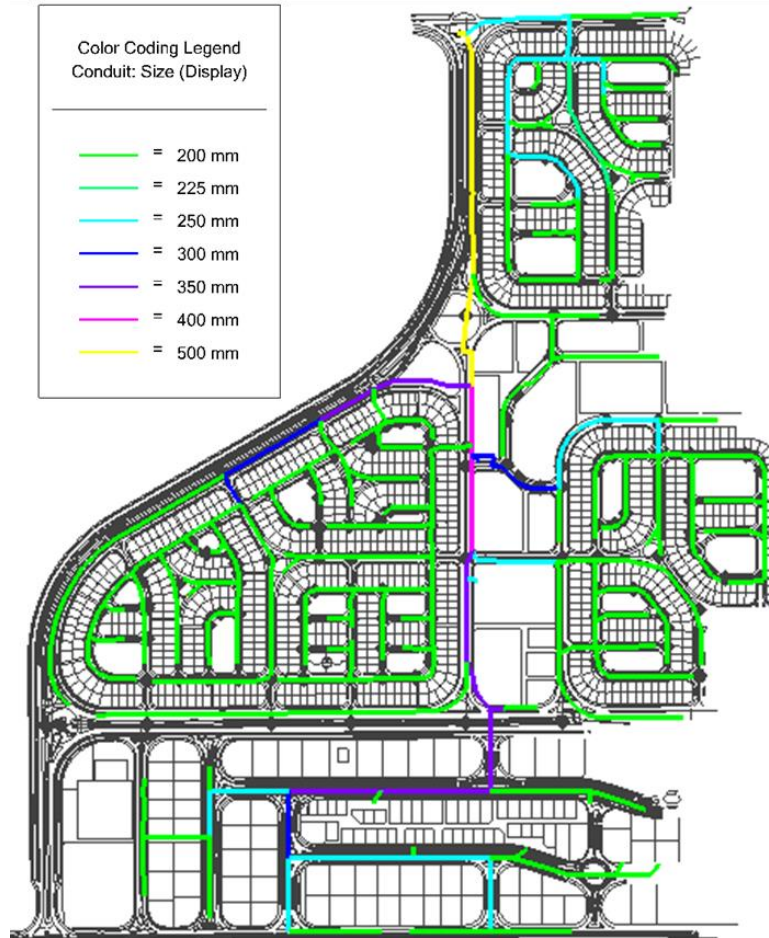


Figure 4.17: Al Academy El-Fareeya Pipes Layout and Diameters

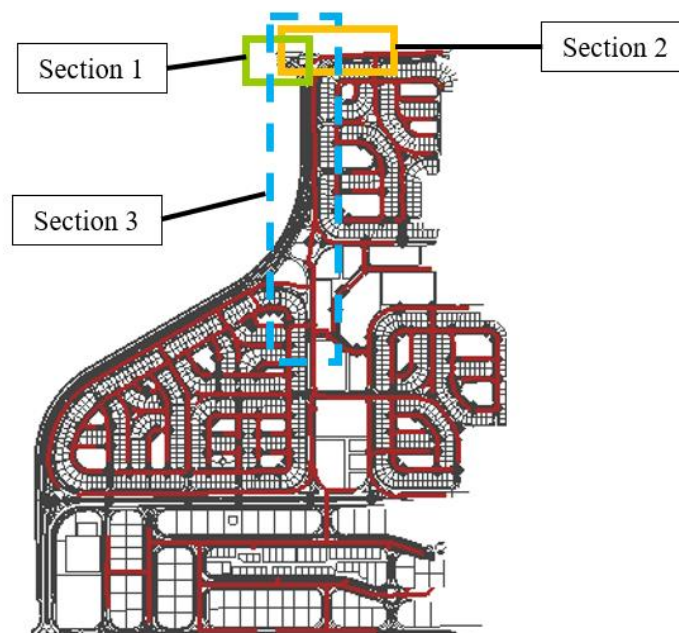


Figure 4.18: Sections that will be assessed for water levels during the simulation

The base scenario simulation is done with only wastewater drainage, the results showed that the drainage network is sufficient for its wastewater discharges, however the velocity in some parts has unacceptable ranges. The velocities ranges between 0.3 m/s to 4.3 m/s at the peak discharge, which is not preferred as the velocity in the gravity conduits as it should be within 0.6 m/s to 1.5 m/s (ECP , 2010) to avoid settlement with low velocities and scouring with the high velocities. Moreover, the pressure pipes that deliver the wastewater to and from the pumping station have a velocity of 2.13 m/s, while it should be in the range of 1 to 1.5 (ECP , 2010). A video for the drainage performance in the three sections are shown in this [link \(https://rb.gy/iypucq\)](https://rb.gy/iypucq), showing the change in water level in the system during the day.

For the 2-years return period simulation, where it discharges both wastewater and rainfall. The results showed that the drainage network is not sufficient, where it has an overflow of 3,919 m<sup>3</sup>/d. The velocities of the gravity conduits range between 0.07 m/s to 4.76 m/s, which is considered an unacceptable range. Moreover, the pressure pipes that deliver the wastewater to and from the pumping station have a velocity of 2.28 m/s, which is also unacceptable. Some of the pipelines were full and flooding during the 2-years return period, which are shown in Figure 4.19. The full daily simulation for the three sections is illustrated in this [link \(https://rb.gy/3uhft4\)](https://rb.gy/3uhft4), showing water completely filling some of the pipelines and manholes, although the pump was working with its maximum pumping rate as shown in Figure 4.20.

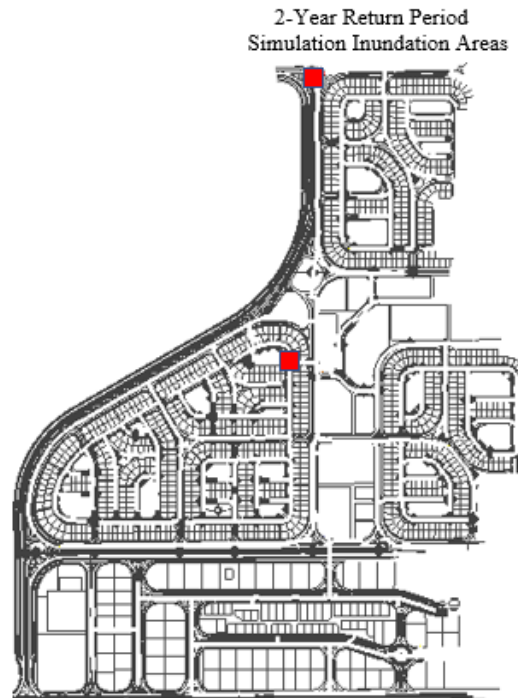


Figure 4.19: 2-Year Return Period Inundation Areas

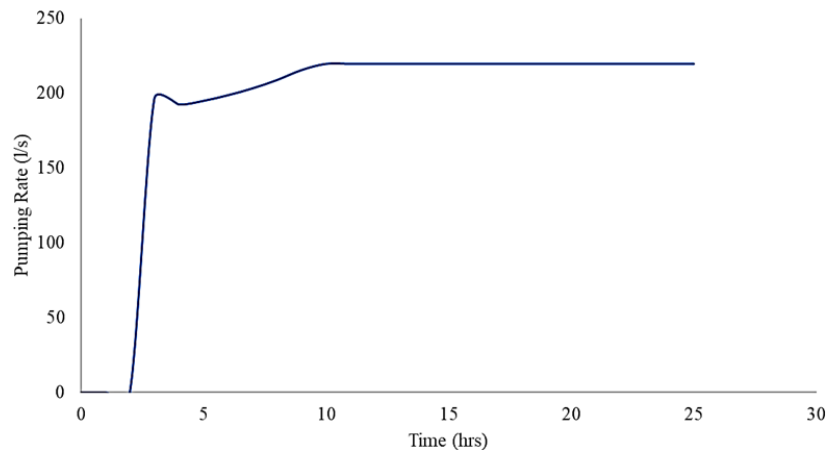


Figure 4.20: 2-year Return Period Rainfall Pumping Operation within 24 Hours

The March 2020 simulation, which discharges both wastewater and rainfall, resulted in a complete failure for the drainage system. The results showed that the drainage network had an overflow of 17,772 m<sup>3</sup>/d, in addition, 30% of the total pipelines were completely full, which caused flooding in the streets and can cause backflow in the households as well. The velocity ranged between 0.01 m/s and the maximum was 6.53 m/s, which is extremely dangerous and can cause breakage in the network; the small velocity shows a stagnation in the pipes, which indicates

that the water is piling up into the system. The Simulated flooded areas show an almost perfect agreement with the flood-prone areas that was recorded by the local authorities Figure 4.21. The full daily simulation for the three sections is illustrated in this [link \(https://rb.gy/iypucq\)](https://rb.gy/iypucq), showing water completely filling pipelines and the water levels reached street levels although the pump was working with its maximum rate from the early hours of the storm. Finally, Table 4.15 shows results' summary of the three scenarios simulated in SewerGEMS.

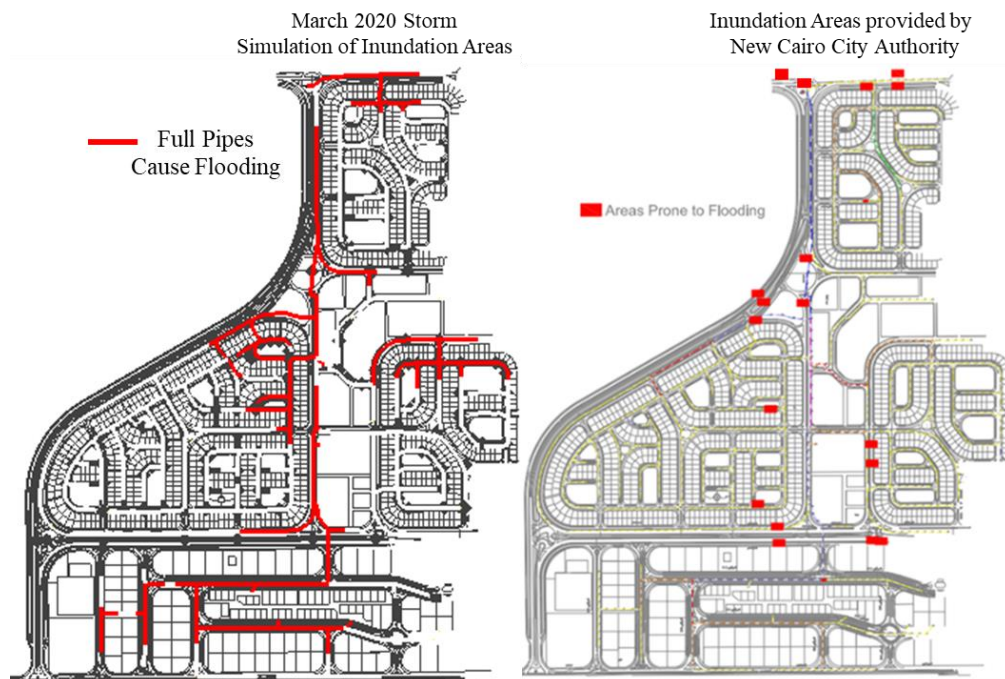


Figure 4.21: Validation of Inundation areas caused by March 2020 Storm against Actual Inundation Areas from site

Table 4.15: Summary of the SewerGEMS Simulation Results

Scenario Name	Velocities (m/s)		Velocities (m/s) Pressure Pump St. Pipes	Is the design Adequate for the load?	System Overflow (m <sup>3</sup> /d)
	Gravity Pipes Min.	Gravity Pipes Max.			
Base Scenario	0.3	4.3	2.13	Yes	-
2-Year Return Period	0.07	4.76	2.28	No	3,919
March 2020 Storm	0.01	6.53	2.28	No	17,772

## 4.5 Discussion

This study contributes to a better understand of the factors affecting urban floods in New Cairo by comparing the effects of rapid urbanization and climate change on increasing surface runoff, while considering the role of drainage design in increasing or mitigating surface flood volumes.

Estimating the runoff values in New Cairo, is a principal factor in the evaluation, which require an accurate information regarding the storm's duration and distribution. However, the available ground observed rainfall data for New Cairo is measured from the nearest ground station that is located about 30 km away and with a temporal resolution of total daily value. This temporal resolution does not represent the distribution of the previously occurred storms, which require at least an hourly observation rainfall data.

Therefore, the research starts by compensating the shortfalls in the ground measured rainfall data through comparing six gridded rainfall products (GPCC, GPCP, TRMM, GPM, PERSIANN and CHIRPS) against observed rainfall from Cairo Station to verify closest product that can represent the rainfall occurred over the study area. The analysis included graphical and statistical comparisons, followed by bias correction for the rainfall product's data and was finalized by validating the assessment through applying the final product in a hydrological model setup to evaluate its performance. The evaluation concluded that GPM, which provide half hourly rainfall data, effectively represents ground measured rainfall data at Cairo station with a small acceptable percentage of underestimation based on monthly rainfall data.

A detailed assessment of urbanization was conducted through monitoring the changes of the spatial urban sprawl, which affected the land use and the ability of the soil to infiltrate rainwater.



The assessment was performed by employing GIS spatial datasets along with Rainfall – Runoff models to study the effect of urbanization on the increase of runoff under different time periods. Seven land use maps from different years (1990, 1995, 2000, 2005, 2010, 2015 and 2020), eight simulated conditions (0%, 10%, 15%, 40%, 65%, 90% and 100% urbanized area percentages) and actual storm distribution driven from GPM were input into the hydrological models, to generate both flash flood hydrographs and runoff values. The urbanization has a direct impact on increasing surface runoff due to changing the natural land use to impervious surfaces that prevent the rainwater to seep into the ground. Moreover, due to poor planning the natural streams and flood plains were not preserved nor integrated within the design, which could have prevented the increasing volumes of runoff as they are natural management systems for flashfloods.

The investigation of whether the current intensities of major storm events occurred in New Cairo is connected to climate change or are mere recurrence of the normal historical trends, was judged by comparing climate change scenarios against ground measured rainfall data. The investigation was based on six bias corrected CC scenarios anticipated from three GCMs (EC-Earth, CNRM and GFDL) under two representative concentration pathways 4.5 and 8.5. The evaluation results showed that the ground observed rainfall data are in a good agreement with CNRM 4.5 scenario. It was the only scenario, within the six scenarios that projected an extreme rainfall event in March 2020. The yearly observed precipitation of New Cairo showed that the extreme rainfall events are becoming more frequent and their intensities is increasing with time, although the total annual precipitation values have a decreasing trend; this agrees with climate change studies reported by the (IPCC) (S. I., et al., 2012). The ground observed rainfall data showed that the threshold of return period intensities increased by only 6% for the 2-year return period and increased by 17% for the 100-year in the period between 2000 to 2020 compared to the

period of 1976 to 1999. Moreover, as a comparison between the two time periods, the 2-year and 5-year rainfall decreased by 30% while the 100-year event occurred soon after a 50-year rainfall event which was proven to have occurred due to climate change as it was projected by CNRM4.5 climate change scenario.

The performance of New Cairo's drainage system is evaluated through analyzing sewer network performance, to assess whether the previously occurred urban flashfloods were due to the effect of climatic changes and urbanization, or the drainage system contributed to the increase of flooded areas as well. The capacity of the drainage networks of seventeen neighborhoods in New Cairo were evaluated through calculating the ability of the sewer networks and pumping stations to accommodate for storms correspond to different return periods, in addition to the wastewater discharge they handle. Moreover, a 1D SewerGEMS urban drainage model was used to simulate three scenarios representing base scenario (discharging wastewater only), small rainfall event (2-year return period and simulating extreme rainfall event (Maximum daily storm in 2020). The simulated flooded areas were verified by flood-prone areas recorded by the local authorities. The drainage design of 70% of the total evaluated neighborhoods showed poor performance, as there are 9 drainage networks and 8 pump station can't afford a 2-years return period storm, in addition to 3 pump stations are not sufficient to discharge the base scenario; therefore, the urban flooding might occur in New Cairo, with the smallest rainfall event.

The results showed that the rapid urban development and changes in land use types, caused significant increase in surface runoff; over a period of 30 years the runoff due to urbanization increased by 140%, while the peak discharge increased by 88% and the time to peak discharge slightly decreased by 5%. Therefore, the increase in impervious surface has a direct impact on increasing surface flows, which stresses the drainage system. Furthermore, the urban drainage has

a distinguished role in increasing the surface runoff. However, upgrading the drainage network can be an effective solution for mitigation. The improvements might not only be applied by replacing pipelines, but it can be through thorough emergency management plans during the storm events.

In New Cairo, climate change effect only has led to an increase in total runoff volumes by 48% from 1990 to 2020 excluding land use effect, while rapid urban expansion led to an increase of 180% for the same period, which is almost three times higher effect than what is induced by the climatic changes. However, having an extreme rainfall event due to CC on an urbanized area magnified the runoff volumes.

As mentioned earlier the results can come with uncertainties, which can be due to the assumptions of land use and land cover runoff coefficients, the usage of simplified equations, data limitation and in some cases inadequate quality of the data. Furthermore, some uncertainties can be due to rainfall products, which come with a percent of uncertainty due to the random errors of their estimate techniques and verifying them as well as the climate change data with only one meteorological station. Finally, using only six ensembles of climate change scenarios might not be enough to study the impact of climate change.

The research indeed highlights the importance of the drainage design, although urbanization and climate change increased urban runoff volumes, however, the deficient performance of the drainage network with the smallest rainfall event increased the flood-prone areas as well as the vulnerability of residential areas to flooding.

# Chapter 5. Conclusion and Recommendation

## 5.1 Summary

Over the past 5 years, Egypt experienced rainfall events resulted in major damages in properties and infrastructures causing sudden standstill for many sectors. Several concerns were raised by public opinion and the scientific society regarding the forthcoming winter periods. Accordingly, accurate models are required to examine the drivers behind urban flash floods occurring in New Cairo to decrease its impacts on humans and society. The study compares the effects of rapid urbanization and climate change on increasing surface runoff, while considering the role of drainage design in raising the vulnerability of urban areas to flooding.

The runoff was analyzed using an actual storm distribution generated based on precipitation events captured by GPM every half an hour, after evaluating its accuracy, bias correct it and validate its hydrological applicability along with five rainfall products against ground observed rainfall data at Cairo Station.

The historical records of the ground observed data (2006 – 2020) were investigated through statistical analysis to confirm whether they follow a Climate Change scenario or are mere recurrence of the normal historical trends; The observed precipitation of New Cairo had a strong correlation with CNRM4.5 climate change scenario. The ground observed records agreed with the IPCC reports, where the extreme rainfall events are becoming more frequent and their intensities is increasing, although the total annual precipitation values have a decreasing trend. The ground observed rainfall data showed that the threshold of return period intensities increased by only 6% for the 2-year return period and increased by 17% for the 100-year in the period between 2000 to

2020 compared to the period of 1976 to 1999. Moreover, as a comparison between the two time periods, the 2-year and 5-year rainfall decreased by 30% while the 100-year event occurred soon after a 50-year rainfall event which was proven to have occurred due to climate change as it was projected by CNRM4.5 CC scenario.

Furthermore, through observing climate change rainfall projections up to 2050, an extreme rainfall event is expected to occur in 2048, larger than March 2020 storm, which is the extremist so far.

The effect of urbanization spread on the increase of urban runoff was conducted through monitoring the urban changes using land use maps acquired from different with eight simulation conditions for the urbanized areas to generate runoff values. It is found that the urbanization amplifies the runoff values through increasing the peak discharge and shortening the time that the peak discharge takes to occur during a rainfall event, which increases the severity of the storms.

The effectiveness of the drainage design for seventeen neighborhoods in New Cairo was studied to validate their accommodation for the normal drainage operation, followed by an evaluation for the performance of the drainage network during small rainfall events and during extreme storms. The results were validated using recorded flood-prone areas and system failures provided by the local authorities. It is found that 70% of the total evaluated neighborhoods in New Cairo showed a poor performance with small rainfall events, with some areas not sufficient to discharge the base scenario which compatible with the municipal authority reports.

Urbanization was found to induce more risk on increasing urban flooding than climate change due to using impervious covers which lead to direct effects on surface flows and induce

overloads on the drainage system. However, having an extreme rainfall event due to CC on an urbanized area magnified the runoff volumes.

This research is important for Egypt as well as developing regions in the world, which are anticipated to undergo rapid urbanization with large-scale land use changes. It shows that although rapid urban expansion increases the vulnerability to flashfloods, the well-designed infrastructure can be an effective mitigation measure when considering climate change projections and land use alterations.

## **5.2 Conclusion**

The findings revealed that, the rapid urbanization has a major effect in increasing surface runoff due to the poor planning, which did not consider the natural flood plains and through increasing the impervious surfaces which amplifies the runoff volumes and stress the drainage system. Moreover, the rainfall patterns recently occurred were influenced by the climate change effect as it increased the frequency of the extreme rainfall events by 17% between the period of 2000 to 2020 compared to the rainfall patterns before 1999. Finally, the urban drainage system plays a significant role in either contribute to the problem by amplify the flood volumes due to under design or aid in mitigation with adequate sizing and design measures. Due to the continuous urban growth with poor planning and impervious surfaces and inadequate drainage design, the vulnerable areas to flash floods are growing, and the severity of urban flooding is projected to increase if appropriate precautions are not adopted.

In order to cope with the increasing runoff volumes, an assessment for the current drainage system and future development plans are essential in the light of climate change. Although the expansion in urban development has the major and inevitable effect on the increase in urban flood

volumes, it could be quantified and alleviated through improved infrastructures, new design policies and adaptation plans. However, the climate change has long-term and unforeseen results, therefore, policy makers should have a better knowledge on the role of climate change and prioritize appropriate mitigation and adaptation strategies.

### 5.3 Suggested Solutions for the Current Situation

There is not only one solution to reduce urban flooding, however, an integrated approach should be followed.

- 1) Depending heavily on pump stations in New Cairo, is one of the main reasons for causing urban flooding, as power outages are more likely to occur during storms. Therefore, using solar power in pump stations could be an opportunity to use a sustainable energy source that will aid during power outages to drain the extra runoff volumes due to storms; moreover, to avoid the costly expenses that come with the pump stations operation.
- 2) Since all the 17 neighborhoods in New Cairo are draining to each other until reaching the final treatment plant destination, a good solution could be sending the combined sewage discharge for each neighborhood directly to the treatment plant separately; hence, if any pump station failed during storms, it won't affect the other neighborhoods as well.
- 3) The final destination, which is the Sokhna Treatment plant is more than 200 meter higher than the New Cairo area; therefore, an urgent need for small gravity channel as an emergency drainage at each district will aid during storm in case of electricity blackouts and will reduce surface runoff. Moreover, planning a new treatment plant with lower elevation than New Cairo would aid in the drainage of extra sewage loads and storm runoff. The emergency gravity channel can be as simple as a French drain on the side of the road where it uses perforated pipelines topped with gravel with different sizes to work as filter for the rainwater as shown in Figure 5.1. In addition, the road cross-section profile needs to be adjusted to drain rainwater effectively to the sides of the roads.



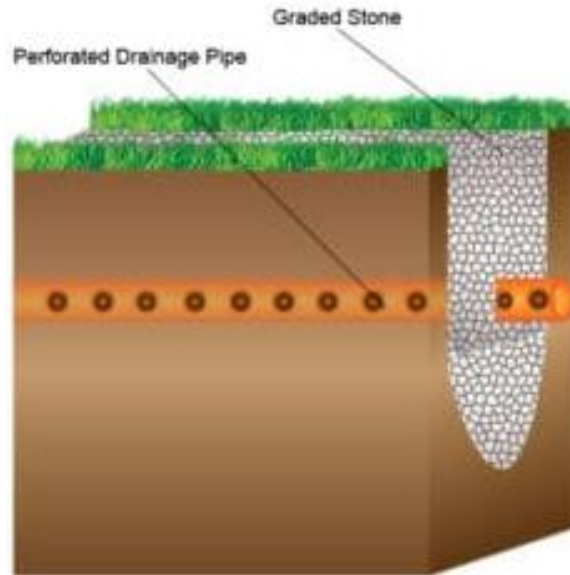


Figure 5.1: Example of simple French drainage to be used on the side of the main roads

- 4) Upgrading pump stations can compensate the upgrade of the whole pipelines system, therefore, a revision and improvement for the capacity of all pump stations is required urgently to accommodate for higher return period storms in addition to the wastewater discharges they handle normally. However, this upgrade will require increasing the capacity of pressurized pipelines that deliver water from pump stations to the treatment plants, as well as, upgrading the treatment plants as well to accommodate for the extra loads.
- 5) Plan for an emergency management strategy during storm events to reduce flood risks. One of the solutions that is followed during heavy rains, is to cutoff water and electricity to reduce wastewater loads and empty the pipeline system to drain only storm water runoff. This strategy reduced the number of neighborhoods having a difficulty in dealing with 2-year storm from 80% of New Cairo's 17 neighborhoods to 30%, assuming that the sewage loads were reduced to 10%. Table 5.1 shows a summary of the effect of the aforementioned solution on 17 neighborhoods in New Cairo.

Table 5.1: Effect of Reducing Wastewater Discharge to only 10% during Storm events on the Capacity of the Drainage System to Accommodate for Storms with Various Return Periods

Name	Drainage Network	Pumping Station
El Banafseg	More than 20 Year Storm	Accommodate All storms
El Miraj	More than 20 Year Storm	More than 20 Year Storm
El Yasmin	Up to 5 Years Storm	Up to 10 Year Storm
West El Yasmin	Can't Afford 2 years Storm	Can't Afford 2 years Storm
Ganoub El Academya Fareeya	Up to 2 years storm	Up to 2 years storm
Ganoub El Academya Ra'esya	Accommodate All storms	Up to 5 Years Storm
Markaz Al Madena	More than 20 Year Storm	Up to 5 Years Storm
Ganoub El Mostasmreen	Accommodate All storms	Up to 10 Year Storm
Shouaifat Fareeya	Up to 2 years storm	Up to 5 Years Storm
Al Hay El Rabee PS1	Can't Afford 2 years Storm	Up to 10 Year Storm
Shouaifat Ra'esya	Up to 2 years storm	Up to 5 Years Storm
Iskan Nekabat	Accommodate All storms	Accommodate All storms
Mokawlon El Arab 1	Accommodate All storms	More than 20 Year Storm
Mokawlon El Arab 2	Accommodate All storms	More than 20 Year Storm
Manteka Sena'yea	More than 10 Year Storm	More than 10 Year Storm
Imtedad Mostasmreen	Accommodate All storms	Up to 5 Years Storm
Gharb El Golf	Up to 2 years storm	Accommodate All storms

- 6) Plan for emergency locations to collect rainwater withing the urban areas like parking lots or excavate in open areas to create ponds that can collect and store rainwater.

## 5.4 Recommendation

The research offers the following recommendations to be further studied.

- 1) Start using a permeable soil whenever available in urban areas instead of the impermeable asphalt, as using interlocking pavers for side roads and for the main roads using Spong asphalt that is absorbent to water that can prevent flooding in urban areas. It is found that increasing the soil permeability can reduce floods in extreme events by 70%.
- 2) Climate change is unavoidable; therefore, policy makers should include its projections during planning new urban areas and within the drainage design capacities.

- 3) Establish consultative board in each governorate responsible for the assessment of rainfall patterns, improving the distribution and number of rain gauges and provide Intensity Duration Frequency (IDF) curves and equations that represent different climate conditions of Egypt for example Eastern Desert Region, Red Sea, Sinai Peninsula, Delta Region and the Mediterranean Region.
- 4) Stating new laws to mandate conducting hydrological studies as part of approvals before planning new urban developments, to preserve natural streamlines that drains storms' runoff and incorporate them in the design phase.
- 5) Add to the Egyptian Code of Practice the minimum return period that the drainage system should be designed on instead of leaving it to the project owner's judgment.
- 6) Conduct more elaborative studies and research on how to extract an actual storm distribution from satellite rainfall products designed for Egypt.
- 7) Evaluate the exact climate change effect on extreme rainfall events in Egypt, in order to give the policy makers a study with high confidence level on how the precipitation patterns in Egypt will change.

## Chapter 6. References

- Abdelmoneim, H., Soliman, M., & Moghazy, H. (2020). Evaluation of TRMM 3B42V7 and CHIRPS Satellite Precipitation Products as an Input for Hydrological Model over Eastern Nile Basin. *Earth Systems and Environment*, 4, 685–698.
- Abedin, S., & Stephen, H. (2019). GIS Framework for Spatiotemporal Mapping of Urban Flooding. *Geosciences*, 9(2), 77.
- Amin, D. (2014). Improvement of Precipitation Estimation Techniques over the Nile Basin. *PhD thesis*. Egypt: Faculty of Engineering, Ain-Shams University.
- AMS. (2013). *Glossary of Meteorology: Regional Climate Model*. Retrieved from American Meteorological Society (AMS): [https://glossary.ametsoc.org/wiki/Regional\\_climate\\_model](https://glossary.ametsoc.org/wiki/Regional_climate_model)
- Aquaveo. (2021). *WMS - The All-in-one Watershed Solution*. Retrieved from AQUAVEO: <https://www.aquaveo.com/software/wms-watershed-modeling-system-introduction>
- Arnone, E., Pumo, D., Francipane, A., La Loggia, G., & Noto, L. (2018). The Role of Urban growth, Climate Change, and their Interplay in Altering Runoff Extremes. *Hydrological Processes*, 32(12), 1755-1770.
- ASFPM. (2020). *Urban Flood Hazards: Challenges and Opportunities*. Association of State Floodplain Managers.

- Awadallah, A., Magdy, M., Helmy, E., & Rashed, E. (2017). Assessment of Rainfall Intensity Equations Enlisted in the Egyptian Code for Designing Potable Water and Sewage Networks. *Advances in Meteorology*.
- Bentley. (2021). *OpenFlows SewerGEMS*. Retrieved from Bentley: <https://www.bentley.com/en/products/product-line/hydraulics-and-hydrology-software/sewergems>
- Bertini, C., Buonora, L., Ridolfi, E., Russo, F., & Napolitano, F. (2020). On the Use of Satellite Rainfall Data to Design a Dam. *Water*.
- Boroujerdy, P., Naeini, M. R., Asanjan, A., Chavoshian, A., Hsu, K., & Sorooshian, S. (2020). Bias Correction of Satellite-Based Precipitation Estimations Using Quantile Mapping Approach in Different Climate Regions of Iran. *Remote Sensing*, 12.
- Bournas , A., & Baltas, E. (2021). Comparative Analysis of Rain Gauge and Radar Precipitation Estimates towards Rainfall-Runoff Modelling in a Peri-Urban Basin in Attica, Greece. *Hydrology*, 8(1), 29.
- Caradot, N., Granger, D., Chapgier, J., Cherqui, F., & Chocat, B. (2011). Urban flood risk assessment using sewer flooding databases. *Water Science & Technology*, 64(4), 832-840.
- Chow, V., Maidment, D., & Mays, L. (1988). *Applied Hydrology* (Vol. 4). (B. Clark, & J. Morris, Eds.) Singapore: McGraw-Hill.
- Dawson, R., Speight, L., Hall, J., Djordjevic, S., Savic, D., & Leandro, J. (2008). Attribution of flood risk in urban areas. *Journal of Hydroinformatics*, 10(4), 275–288.

- Dembélé, M., & Zwart, S. J. (2016). Evaluation and comparison of satellite-based rainfall products in Burkina Faso, West Africa. *International Journal of Remote Sensing*, 1366-5901.
- Douglas, I., Alam, K., Maghenda, M., McDonnell, Y., Mclean, L., & Campbell, J. (2008). Unjust waters: climate change, flooding and the urban poor in Africa. *Environment and Urbanization*, 20(1), 187-205.
- Ebert, E. (2007). Methods for Verifying Satellite Precipitation Estimates. In V. Levizzani, P. Bauer, & F. Joseph Turk, *Measuring Precipitation from Space: EURAINSAT and the Future* (pp. 345-356). Netherlands: Springer.
- ECP. (2010). *Egyptian Code of Practice (102) for Designing Basis of Water and Waste Water Drainage Networks*. Egypt: Ministry of Housing, Utility and Urban Communities.
- ECP. (1998). *Egyptian Code of Practice (102) for Designing Basis of Water and Waste Water Drainage Networks*. Cairo: Ministry of Housing, Utilities and Urban Communities.
- Egypt's Cabinet Information and Decision Support Centre. (2011). *Egypt's National Strategy for Adaptation to Climate Change and Disaster Risk Reduction*. Cairo: Egypt's National Strategy.
- ElGanzori, A. (2012). *Towards a Climate Change Adaptation Strategy for the Water Sector in Egypt*. Cairo: UNESCO.
- EMA. (2021). Egyptian Meteorological Authority (EMA). Retrieved from <http://ema.gov.eg/wp/>
- ESRI. (2012). *ArcGIS*. Retrieved from Environmental Systems Research Institute (ESRI): <https://www.esri.com/en-us/arcgis/about-arcgis/overview>

- Farr, T. G., & Kobrick, M. (2000). Shuttle Radar Topography Mission produces a wealth of data. *Eos Trans. AGU*, 81, 583-583.
- Funk, C., Peterson, P., Lansfeld, M., Pedreros, D., Verdin, J., Shukla, S., . . . Michaelsen, J. (2015). The climate hazards infrared precipitation with stations—a new environmental record for monitoring extremes. *Sci Data*, 2.
- Galloway, G., Reilly, A., Ryoo, S., Riley, A., Haslam, M., Brody, S., . . . Parker, S. (2018). *The Growing Threat of Urban Flooding: A National Challenge*. University of Maryland, Center for Disaster Resilience, and Texas A&M University, Galveston Campus, Center for Texas Beaches and Shores. College Park: A. James Clark School of Engineering.
- Golmohammadi, G., Prasher, S., Madani, A., & Rudra, R. (2014). Evaluating Three Hydrological Distributed Watershed Models: MIKE-SHE, APEX, SWAT. *Hydrology*, 20-39. doi:10.3390/hydrology1010020
- Huang, Q., Wang, J., Li, M., Fei, M., & Dong, J. (2017). Modeling the influence of urbanization on urban pluvial flooding: a scenario-based case study in Shanghai, China. *Natural Hazards volume*, 87, 1035–1055.
- Huffman, G., & Pendergrass, A. (2021). *The Climate Data Guide: TRMM: Tropical Rainfall Measuring Mission*. (N. C. Staff, Editor) Retrieved from <https://climatedataguide.ucar.edu/climate-data/trmm-tropical-rainfall-measuring-mission>
- Huffman, G., Bolvin, D., Nelkin, E., & Adler, R. (2016). *TRMM (TMPA) Precipitation L3 1 day 0.25 degree x 0.25 degree V7*. (A. Savtchenko, Editor) Retrieved from Goddard Earth Sciences Data and Information Services Center (GES DISC): 10.5067/TRMM/TMPA/DAY/7

- Huffman, G., Bolvin, D., Nelkin, E., Wolff, D., Adler, R., Gu, G., . . . Stocker, E. (2007). The TRMM Multisatellite Precipitation Analysis (TMPA): Quasi-Global, Multiyear, Combined-Sensor Precipitation Estimates at Fine Scales. *Journal of Hydrometeorology*, 8(1), 38-55.
- Huong, H., & Pathirana, A. (2013). Urbanization and climate change impacts on future urban flooding in Can Tho city, Vietnam. *Hydrological Earth Systems Sciences*, 17(1), 379–394.
- IFRC. (2020). *Egypt: Flash Floods Emergency Plan of Action (EPoA) DREF Operation n° MDREG015*. Egypt: International Federation of Red Cross and Red Crescent Societies.
- IPCC. (2014). *Impacts, adaptation, and vulnerability. Contribution of Working Group II to the Fifth Assessment Report of the Intergovernmental Panel on Climate Change*. Cambridge: Cambridge University Press.
- Jamal, H. (2017). *How to Measure Rainfall / Precipitation*. Retrieved from About Civil.
- JAXA. (2021). *What's TRMM?* Retrieved from [https://www.eorc.jaxa.jp/TRMM/about/top\\_e.html](https://www.eorc.jaxa.jp/TRMM/about/top_e.html)
- Jung, M., Kim, H., Mallari, K., Pak, G., & Yoon, J. (2015). Analysis of Effects of Climate Change on Runoff in an Urban Drainage System: A Case Study from Seoul, Korea. *Water Sciences & Technology*, 71(5), 653–660.
- Kent, K., Woodward, D., Hoeft, C., Humpal, A., & Cerrelli, G. (2010). Chapter 15: Time of Concentration. In *Part 630 Hydrology - National Engineering Handbook*. United States Department of Agriculture.



- Kleidorfer, M., Mikovits, C., Tonnies, A., Huttenlau, M., Einfalt, T., & Rauch, W. (2014). Impact of a Changing Environment on Drainage System Performance. *Procedia Engineering*, 70, 943-950.
- Kleidorfer, M., Modrel, M., Sitzenfrei, R., Urich, C., & Rauch, W. (2009). A case independent approach on the impact of climate change effects on combined sewer system performance. *Water Sciences and Technology*, 60(6), 1555-64.
- Lakew, H. B., & Moges, S. A. (2021). Comparison of Spatial Interpolation Techniques of Rainfall for Hydrological Applications in a Complex Mountainous Region of the Upper Blue Nile Basin. *Nile and Grand Ethiopian Renaissance Dam*, 461-474.
- Larsen, A., Gergersen, I., Christensen, B., Linde, J., & Mikkelsen, P. (2009). Potential Future Increase In Extreme One-Hour Precipitation Events Over Europe Due To Climate Change. *Water Science & Technology*, 60(9), 2205–2216.
- Luo, M., Liu, T., Duan, Y., Frankl, A., Bao, A., & Maeyer, P. D. (2018). Comparing Bias Correction Methods Used in Downscaling Precipitation and Temperature from Regional Climate Models: A Case Study from the Kaidu River Basin in Western China. *Water*.
- Mabrouk, N., & Sharnouby, I. (2018). Stories After the Disaster. Al Dostor Newspaper.
- Mahmood, M., Alagib, N., Horn, F., & Saad, S. (2017). Lessons learned from Khartoum flash flood impacts: An integrated Assessment. *Science of The Total Environment*, 601-602, 1031-1045.

- Mahmoud, S., & Gan, T. (2018). Urbanization and climate change implications in flood risk management: Developing an efficient decision support system for flood susceptibility mapping. *Science of The Total Environment*, 636(3), 152-167.
- Mei, Y., Anagonostou, E., Nikolopoulos, E., & Borga, M. (2014). Error Analysis of Satellite Precipitation Products in Mountainous Basins. *Journal of Hydrometeorology*, 1778-1793.
- Miller, J., Kim, H., Kjeldsen, T., Packman, J., Grebby, S., & Dearden, R. (2014). Assessing the impact of urbanization on storm runoff in a peri-urban catchment using historical change in impervious cover. *Journal of Hydrology*, 515, 59-70.
- Moore, D., Notz, W., & Flinger, M. A. (2013). *The basic practice of statistics* (Vol. 6). New York, NY: Freeman and Company.
- Morad, N., Youssef, N., & Ibrahim, S. (2020). Assessment Of Flash Flood “April 2018” And Its Effect On Wadi Degla And Wadi El-Halazouni - East Cairo - Egypt. *Egyptian Journal Deser Res.*, 70(1), 25-57.
- Moriasi, D., Arnold, J., Van Liew, M., Bingner, R., Harmel, R., & Veith, T. (2007). Model Evaluation Guidelines For Systematic Quantification Of Accuracy In Watershed Simulations. *American Society of Agricultural and Biological Engineers*, 50(3), 885–900.
- MoSS. (2020). *Ministry of Social Solidarity*.
- NASA. (2021). *IMERG: Integrated Multi-satellitE Retrievals for GPM*. Retrieved from <https://gpm.nasa.gov/data/IMERG#IMERGOVERVIEW>

- NCAR. (2017). *The Climate Data Guide: GPM: Global Precipitation Measurement Mission*.  
<https://climatedataguide.ucar.edu/climate-data/gpm-global-precipitation-measurement-mission>: National Center for Atmospheric Research.
- NCAR. (2020). *The Climate Data Guide: GPCC: Global Precipitation Climatology Centre. National Center for Atmospheric Research*. Retrieved from  
<https://climatedataguide.ucar.edu/climate-data/gpcc-global-precipitation-climatology-centre>.
- New Cairo City Authority. (2016).
- New Urban Communities Authority. (2018).
- Nguyen, P., Sorooshian, S., Hsu, K., Gupta, H., Gao, X., Braithwaite, D., & AghaKouchak, A. (2019). The CHRS Data Portal, an easily accessible public repository for PERSIANN global satellite precipitation data. *Nature Scientific Data*, 6. Retrieved from CHRS:  
<https://chrsdata.eng.uci.edu/>
- NOAA. (2020). *Climate Modeling*. Retrieved from Geophysical Fluid Dynamics Laboratory:  
[https://www.gfdl.noaa.gov/wp-content/uploads/files/model\\_development/climate\\_modeling.pdf](https://www.gfdl.noaa.gov/wp-content/uploads/files/model_development/climate_modeling.pdf)
- Notaro, V., Liuzzo, L., Freni, G., & La Loggia, G. (2015). Uncertainty Analysis in the Evaluation of Extreme Rainfall Trends and Its Implications on Urban Drainage System Design. *Water*.
- Olawoyin, R., & Acheampong, P. K. (2017). Objective assessment of the Thiessen polygon method for. *Ghana Journal of Geography*, 9(2), 151–174.

- Parkinson, J. (2003). Drainage and stormwater management strategies for low-income urban communities. *Environment&Urbanization*, 15(2).
- Pendergrass, A., & NCAR. (2016). *The Climate Data Guide: GPCP (Daily): Global Precipitation Climatology Project*. Retrieved from <https://climatedataguide.ucar.edu/climate-data/gpcp-daily-global-precipitation-climatology-project>.
- Pendergrass, A., Wang, J., & NCAR. (2020). *The Climate Data Guide: GPCP (Monthly): Global Precipitation Climatology Project*. Retrieved from NCAR: <https://climatedataguide.ucar.edu/climate-data/gpcp-monthly-global-precipitation-climatology-project>
- Peng, J., Liu, T., Huang, Y., Ling, Y., Li, Z., Bao, A., . . . De Maeyer, P. (2021). Satellite-Based Precipitation Datasets Evaluation Using Gauge Observation and Hydrological Modeling in a Typical Arid Land Watershed of Central Asia. *Remote Sensing*, 13.
- RICCAR. (2020). *Background*. Retrieved from United Nations Economic and Social Commission for Western Asia (ESCWA): <http://www.riccar.org/basic-page/background>
- S. I., Nicholls, N., Easterling, D., Goodess, C., Kanae, S., Kossin, J., . . . Zhang, X. (2012). *Changes in Climate Extremes and their Impacts on the Natural Physical Environment*. In : *Managing the Risks of Extreme Events and Disasters to Advance Climate Change Adaptation A Special Report of the Intergovernmental Panel on Climate Change (IPCC)*. Cambridge, UK, and New York, NY, USA: Cambridge University Press.
- Saber, M., Abdrabo, K. I., Habiba, O. M., Kantosh, S. A., & Sumi, T. (2020). *Impacts of Triple Factors on Flash Flood Vulnerability in Egypt: Urban Growth, Extreme Climate, and Mismanagement* (Vol. 10). Geosciences.

- Saber, M., Abdrabo, K., Habiba, O., Kanotsh, S., & Sumi, T. (2020). Impacts of Triple Factors on Flash Flood Vulnerability in Egypt: Urban Growth, Extreme Climate, and Mismanagement. *Geosciences*, 10(1).
- Saleh, S. (2021). *New Cairo City Authority Comments on the frequent Wastewater Flooding in New Cairo*. Cairo: El-Watan News.
- Salem, M., & El-Sayed, E. (2017). Historical Satellite Data Analysis to Enhance Climate Change Adaption and Hydrologic Models in Egypt. *Journal of Power and Energy Engineering*, 5(8), 56-71.
- Salem, N., Shahid, S., Dewan, A., Ismail, T., & Alias, N. (2020, May 15). Performance of five high resolution satellite-based precipitation products in arid region of Egypt: An Evaluation. *Atmospheric Research*, 236.
- Schumann, A. H. (1998). Thiessen polygon. *Encyclopedia of Hydrology and Lakes*, 648-649.
- Shrestha, M., & Dangol, P. (2020). Introduction to Satellite Rainfall Estimates. Nepal.
- Shrestha, M., Acharyaa, S., & Shrestha, P. (2017). Bias correction of climate models for hydrological modelling – are simple methods still useful? *Meteorological Applications*, 24, 531–539.
- Simon, P. N., & Hashemi, M. R. (2018). *Fundamentals of Ocean Renewable Energy*.
- Soriano, E., Mediero, L., & Garijo, C. (2019). Selection of Bias Correction Methods to Assess the Impact of Climate Change on Flood Frequency Curves. *Water*.

- Spinoni, J., Barbosa, P., Bucchignani, E., Cassano, J., Cavazos, T., Christensen, J. H., . . . Dosio, A. (2020). Future Global Meteorological Drought Hot Spots: A Study Based on CORDEX Data. *Journal of Climate*, 33(9), 3635–3661.
- The World Bank. (2011). *Five Feet High and Rising: Cities and Flooding in the 21st Century (Transport, Energy & Urban Sustainable Development Unit)*. Washington, D.C: The World Bank.
- Thiessen, A. H. (1911). Precipitation for large areas. *Monthly Weather Review*, 39, 1082–1084.
- USAID, & UCSB. (2021). *CHIRPS: Rainfall Estimates from Rain Gauge and Satellite Observations*. Retrieved from University of California, Santa Barbara (UCSB): <https://www.chc.ucsb.edu/data/chirps>
- USEPA. (2021). Climate Change Indicators: Heavy Precipitation. *United States Environmental Protection Agency*.
- USGS. (2021). Landsat-7 image courtesy of the U.S. Geological Survey.
- van Vuuren, D., Edmonds, J., Kainuma, M., Riahi, K., Thomson, A., Hibbard, k., . . . Rose, S. (2011). The representative concentration pathways: an overview. 109, 5.
- Verner , D. (2012). *Adaptation to a Changing Climate in the Arab Countries: A Case for Adaptation Governance and Leadership in Building Climate Resilience*. MENA Development. Washington D.C: World Bank.
- Willems, P., Arnbjerg-Nielsen, K., Olsson, J., & Nguyen, V. (2012). Climate change impact assessment on urban rainfall extremes and urban drainage: Methods and shortcomings. *Atmospheric Research*, 103, 106-118.

WMO; Cap-Net. (2007). *Urban Flood Management*. World Meteorological Organization.

Zhou, Q. (2014). A Review of Sustainable Urban Drainage Systems Considering the Climate Change and Urbanization Impacts. *Water*, 6(4), 976-992.

Zhou, Q., Leng, G., Su, J., & Ren, Y. (2018). Comparison of urbanization and climate change impacts on urban flood volumes: Importance of urban planning and drainage adaptation. *Science of the Total Environment*.

Zhu, D., Wang, G., Ren, Q., & L., A. (2020). Hydrological evaluation of hourly merged satellite–station precipitation product in the mountainous basin of China using a distributed hydrological model. *Meteorological Applications*, 27(2).

Ziese, M., Rauthe-Schöch, A., Becker, A., Finger, P., Rustemeier, E., & Schneider, U. (2020). GPCC Full Data Daily Version 2020 at 1.0°: Daily Land-Surface Precipitation from Rain-Gauges built on GTS-based and Historic Data. *DWD*.

## Appendix A. Identify the Nearest Ground Station to the Study Area

### Using TPM Method

The closest rainfall station is chosen according to Thiessen Polygon Method (TPM). TPM is an averaging method used to identify the area of influence of rainfall stations in a catchment (Thiessen, 1911). It assumes that rainfall at any station is effective until midway to the next station in all directions. The Thiessen polygons are constructed by connecting lines between the meteorological stations available in the study area and for each connecting line a perpendicular bisector is drawn until all lines connects, which identify the area of influence of each station as shown in Figure A-1 (Schumann, 1998; Jamal, 2017). TPM is a popular method that is used extensively in hydrological studies (Olawoyin & Acheampong, 2017; Bournas & Baltas, 2021; Lakew & Moges, 2021)

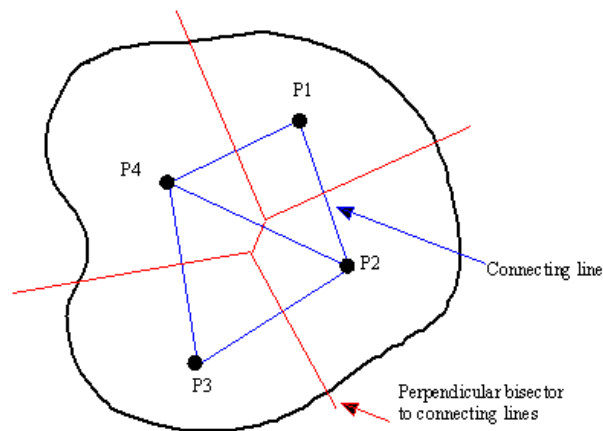


Figure A-1: Thiessen Polygon Method (Jamal, 2017)

Subsequently, the locations of rainfall stations around New Cairo were identified from EMA as shown in Figure A-2; these stations are Cairo, Katamya and Helwan.



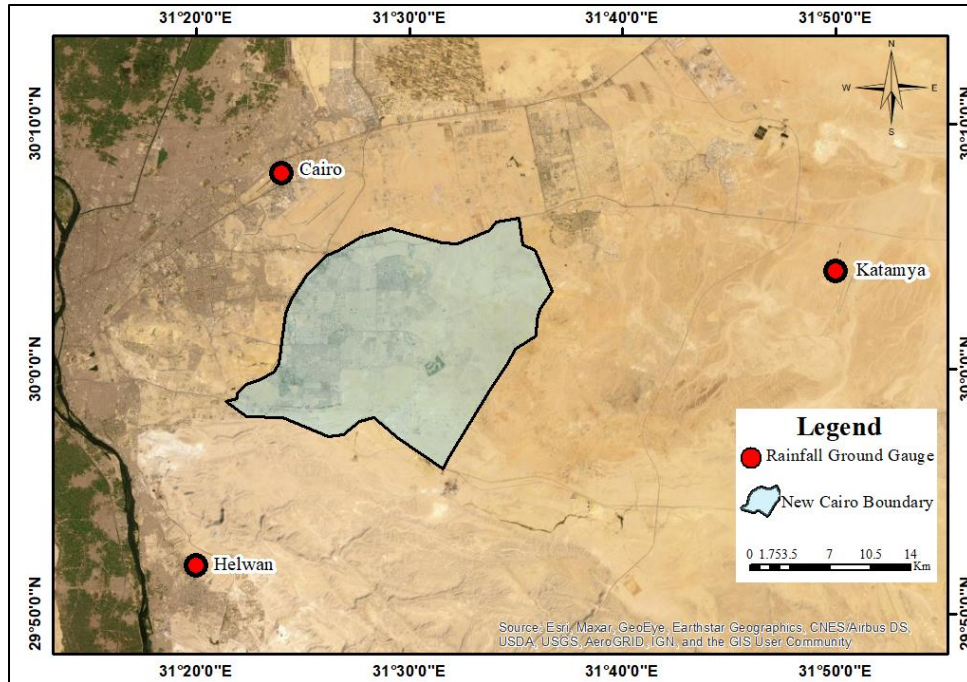


Figure A-2: Rainfall Stations Around New Cairo

By using the Thiessen Polygon method as shown in Figure A-3, it is clear that Cairo station covers all the urbanized areas in New Cairo and it can be used to extract rainfall data that historically fallen over the city.

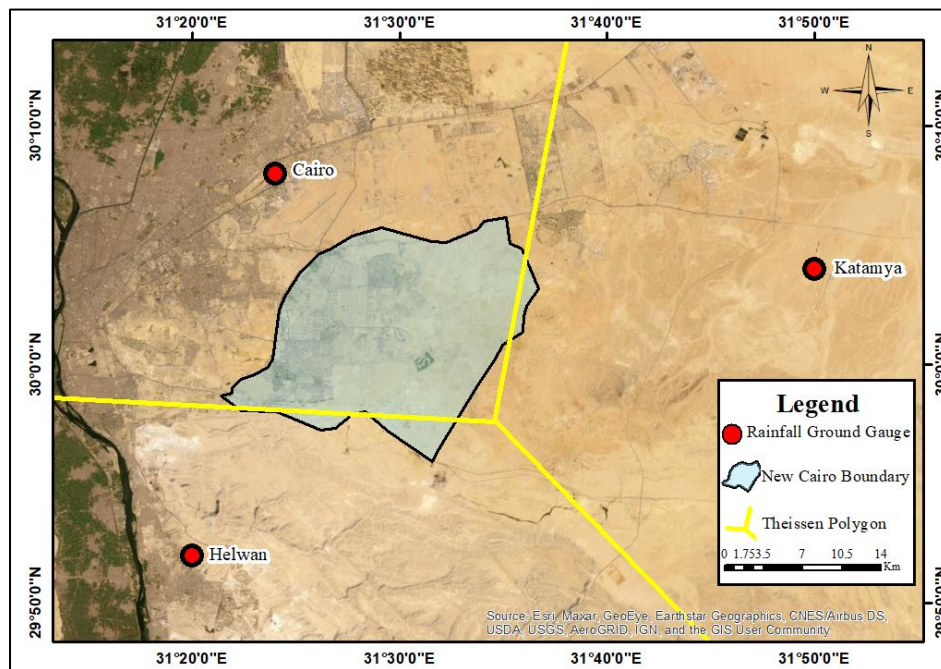


Figure A-3: Thiessen Polygon for stations around New Cairo

## **Appendix B. Satellite Rainfall Data-Sets Detailed Description and Analysis Equations**

This appendix compiles a detailed description of the satellite rainfall products showing their sources description and the available rain products. Moreover, the appendix includes detailed description of the statistical equations used for the analysis of satellite rainfall products

### **Description of Gridded Rainfall Data**

#### **A. Global Precipitation Climatology Centre (GPCC)**

GPCC provides rainfall data measured from ground rainfall stations from all over the globe and provide it online in the form of grids. GPCC provides range of data with various spatial resolution and time coverages according to intended application for the rainfall data. The daily and monthly rainfall data were downloaded in order to conduct a hydrological study and to study the extreme rainfall events, however, the rainfall data is not bias corrected against the changes of the number of stations per grid and from the general gauge errors (NCAR, 2020). The GPCC provides rainfall data with temporal distribution of total daily and total monthly rainfall. The monthly product of GPCC is offered with different resolutions which are  $0.25^\circ$ ,  $0.5^\circ$ ,  $1.0^\circ$ ,  $2.5^\circ$ , while the daily data has only one resolution of  $1.0^\circ$  (Ziese, et al., 2020). The rainfall data is available for total 37 years from 1982 to 2019 for the daily data. Figure B-1 shows the statistical analysis of the daily and monthly of GPCC, which extracted for the location of Cairo Station.

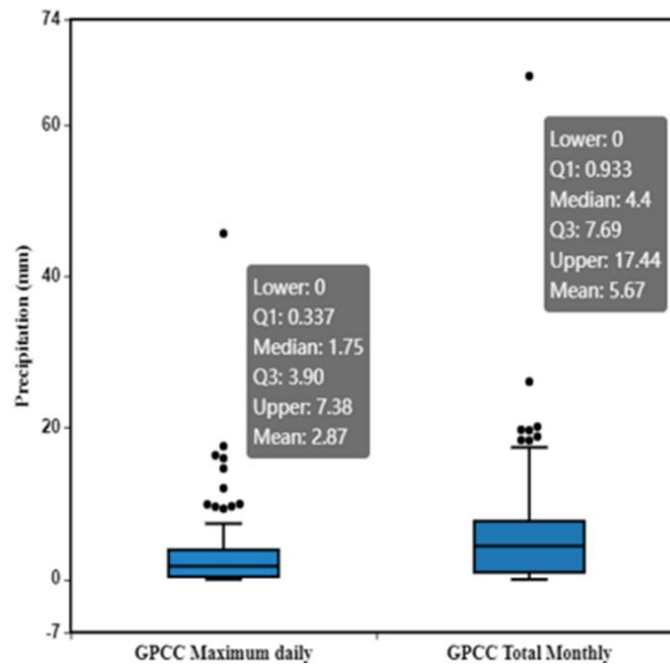


Figure B-1: Daily and Monthly GPCP Rainfall Data Statistical Features (Mean, Median, Minimum, Maximum and Extreme values as outliers)

## B. Global Precipitation Climatology Project (GPCP)

GPCP measures rainfall data through combining precipitation data from various sources and benefits from the strength of each type to reach a final merged rainfall product. The GPCP data offers only daily and monthly data with a resolution of  $2.5^\circ$  for the monthly and  $1^\circ$  for the daily. The monthly rainfall data is available for total 41 years from 1979 to 2020, while the daily data is available for 25 years from 1996 to 2021, therefore, the data is extracted between 1996 to 2020 as it is the common period between the monthly and daily data (Pendergrass & NCAR, 2016; Pendergrass, Wang, & NCAR, 2020). Figure B-2 shows the statistical analysis of the daily and monthly data of GPCP, which extracted for the location of Cairo Station.

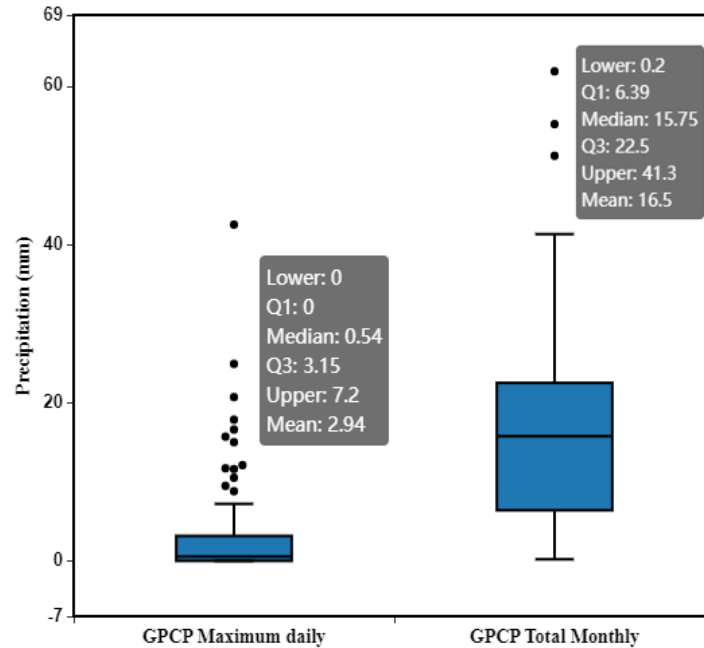


Figure B-2: Daily and Monthly GPCP Rainfall Data Statistical Features (Mean, Median, Minimum, Maximum and Extreme values as outliers)

### C. Tropical Rainfall Measuring Mission (TRMM)

TRMM is a polar orbiting satellite. It was the first precipitation radar launched in 1997 and aimed to measure precipitation over the tropical and subtropical regions through combining Thermal Infrared (TIR) data from geostationary satellites with Passive Microwave (PM) data from different sources (Amin, 2014). The spatial resolution of TRMM is  $0.25^\circ$  i.e., 27.75 km and its time coverages are 3 hours, daily or monthly (JAXA, 2021; Huffman & Pendergrass, 2021). TRMM data, which is called TMPA was discontinued at the end of December 2019 (Huffman G. , Bolvin, Nelkin, & Adler , 2016; Huffman G. , et al., 2007). The TRMM data covers 21 years from 1998 to 2019; for the purpose of this research the daily and monthly data are extracted for the location of Cairo Station and their statistical features are shown in Figure B-3.

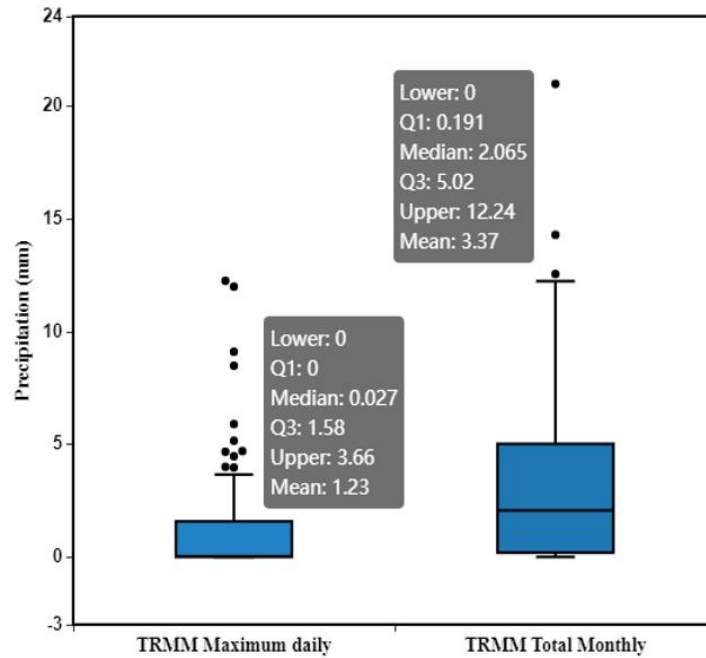


Figure B-3: Daily and Monthly TRMM Rainfall Data Statistical Features (Mean, Median, Minimum, Maximum and Extreme values as outliers)

#### D. The Global Precipitation Measurement Mission (GPM)

GPM is the successor of TRMM. Unlike TRMM it can measure light rain events (NCAR, 2017). The rainfall data from GPM is called IMERG (Integrated Multi-Satellite Retrievals for GPM), which is an algorithm combines and calibrate rainfall data from TRMM and other products for the period of 2000 to 2015. The spatial resolution of GPM is  $0.1^\circ$  which is about 10 km and its temporal coverages are 30 minutes, 1 day and 1 month (NASA, 2021). Finally, the GPM covers 21 years starting from June 2000 until present. The GPM's statistical Analysis of the rainfall data extracted for the location of Cairo Station is shown in Figure B-4.

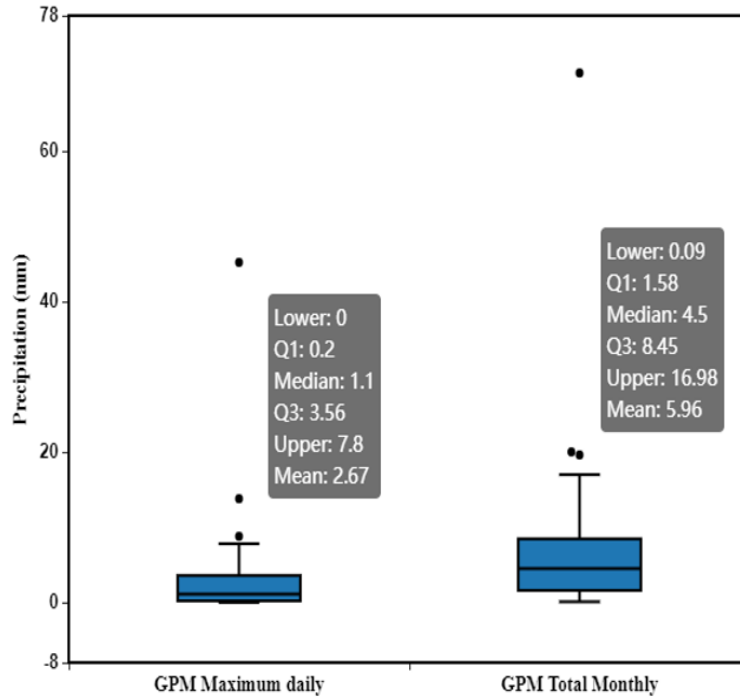


Figure B-4: Daily and Monthly GPM Rainfall Data Statistical Features (Mean, Median, Minimum, Maximum and Extreme values as outliers)

#### E. Precipitation Estimation from Remotely Sensed Information using Artificial Neural Network (PERSIANN)

PERSIANN is an algorithm that measure rainfall data by importing images either from geostationary satellites or daytime visible images and through using infrared illumination it classifies the image and estimate rainfall (Nguyen, et al., 2019). The PERSIANN data has a resolution of  $0.25^\circ \times 0.25^\circ$  and its temporal coverages are hourly, 3-hourly, 6-hourly, daily, monthly and yearly. PERSIANN covers 21 years from March 2000 until present. PERSIANN's statistical analysis of the daily and monthly data extracted for the location of Cairo Station are shown in Figure B-5.

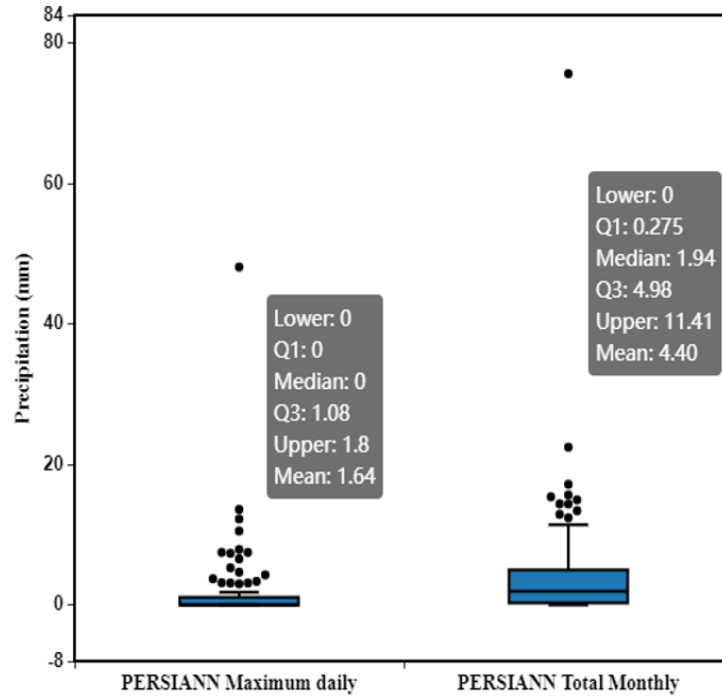


Figure B-5: Daily and Monthly PERSIANN Rainfall Data Statistical Features (Mean, Median, Minimum, Maximum and Extreme values as outliers)

#### F. Climate Hazards Group Infra-Red Precipitation with Station (CHIRPS)

CHIRPS is a combination between the rain gauges data and satellite data in order to get an average rainfall record in areas with scarce precipitation measurements. The CHIRPS data has two resolutions either  $0.05^\circ$  or  $0.25^\circ$ . Furthermore, its temporal resolutions are daily, pentad, decade, monthly, 2-monthly, 3-monthly and annual. The rainfall data is available for 40 years starting from 1981 until present (USAID & UCSB, 2021). In this research, the used data are monthly and daily CHIRPS data with resolution of  $0.05^\circ$ . Finally, the statistical analyses of the daily and monthly data extracted at the location of Cairo Station are shown in Figure B-6.

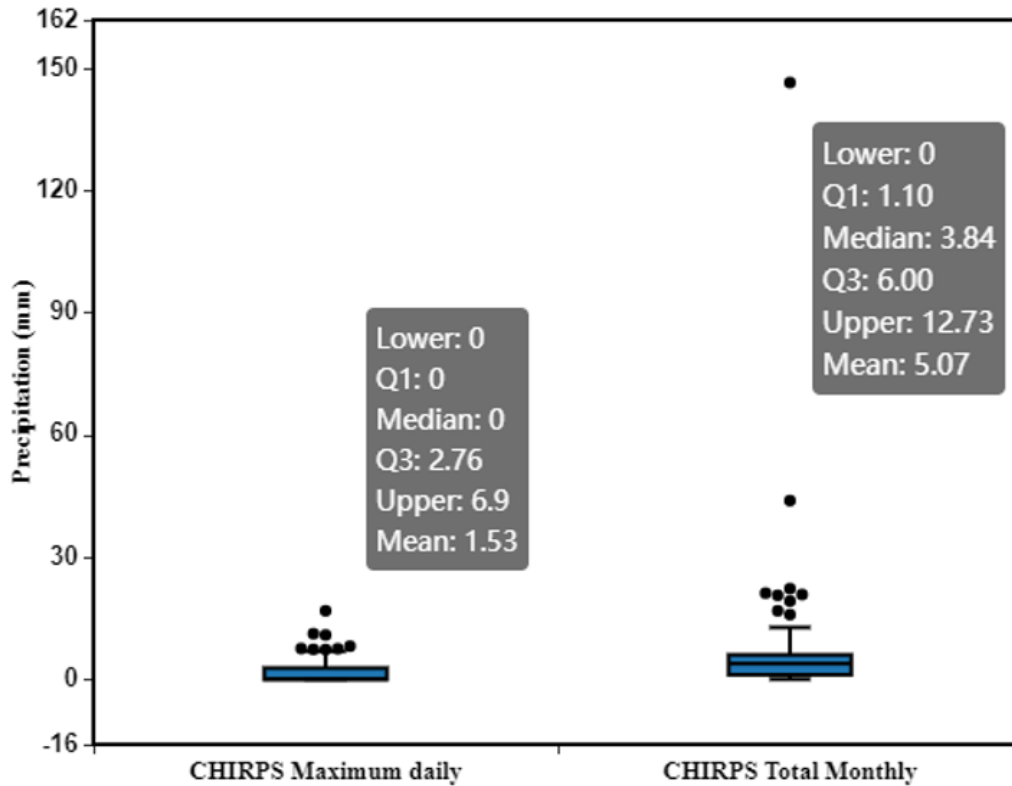


Figure B-6: Daily and Monthly CHIRPS Rainfall Data Statistical Features (Mean, Median, Minimum, Maximum and Extreme values as outliers)

## Statistical Equations' Description

### A. Mean Absolute Error (MAE)

The mean absolute error measure the average difference between the observational data and satellite measured data. Zero means a perfect fit, however, the lower the MAE the better the data.

$$\text{Mean Absolute Error (MAE)} = \frac{1}{n} \sum_{i=1}^n |P_i - O_i|$$

Equation 3: Mean  
Absolute Error  
(MAE)

Where, P is the satellite data, O is the observed ground measured data, n is the number of total population data.



## B. Root Mean Square Error (RMSE)

It is an indicator of a perfect match between the ground data and satellite data. The value of RMSE depends on the scale and order of the data (Simon & Hashemi, 2018). In general, the lower RMSE the better fit between data.

$$\text{Root Mean Square Error (RMSE)} = \sqrt{\frac{\sum_{i=1}^n (P_i - O_i)^2}{n}}$$

Equation 4: Root Mean Square Error (RMSE)

## C. The coefficient of determination $R^2$

It measures the variance in the satellite data. It ranges between 0 and 1. The higher the value of  $R^2$  the less variance the satellite data have and the better fit.  $R^2$  larger than 0.5 is considered satisfactory (Golmohammadi, Prasher, Madani, & Rudra, 2014). However, the  $R^2$  method is overly sensitive to extreme values.

$$\text{Coefficient of Determination (R}^2\text{)} = \left[ \frac{\sum_{i=1}^n (O_i - \bar{O})(P_i - \bar{P})}{\sqrt{\sum_{i=1}^n (O_i - \bar{O})^2} \sqrt{\sum_{i=1}^n (P_i - \bar{P})^2}} \right]^2$$

Equation 5: Coefficient of Determination ( $R^2$ )

Where,  $\bar{O}$  is the mean value for ground measured data, and  $\bar{P}$  is the mean value for satellite data.

## D. The percentage of bias (PBIAS)

It measures whether the satellite data overestimates or underestimates precipitation compared to the ground measured data. The optimal value for PBIAS is zero, negative values indicate over estimation and positive value indicates under estimation.

$$\text{Percent Bias (PBIAS)} = \left[ \frac{\sum_{i=1}^n (O_i - P_i) * 100}{O_i} \right]$$

Equation 6: Percent Bias (PBias)

#### E. The RMSE-observations standard deviation ratio (RSR)

It is the ration between the mean square error and the standard deviation of the ground data and it is one of the criteria used for measuring the performance of model. The optimum value of RSR is Zero, however, in general the lower the RSR value the better data.

$$RMSE - Observation Standrd Deviation (RSR) = \frac{RMSE}{STDEV_{Obs}}$$

Equation 7: RMSE-  
Observation  
Standrd Deviation  
(RSR)

Where,  $STDEV_{Obs}$  is the standard deviation of observed data.

#### F. Nash Sutcliffe Efficiency (NSE)

The NSE is a coefficient that evaluates the prediction efficiency of a hydraulic model. It ranges between  $-\infty$  to 1.0, where 1 is the optimum value. The range between 0 to 1 are viewed as satisfactory, however, the recommended NSE ranges are  $>0.75$  Very good fit, 0.64 to 0.74 good fit, 0.5 to 0.64 satisfactory, less than 0.5 unsatisfactory. On the other hand, less than 0 is unsatisfactory performance for the satellite data (Moriasi, et al., 2007).

$$Nash\ Sutcliffe\ Efficiency\ (NSE) = 1 - \left[ \frac{\sum_{i=1}^n (O_i - P_i)^2}{\sum_{i=1}^n (O_i - \bar{O})^2} \right]$$

Equation 8: Nash  
Sutcliffe Efficiency  
(NSE)

### The Graphical Comparison Figures

The graphical comparison is done through box plot and scatter plot. Figure B-7 and Figure B-8 show a box plot for the key features of the monthly and daily data sets like mean, maximum and extreme rainfall values; moreover, Figure B-9 and Figure B-10 are scatter charts of the Cairo station rainfall data plotted against each rainfall products data set for the monthly and daily rainfall values. From the charts, the closest rainfall products to the ground measured rainfall are GPCC and GPM.

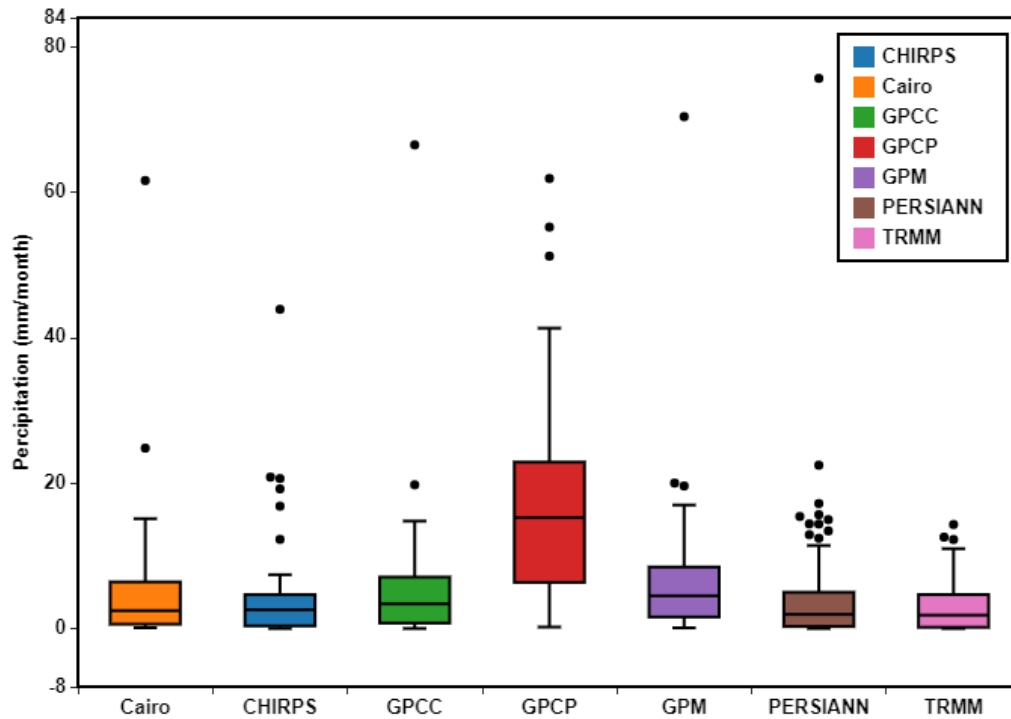


Figure B-7: Graphical comparison of monthly rainfall data for ground observed data vs. gridded rainfall products showing (Mean, Median, Minimum, Maximum and Extreme values as outliers)

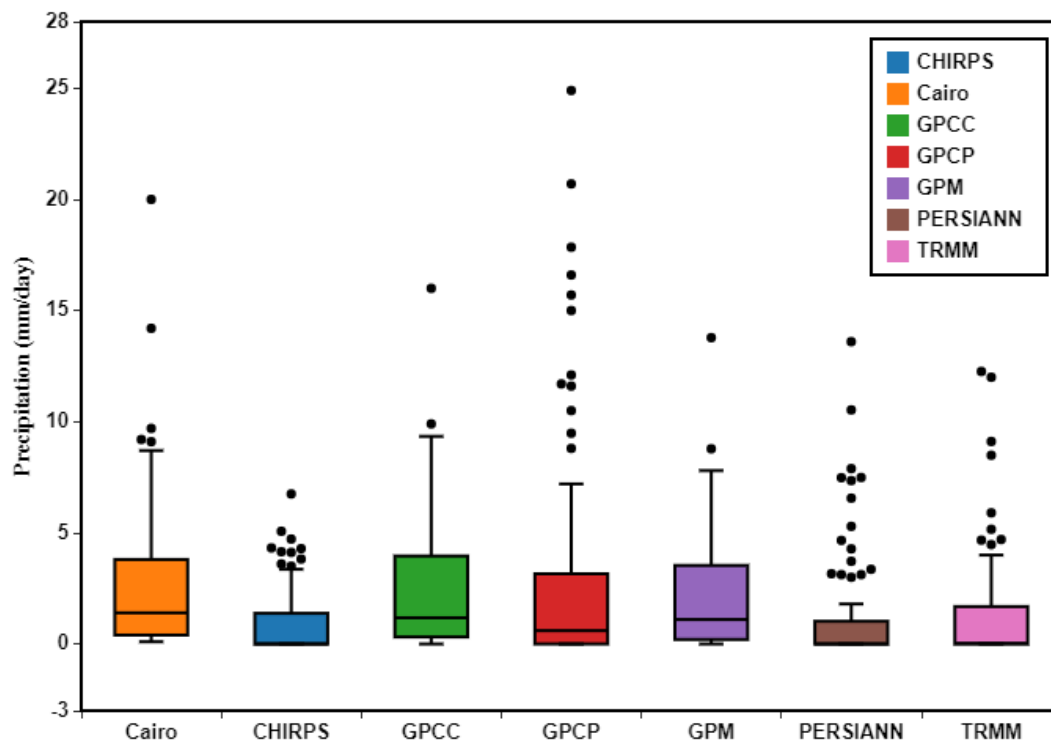


Figure B-8: Graphical comparison of daily rainfall data for ground observed data vs. gridded rainfall products showing (Mean, Median, Minimum, Maximum and Extreme values as outliers)

The monthly data box plot show GPCC as the most comparable to Cairo Station in terms of the upper and lower bounds as well as the extreme events. Followed by GPM as it gives the impression that it overestimates the rainfall values; as for the daily data box plot, the same observation applies, where GPCC and GPM are the closest.

Similarly, the scatter plot of monthly and daily data show that GPCC has the strongest correlation to ground measured data with  $R^2=0.41$  for the monthly data and 0.40 for the daily data. Moreover, the GPM has a similar value with  $R^2=0.4$  for monthly data and 0.37 for daily data. However, the  $R^2$  value should exceed 0.5 to be accepted.

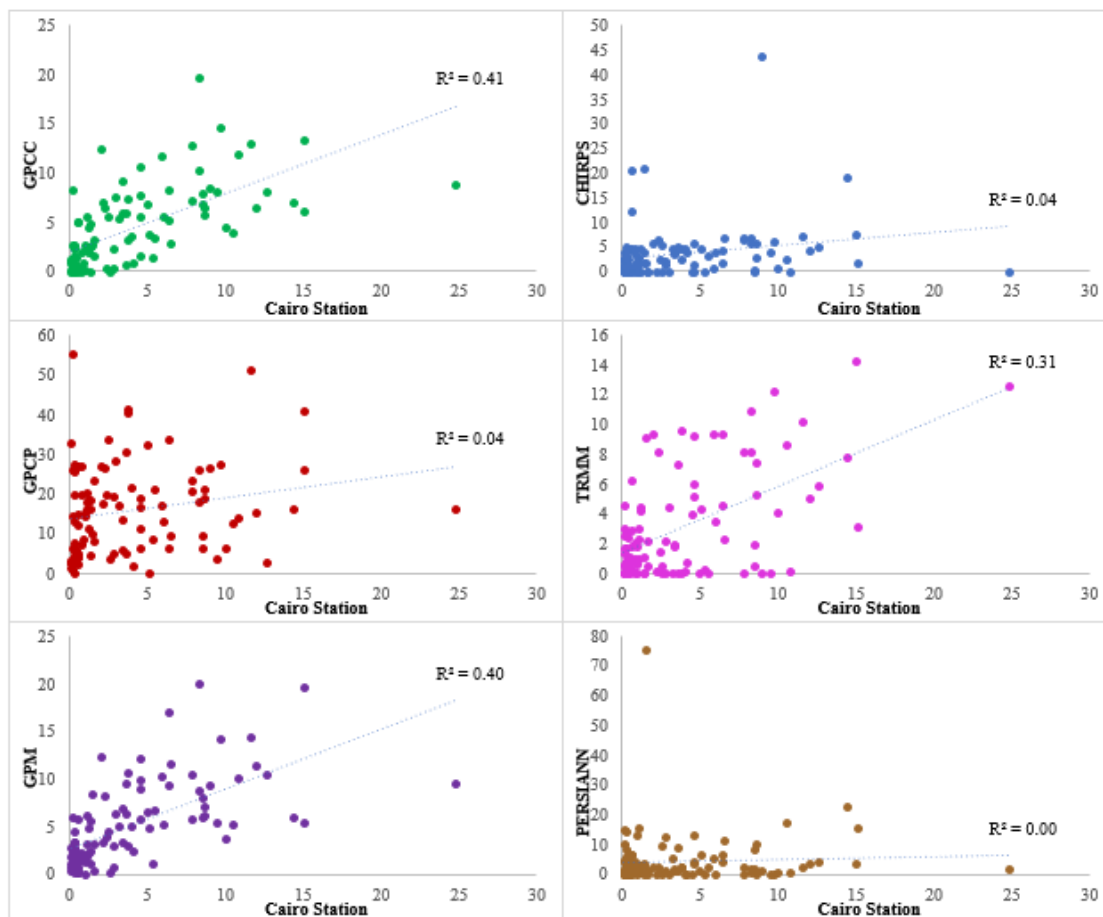


Figure B-9: Scatter plot showing correlation between six gridded rainfall products and ground observed data for monthly precipitation

It worth noting that the remotest product to represent Cairo station rainfall measurement is PERSIANN in terms of the monthly rainfall data as  $R^2$  value is near to zero resembling no coherence at all. On the other hand, for the daily data the weakest product to represent the rainfall is GPCP with  $R^2$  value of 0.01. However, although the results of the graphical representation are promising they should be coupled with the statistical validation to include each data point.

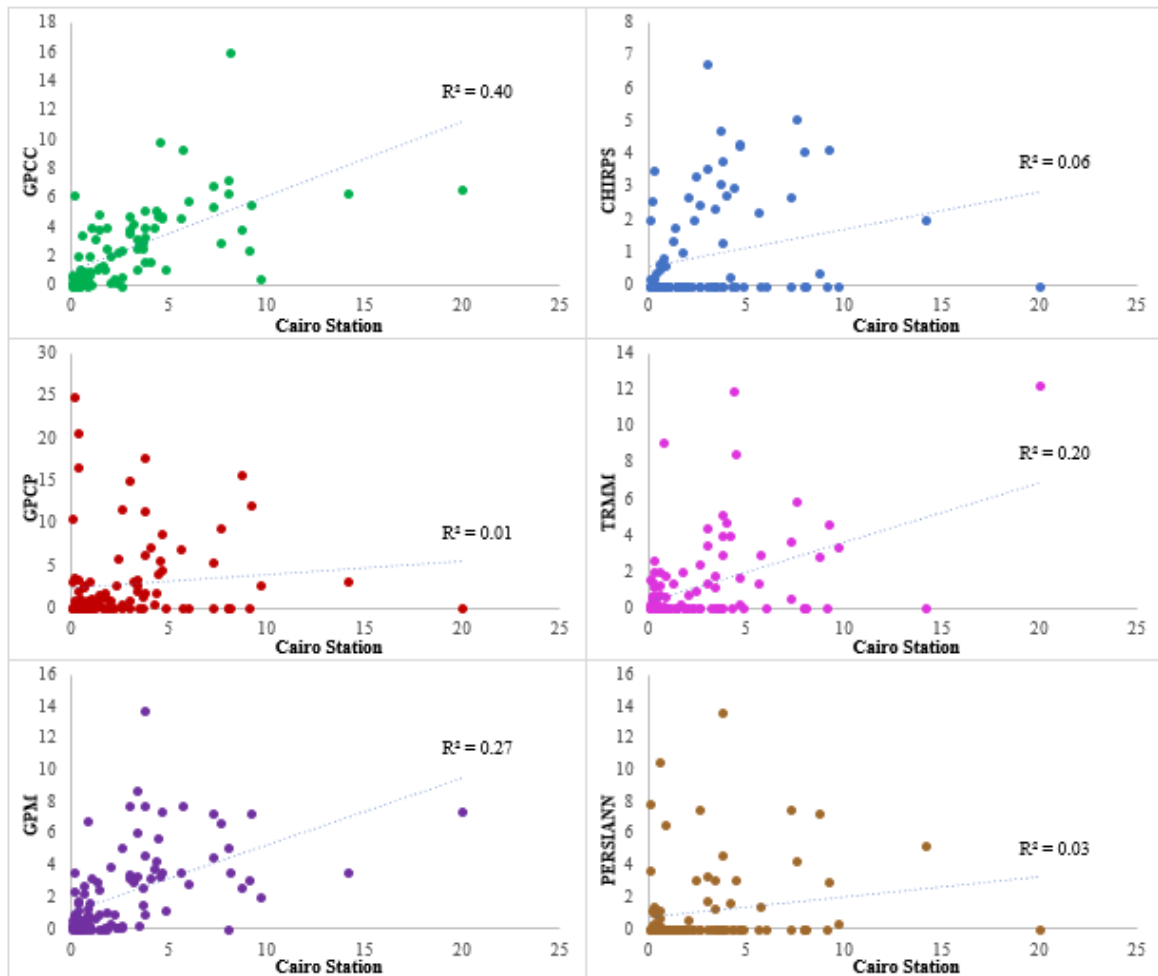


Figure B-10: Scatter plot showing correlation between six gridded rainfall products and ground station data for daily precipitation

## Appendix C. Rainfall Runoff Model Detailed Inputs

### A. Identifying Watersheds Affecting New Cairo

The study area of the New Cairo is located in the north of the Eastern Desert between longitudes  $31^{\circ}27'42.70''\text{E}$  &  $31^{\circ}27'37.73''\text{E}$  and latitude  $29^{\circ}55'53.52''\text{N}$  &  $30^{\circ}5'26.08''\text{N}$ . The New Cairo is bounded by Ain-Sokhna Road from the South, the ring road from the west, Suez-Rd. from the north and the New Capital from the east. Before urbanization New Cairo was constructed on a fluvial area. Figure C-1 shows New Cairo in 1990 before urbanization; as observed from the figure there are streamlines passing inside the New Cairo's boundaries, which represent water streams. The watershed affecting New Cairo were identified by the topographic maps, which show the land use before urbanization included the valleys streams. Four topographic maps were used to show the area produced in 1973, with resolution 1:50,000. Using WMS and the SRTM digital elevation (Farr & Kobrick, 2000), the watersheds are defined and modified according to the topographic maps as shown in Figure C-2.

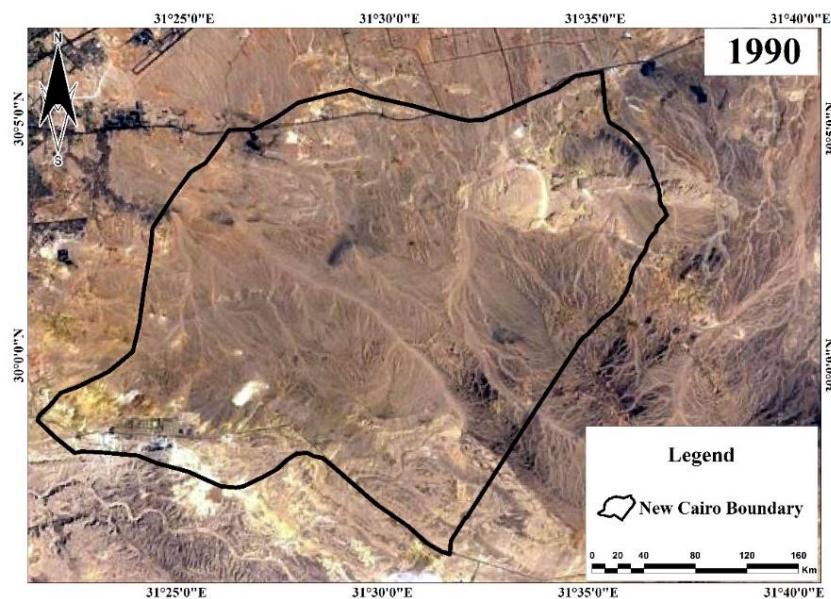


Figure C-1: Satellite image from 1990 showing New Cairo area before urbanization and some streamlines appear to exist

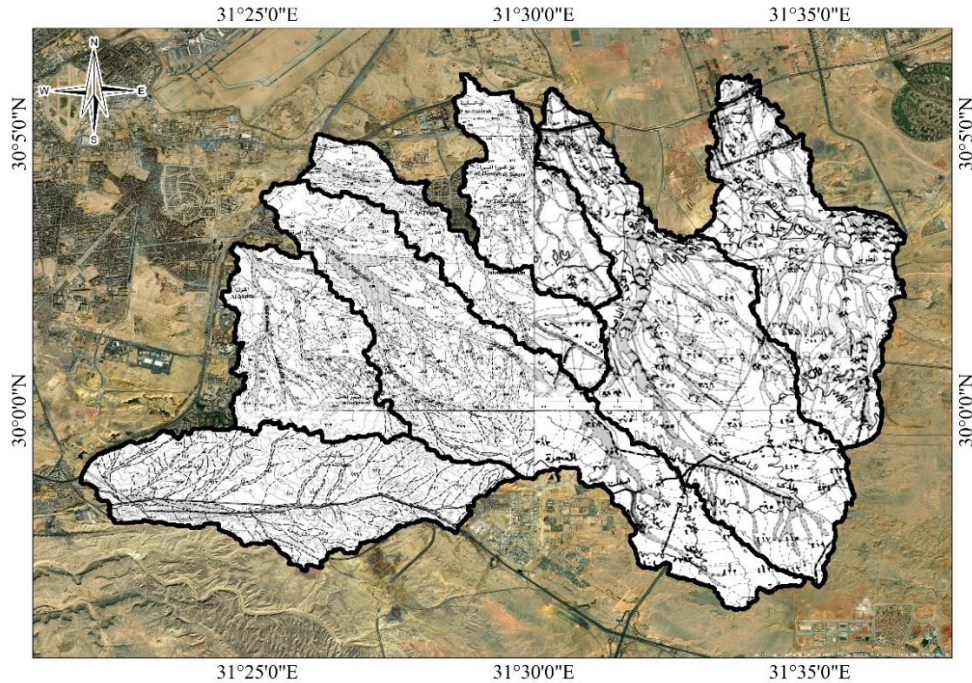


Figure C-2: Boundaries of seven watersheds affecting the area of New Cairo, modified according to the topographic map.

The results of the digital elevation model and the topographic maps showed that there were seven basins passed through New Cairo. Figure C-3 show the names and characteristics of the basins and drainage network of watersheds affecting New Cairo, moreover, it shows their areas and basins' lengths. Figure C-3 shows the morphological properties of the basins like their time of concentration and lag time. The elevation upstream the watersheds is 482 asl and the downstream is 130 asl, while the slopes average between  $0^{\circ}$  and  $5^{\circ}$ , and reaches  $13^{\circ}$  on the western side of the catchment area which increases the probability of runoff.



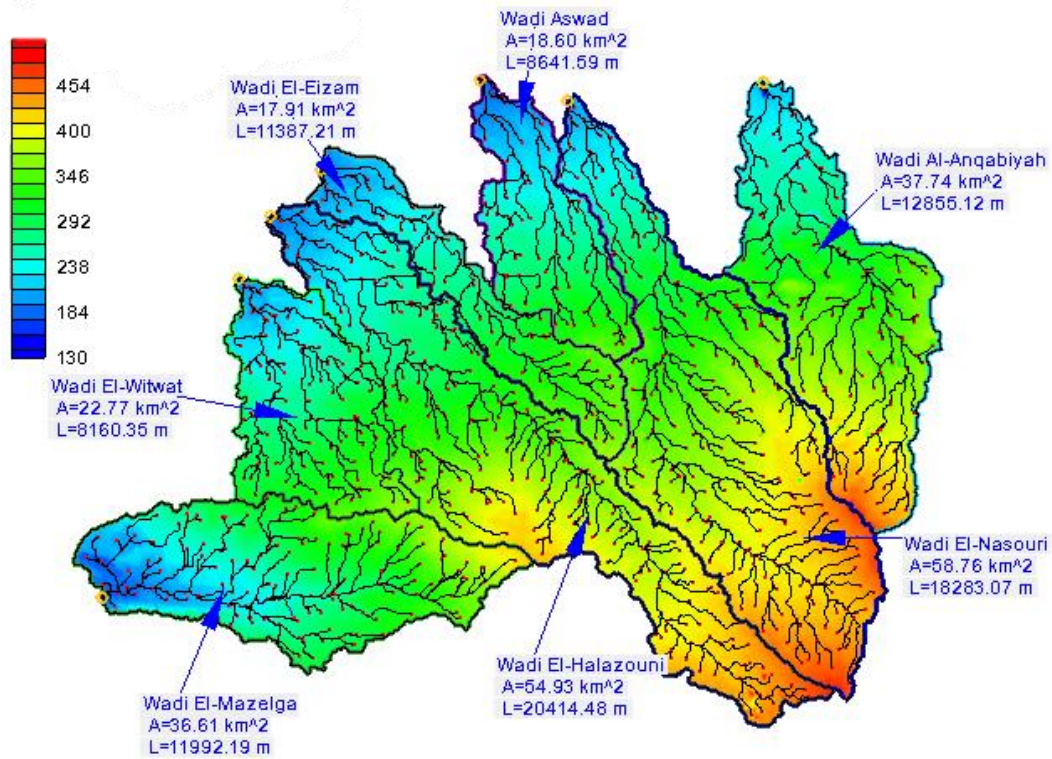


Figure C-3: Names and shapes of basins affecting New Cairo with their names, basins areas and lengths

Table C-1: Morphological Properties of Watersheds Upstream New Cairo

Basin No.	Basin Name	Basin Area (km <sup>2</sup> )	Basin Length (km)	T <sub>c</sub> (hr.)	T <sub>L</sub> (hr.)
1B	Wadi Aswad	18.6	8.64	4.57	2.74
2B	Wadi Al-Anqabiyah	37.74	12.85	5.93	3.56
3B	Wadi El-Nasouri	58.76	18.28	8.60	5.16
4B	Wadi El-Eizam	17.91	11.38	5.80	3.48
6B	Wadi El-Halazouni	54.93	20.41	9.10	5.46
7B	Wadi El-Witwat	22.77	81.60	4.80	2.88
8B	Wadi El-Mazelga	36.61	11.99	4.48	2.69

The soil description is particularly crucial factor to calculate the infiltration corresponds to each rainfall event, thus, estimate the runoff values. The infiltration rates are defined according to the land use and soil type. The infiltration rate is defined according to its geological soil types, the



exact soil mapping and description is mentioned. As for the urban areas, the infiltration is defined by the land use and cover as described in Table C-2.

## B. Soil Data

The runoff is considered an excess rainfall after the soil initial abstraction during the rainfall event. The initial abstraction quantity is based on the type of the soil in the watershed. To calculate the runoff values the Curve number (CN) method is adopted from Soil Conservation Service's (SCS). The CN method divides the soil into four groups (A, B, C, D), A is the soil group that has a highest infiltration rate, B represent soil group with medium rate, C is low infiltration rate and finally D represent impermeable soil. For each soil group a soil CN is defined according to the land use. Therefore, as a first step the soil type and its geological group should be defined to determine the ability of the soil to infiltrate rainwater, then the land use should be defined to choose the correct CN. The CN for relevant land uses in this research is mentioned in Table C-2.

Table C-2: Morphological Properties of Watersheds Upstream New Cairo

Cover Description		Curve Numbers for Soil Groups			
Cover type	Hydrologic Condition	A	B	C	D
<b>Fully Developed urban areas</b>					
Open space (lawns, parks, golf courses, cemeteries, etc.)	Poor condition (grass cover < 50%)	68	79	86	89
	Fair condition (grass cover 50% to 75%)	49	69	79	84
Residential districts	1/8 acre or less (town houses)	77	85	90	92
Paved parking lots, roofs, driveways, streets and roads	Impervious Areas	98	98	98	98
<b>Arid and Simi Arid Regions</b>					
Desert shrub – major plants include saltbrush, greasewood, creosotebush, blackbrush, bursage, palo verde, mesquite, and cactus.	Poor	63	77	85	88
	Fair	55	72	81	86
	Good	49	68	79	84

After determining the CN, the excess runoff is calculated through the following set of equations for each time step as follows.

$$Q = \frac{(P - I_a)^2}{P - I_a + S} \quad \text{Equation 9: Excess Rainfall}$$

$$I_a = 0.2 S \quad \text{Equation 10: Initial Abstraction}$$

$$S = \frac{100}{CN} - 10 \quad \text{Equation 11: Potential Maximum Soil Retention}$$

Where, Q is the excess rainfall (cumulative), P is the rainfall depth,  $I_a$  is the initial abstraction, S is the potential maximum soil retention after the start of rainfall event.

### C. Identifying Geological Groups of the Study Area

The geological map (Figure C-4) shows that the Eocene and Miocene rocks cover the area and consist of the following units arranged from the components which covers the most area to the least (Morad, Youssef, & Ibrahim, 2020).

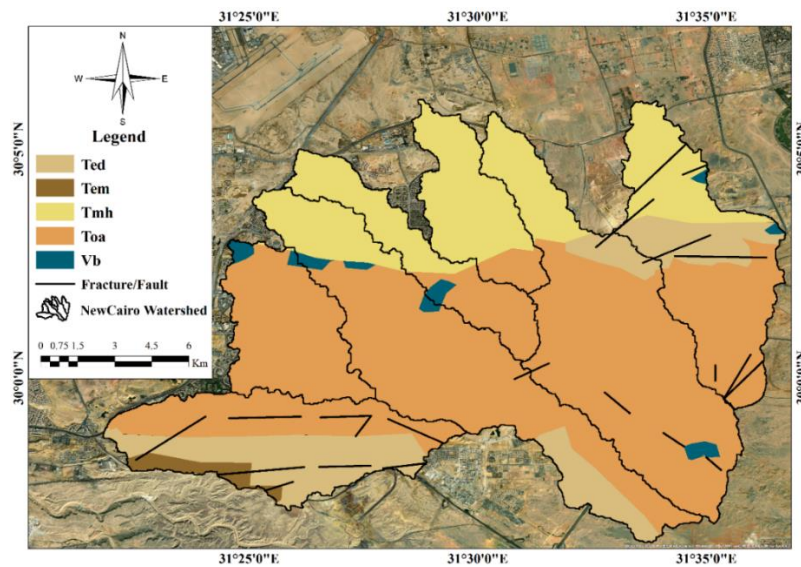


Figure C-4: Geological Map of the watershed affecting New Cairo, showing the soil types

**The Toa Component:** This component dominates New Cairo it is about 60% of the watershed and it is called Gebel El-Ahmar Formation. It is petrified forest that consists of vividly colored sand and gravel and silicified wood and it indicates fluvial depositions. It has a medium capacity to absorb water.

**The Tmh Component:** This component represents about 22% of the watershed located exclusively in the downstream. It consists of fluviatile Sand and gravel, which is represent an ancient flooding area known as Hagul Formation or Upper Miocene. It is also underlain by marine limestone with sandy layers at the base. This component has a weak ability to drain water.

**The Ted Component:** This component covers about 14% of the watershed located mostly in the upstream and a small portion in the northern part; it consists of slurry and fossil limestone of shallow marine origin with interactions of sandstone with a marine origin, which is equivalent to the Qasr al-Sagha component, and these rocks have a weak ability to absorb water.

**The Vb Component:** This component covers a small, scattered portion of the watershed about 1.4%. It consists of basaltic dikes, sills and flows. Vb has an average capacity to drain water.

**The Tem Component:** This component covers a small area of the watershed about 1.2% in the southwest of the drainage area. It consists of medium to dense layers of fossil limestone of shallow marine origin with overlaps of Chert and above it the Al-Jyushi component located below the Jabal Hawf component and the Muqattam group and these rocks have a medium capacity to absorb water.

The area contains few faults of different directions in the south and east part of the watershed, which affect the movement and direction of surface and ground water.

#### D. Identifying Land Use of the Study Area

Table C-3 shows a detailed description of the Watersheds showed in Figure C-3, this description aid in identifying the land use of the area before urbanization, accordingly, identify the potential of soil infiltration of New Cairo as shown in Table C-4 and Table C-5.

Table C-3: Detailed Description of Each Basin Affecting New Cairo

Basin No.	Description
Wadi Aswad	It starts from the middle of the watershed until downstream, it passes between Aldawra El-Samraa Hill and El-Fengan Hill, currently it is blocked by new developments in New Cairo but still under construction
Wadi Al-Anqabiyah	It is located upstream Wadi Aswad and passes through El-Malahez Hill, there are no signs of flooding streams at it is now under construction starting from the New Capital and ending at New Cairo.
Wadi El-Nasouri	It starts from El-Rowaysat Mountain and passes through El-Nasouri Mountain, it is currently blocked with New Developments that are under construction in New Cairo.
Wadi El-Eizam	It is located in the middle of the watershed and it is currently blocked with fully developed urbanized area.
Wadi El-Halazouni	It is one of the biggest basins affecting New Cairo, however, most of the urban areas in New Cairo located within the boundaries of this basins, it is still a little active as some areas within the city shows water streamlines after rainfall events.
Wadi El-Witwat	It was a small watershed and it is totally blocked with fully development urban area.
Wadi El-Mazelga	It is located in the far west of the watershed, it contined petrified forest area that is now changed into an urban area.

Table C-4: Summary of the geological soil types in New Cairo Watershed and their percentage area and the final CN Value for Rural Areas

Soil Type	Percent of total Area	CN Soil Group	CN	Weighted CN for Rural Areas
Toa	62%	B	77	79.8
Tmh	22%	C	85	
Ted	14%	C	85	

Soil Type	Percent of total Area	CN Soil Group	CN	Weighted CN for Rural Areas
Vb	1%	B	77	
Tem	1%	B	77	

Table C-5: CN for Urban land use and cover used in this research

Land Cover	Description	CN	Weighted CN
Fully Urbanized Areas	Paved Roads (50%)	98	94
	Buildings (50%)	90	
Green Areas	Compounds with green areas $\geq 50\%$	89	89
Construction Areas	Urban areas under Construction	85	85

## E. Rainfall Calculations

The rainfall data required are the storm magnitude identified according to the chosen return period and Actual storm distribution for New Cairo derived from GPM as discussed in the research.

The return periods rainfall amounts are calculated through extracting the maximum daily rainfall occurred in each recorded year, then the data points extracted from each year is fitted on as many probability distributions as possible to determine the most appropriate and accurate distribution that fit the available data. In order to save time on the fitting, a statistical analysis program was used to perform the analysis of different probability distributions, which are:

Exponential	GEV	Gumbel	Weibull
Generalized Pareto	Halphen	Normal	Lognormal
Lognormal (3 Param)	Gamma	Inverse Gamma	Person Type 3
	Generalized Gamma	Log-Pearson	

The fitted distribution will be then useful in determining the expected values of rain at different return periods. The most representative distribution for both Cairo Station and GPM was lognormal distribution as shown in Figure C-5 and Figure C-6. Table C-6 shows the rainfall values calculated for each return period for Cairo Station.

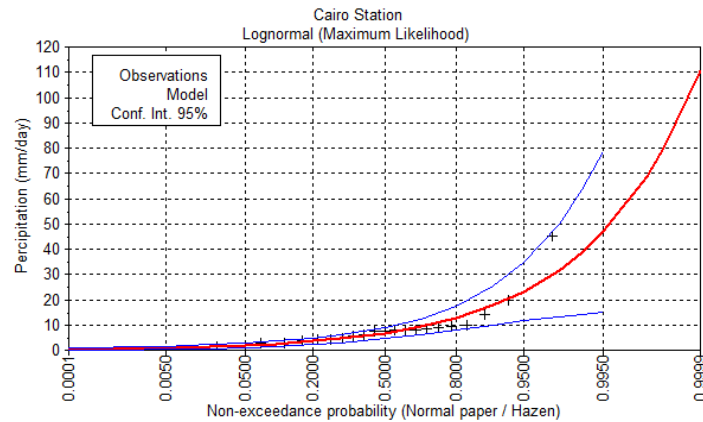


Figure C-5: Probability Distribution fit for Cairo Station

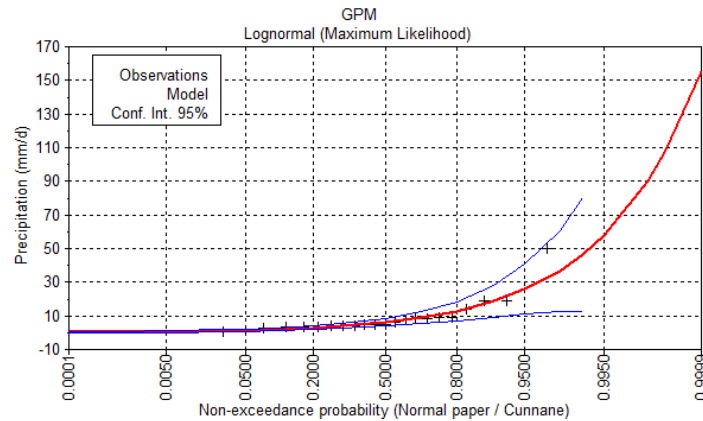


Figure C-6: Probability Distribution Fit for GPM

Table C-6: Rainfall corresponds to each return period for the rainfall runoff model

Return Period	Cairo	
	Rainfall (mm/d)	Confidence Interval
2	6.75	4.58 - 8.92
5	12.7	7.92 - 17.5
10	17.7	9.93 - 25.5
20	23.3	11.6 - 34.9
50	31.6	13.4 - 49.9
100	38.8	14.3 - 63.3
200	46.8	14.9 - 78.7

## Appendix D. SewerGEMS Model Structure and Details and Results

### A. Building the Model

There are Three main components required by the SewerGEMS model, firstly, the drainage system inputs that includes as built sewer design drawings, sewage load and the outfall which is a pump station with its pump definition.

Secondly, the hydrologic input that includes precipitation values correspond to the desired return period, the sub-catchments areas, and imperviousness properties of the land use. The storm values are taken according to the simulated return period as mentioned in Table C-6. The rainfall distribution is extract from selected satellite rainfall product as shown in Figure D-1, which is a 24-hour storm distribution. On the other hand, the drainage discharge is assumed to follow the water consumption pattern hydrograph provided by the Egyptian Code of Practice Figure D-1.

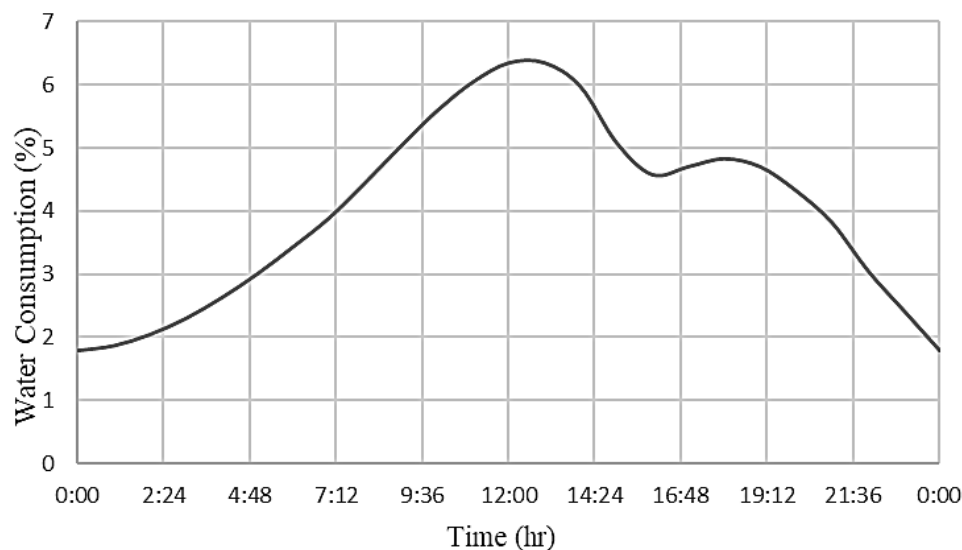


Figure D-1: Water Consumption Pattern in Egypt (ECP, 1998)

The final input is the urban land use and it is defined by the rational coefficient. The rational coefficient is a predicted value that depends on the designer judgment and it is taken based on the land use of the catchment; it ranges from zero to one, where zero means that the rainfall quantity

is totally seeped into the ground, while one means that the catchment is totally impervious. The runoff coefficient value is identified according to Table 3.4 that is adopted from The Egyptian Code of Practice (ECP , 2010).

## B. Results of Runoff Using Ration Method

Table D-1: Calculated Runoff Corresponds to 2-Year Storm

No.	Name	Area (Km <sup>2</sup> )	Runoff of 2-yrs Freq. m <sup>3</sup> /d	Percentage Used by Rainfall of the Total Network Capacity
1	El Banafseg	2.24	9,036.28	22%
2	El Miraj	4.25	18,695.77	31%
3	El Yasmin	9.49	39,661.98	57%
4	West El Yasmin	5.83	22,859.23	120%
5	Ganoub El Academya Fareeya	2.88	12,330.20	65%
6	Ganoub El Academya Ra'esya	3.13	13,483.76	12%
7	Markaz Al Madena	15.30	60,196.04	29%
8	Ganoub El Mostasmreen	4.07	9,380.61	6%
9	Shouaifat Fareeya	0.58	2,258.61	65%
10	Al Hay El Rabee PS1	5.17	18,149.59	121%
11	Shouaifat Ra'esya	11.23	47,043.40	69%
12	Iskan Nekabat	1.99	7,971.02	16%
13	Mokawlon El Arab 1	3.27	11,805.35	9%
14	Mokawlon El Arab 2	2.19	6,210.99	5%
15	Manteka Sena'yea	5.04	16,221.00	40%
16	Imtedad Mostasmreen	6.11	8,247.02	2%
17	Gharb El Golf	2.17	8,425.37	89%

Table D-2: Calculated Runoff Corresponds to 5-Year Storm

No.	Name	Area (Km <sup>2</sup> )	Runoff of 5-yrs Freq. m <sup>3</sup> /d	Percentage Used by Rainfall of the Total Network Capacity
1	El Banafseg	2.24	17,001.59	41.88%



2	<b>El Miraj</b>	4.25	35,175.75	58.14%
3	<b>El Yasmin</b>	9.49	74,623.28	107.92%
4	<b>West El Yasmin</b>	5.83	43,009.22	226.36%
5	<b>Ganoub El Academya Fareeya</b>	2.88	23,199.04	122.10%
6	<b>Ganoub El Academya Ra'esya</b>	3.13	25,369.45	11.98%
7	<b>Markaz Al Madena</b>	15.30	113,257.74	43.70%
8	<b>Ganoub El Mostasmreen</b>	4.07	17,649.45	10.87%
9	<b>Shouaifat Fareeya</b>	0.58	4,249.53	121.42%
10	<b>Al Hay El Rabee PS1</b>	5.17	34,148.13	227.65%
11	<b>Shouaifat Ra'esya</b>	11.23	88,511.28	130.64%
12	<b>Iskan Nekabat</b>	1.99	14,997.33	29.41%
13	<b>Mokawlon El Arab 1</b>	3.27	22,211.55	17.14%
14	<b>Mokawlon El Arab 2</b>	2.19	11,685.85	9.02%
15	<b>Manteka Sena'yea</b>	5.04	30,519.50	75.17%
16	<b>Imtedad Mostasmreen</b>	6.11	15,516.61	4.49%
17	<b>Gharb El Golf</b>	2.17	15,852.18	166.87%

Table D-3: Calculated Runoff Corresponds to 10-Year Storm

<b>No.</b>	<b>Name</b>	<b>Area (Km<sup>2</sup>)</b>	<b>Runoff of 10-ysrs Freq. m<sup>3</sup>/d</b>	<b>Percentage Used by Rainfall of the Total Network Capacity</b>
1	<b>El Banafseg</b>	2.24	23,695.13	58%
2	<b>El Miraj</b>	4.25	49,024.47	81%
3	<b>El Yasmin</b>	9.49	104,002.53	150%
4	<b>West El Yasmin</b>	5.83	59,941.98	315%
5	<b>Ganoub El Academya Fareeya</b>	2.88	32,332.52	170%
6	<b>Ganoub El Academya Ra'esya</b>	3.13	35,357.43	17%
7	<b>Markaz Al Madena</b>	15.30	157,847.40	61%
8	<b>Ganoub El Mostasmreen</b>	4.07	24,598.05	15%
9	<b>Shouaifat Fareeya</b>	0.58	5,922.58	169%
10	<b>Al Hay El Rabee PS1</b>	5.17	47,592.27	317%
11	<b>Shouaifat Ra'esya</b>	11.23	123,358.24	182%
12	<b>Iskan Nekabat</b>	1.99	20,901.79	41%
13	<b>Mokawlon El Arab 1</b>	3.27	30,956.25	24%

No.	Name	Area (Km <sup>2</sup> )	Runoff of 10-yrs Freq. m <sup>3</sup> /d	Percentage Used by Rainfall of the Total Network Capacity
14	Mokawlon El Arab 2	2.19	16,286.58	13%
15	Manteka Sena'yea	5.04	42,535.06	105%
16	Imtedad Mostasmreen	6.11	21,625.51	6%
17	Gharb El Golf	2.17	22,093.20	233%

Table D-4: Calculated Runoff Corresponds to 20-Year Storm

No.	Name	Area (Km <sup>2</sup> )	Runoff of 20-yrs Freq. m <sup>3</sup> /d	Percentage Used by Rainfall of the Total Network Capacity
1	El Banafseg	2.24	31,191.90	77%
2	El Miraj	4.25	64,535.04	107%
3	El Yasmin	9.49	136,907.28	198%
4	West El Yasmin	5.83	78,906.68	415%
5	Ganoub El Academya Fareeya	2.88	42,562.02	224%
6	Ganoub El Academya Ra'esya	3.13	46,543.96	22%
7	Markaz Al Madena	15.30	207,787.83	80%
8	Ganoub El Mostasmreen	4.07	32,380.49	10%
9	Shouaifat Fareeya	0.58	7,796.39	223%
10	Al Hay El Rabee PS1	5.17	62,649.71	418%
11	Shouaifat Ra'esya	11.23	162,386.84	240%
12	Iskan Nekabat	1.99	27,514.78	54%
13	Mokawlon El Arab 1	3.27	40,750.32	31%
14	Mokawlon El Arab 2	2.19	21,439.40	17%
15	Manteka Sena'yea	5.04	55,992.48	138%
16	Imtedad Mostasmreen	6.11	28,467.48	8%
17	Gharb El Golf	2.17	29,083.14	306%

Table D-5: Calculated Runoff Corresponds to 50-Year Storm

No.	Name	Area (Km <sup>2</sup> )	Runoff of 50-yrs Freq. m <sup>3</sup> /d	Percentage Used by Rainfall of the Total Network Capacity
1	El Banafseg	2.24	42,303.18	104%
2	El Miraj	4.25	87,523.91	145%
3	El Yasmin	9.49	185,676.82	269%
4	West El Yasmin	5.83	107,015.06	563%
5	Ganoub El Academya Fareeya	2.88	57,723.60	304%
6	Ganoub El Academya Ra'esya	3.13	63,124.00	30%
7	Markaz Al Madena	15.30	281,806.67	109%
8	Ganoub El Mostasmreen	4.07	43,915.17	14%
9	Shouaifat Fareeya	0.58	10,573.64	302%
10	Al Hay El Rabee PS1	5.17	84,966.99	566%
11	Shouaifat Ra'esya	11.23	220,232.80	325%
12	Iskan Nekabat	1.99	37,316.19	73%
13	Mokawlon El Arab 1	3.27	55,266.52	43%
14	Mokawlon El Arab 2	2.19	29,076.61	22%
15	Manteka Sena'yea	5.04	75,938.29	187%
16	Imtedad Mostasmreen	6.11	38,608.25	11%
17	Gharb El Golf	2.17	39,443.23	415%

Table D-6: Calculated Runoff Corresponds to 100-Year Storm

No.	Name	Area (Km <sup>2</sup> )	Runoff of 100-yrs Freq. m <sup>3</sup> /d	Percentage Used by Rainfall of the Total Network Capacity
1	El Banafseg	2.24	51,941.88	128%
2	El Miraj	4.25	107,466.07	178%
3	El Yasmin	9.49	227,982.94	330%
4	West El Yasmin	5.83	131,398.24	692%
5	Ganoub El Academya Fareeya	2.88	70,875.81	373%
6	Ganoub El Academya Ra'esya	3.13	77,506.68	37%
7	Markaz Al Madena	15.30	346,015.78	133%
8	Ganoub El Mostasmreen	4.07	53,921.16	17%

No.	Name	Area (Km <sup>2</sup> )	Runoff of 100-yrs Freq. m <sup>3</sup> /d	Percentage Used by Rainfall of the Total Network Capacity
9	Shouaifat Fareeya	0.58	12,982.82	371%
10	Al Hay El Rabee PS1	5.17	104,326.56	696%
11	Shouaifat Ra'esya	11.23	270,412.42	399%
12	Iskan Nekabat	1.99	45,818.61	90%
13	Mokawlon El Arab 1	3.27	67,858.89	52%
14	Mokawlon El Arab 2	2.19	35,701.66	28%
15	Manteka Sena'yea	5.04	93,240.69	230%
16	Imtedad Mostasmreen	6.11	47,405.07	14%
17	Gharb El Golf	2.17	48,430.30	510%

Table D-7: Calculated Runoff Corresponds to Maximum Predicted Storm

No.	Name	Area (Km <sup>2</sup> )	Runoff of Max Storm m <sup>3</sup> /d	Percentage Used by Rainfall of the Total Network Capacity
1	El Banafseg	2.24	80,322.49	198%
2	El Miraj	4.25	166,184.64	275%
3	El Yasmin	9.49	352,550.93	510%
4	West El Yasmin	5.83	203,193.16	1069%
5	Ganoub El Academya Fareeya	2.88	109,601.77	577%
6	Ganoub El Academya Ra'esya	3.13	119,855.69	57%
7	Markaz Al Madena	15.30	535,075.95	206%
8	Ganoub El Mostasmreen	4.07	83,383.24	26%
9	Shouaifat Fareeya	0.58	20,076.53	574%
10	Al Hay El Rabee PS1	5.17	161,329.73	1076%
11	Shouaifat Ra'esya	11.23	418,163.54	617%
12	Iskan Nekabat	1.99	70,853.52	139%
13	Mokawlon El Arab 1	3.27	104,936.43	81%
14	Mokawlon El Arab 2	2.19	55,208.76	43%
15	Manteka Sena'yea	5.04	144,186.64	355%
16	Imtedad Mostasmreen	6.11	73,306.81	21%
17	Gharb El Golf	2.17	74,892.21	788%

### C. Pump Stations Capacity Calculations

Table D-8: Pump Stations Evaluation for Base Scenario (Wastewater Only)

No.	Name	Wastewater Discharge (l/s)	Percentage of Total Capacity of Pump Station (%)
1	El Banafseg	260.42	27.70%
2	El Miraj	393.52	35.14%
3	El Yasmin	637.73	68.43%
4	West El Yasmin	85.65	38.93%
5	Ganoub El Academya Fareeya	115.74	52.61%
6	Ganoub El Academya Ra'esya	1,068.75	98.15%
7	Markaz Al Madena	1,593.75	98.24%
8	Ganoub El Mostasmreen	1,603.01	107.04%
9	Shouaifat Fareeya	18.75	34.72%
10	Al Hay El Rabee PS1	133.36	26.67%
11	Shouaifat Ra'esya	435.79	37.45%
12	Iskan Nekabat	143.76	21.14%
13	Mokawlon El Arab 1	1,041.67	50.67%
14	Mokawlon El Arab 2	983.80	68.41%
15	Manteka Sena'yea	200.23	42.60%
16	Imtedad Mostasmreen	1,952.48	134.87%
17	Gharb El Golf	46.61	5.48%

Table D-9: Pump Stations Evaluation for Wastewater Combined with 2-year scenario

No.	Name	Wastewater and 2-year Rainfall Discharge (l/s)	% Used of total pump capacity	Excess Water Amount (m <sup>3</sup> /d)
1	El Banafseg	345.37	36.74%	-
2	El Miraj	571.09	50.99%	-
3	El Yasmin	1,643.16	102.70%	3,728.85
4	West El Yasmin	299.89	136.31%	6,902.07
5	Ganoub El Academya Fareeya	232.50	105.68%	1,080.42
6	Ganoub El Academya Ra'esya	3,657.62	140.14%	78,803.41

No.	Name	Wastewater and 2-year Rainfall Discharge (l/s)	% Used of total pump capacity	Excess Water Amount (m <sup>3</sup> /d)
7	Markaz Al Madena	5,815.67	137.49%	58,198.12
8	Ganoub El Mostasmreen	7,499.01	139.39%	124,884.43
9	Shouaifat Fareeya	39.88	73.86%	-
10	Al Hay El Rabee PS1	301.00	60.20%	-
11	Shouaifat Ra'esya	1,221.02	77.77%	-
12	Iskan Nekabat	218.64	32.15%	-
13	Mokawlon El Arab 1	2,590.78	74.02%	-
14	Mokawlon El Arab 2	3,630.03	90.08%	-
15	Manteka Sena'yea	339.14	72.16%	-
16	Imtedad Mostasmreen	13,479.84	170.42%	356,350.12
17	Gharb El Golf	125.46	14.76%	-

Table D-10: Pump Stations Evaluation for Wastewater Combined with 5-year scenario

No.	Name	Wastewater and 5-year Rainfall Discharge (l/s)	% Used of total pump capacity	Excess Water Amount (m <sup>3</sup> /d)
1	El Banafseg	432.46	46.01%	-
2	El Miraj	753.12	67.24%	-
3	El Yasmin	2,205.16	137.82%	52,286.16
4	West El Yasmin	519.50	236.14%	25,876.55
5	Ganoub El Academya Fareeya	352.20	160.09%	11,421.95
6	Ganoub El Academya Ra'esya	4,780.94	183.18%	97,984.28
7	Markaz Al Madena	7,517.43	177.72%	186,049.46
8	Ganoub El Mostasmreen	9,283.12	172.55%	151,180.47
9	Shouaifat Fareeya	61.55	113.98%	652.21
10	Al Hay El Rabee PS1	472.85	94.57%	-
11	Shouaifat Ra'esya	1,870.03	119.11%	25,270.71
12	Iskan Nekabat	295.40	43.44%	-
13	Mokawlon El Arab 1	3,428.75	97.96%	-
14	Mokawlon El Arab 2	4,524.85	112.28%	68,025.89
15	Manteka Sena'yea	481.54	102.45%	996.91

No.	Name	Wastewater and 5-year Rainfall Discharge (l/s)	% Used of total pump capacity	Excess Water Amount (m <sup>3</sup> /d)
16	Imtedad Mostasmreen	16,361.84	206.85%	510,035.34
17	Gharb El Golf	206.29	24.27%	-

Table D-11: Pump Stations Evaluation for Wastewater Combined with 10-year scenario

No.	Name	Wastewater and 10-year Rainfall Discharge (l/s)	% Used of total pump capacity	Excess Water Amount (m <sup>3</sup> /d)
1	El Banafseg	504.02	53.62%	-
2	El Miraj	902.69	80.60%	-
3	El Yasmin	2,666.95	166.68%	92,184.65
4	West El Yasmin	699.95	318.16%	41,467.47
5	Ganoub El Academya Fareeya	450.55	204.79%	19,919.36
6	Ganoub El Academya Ra'esya	5,703.94	218.54%	113,744.79
7	Markaz Al Madena	8,915.73	210.77%	291,102.14
8	Ganoub El Mostasmreen	10,749.09	199.80%	172,787.35
9	Shouaifat Fareeya	79.35	146.94%	2,190.24
10	Al Hay El Rabee PS1	614.05	122.81%	9,854.17
11	Shouaifat Ra'esya	2,403.31	153.08%	59,953.87
12	Iskan Nekabat	358.47	52.72%	-
13	Mokawlon El Arab 1	4,117.28	117.64%	6,620.53
14	Mokawlon El Arab 2	5,260.10	130.52%	112,901.48
15	Manteka Sena'yea	598.54	127.35%	11,106.03
16	Imtedad Mostasmreen	18,729.91	236.79%	638,044.97
17	Gharb El Golf	272.71	32.08%	-

Table D-12: Pump Stations Evaluation for Wastewater Combined with 20-year scenario

No.	Name	Wastewater and 20-year Rainfall Discharge (l/s)	% Used of total pump capacity	Excess Water Amount (m <sup>3</sup> /d)
1	El Banafseg	584.72	62.20%	-
2	El Miraj	1,071.35	95.66%	-
3	El Yasmin	3,187.69	199.23%	137,176.57
4	West El Yasmin	903.43	410.65%	59,048.72
5	Ganoub El Academya Fareeya	561.45	255.21%	29,501.55
6	Ganoub El Academya Ra'esya	6,744.77	258.42%	131,517.28
7	Markaz Al Madena	10,492.54	248.05%	409,565.80
8	Ganoub El Mostasmreen	12,402.20	230.52%	197,152.56
9	Shouaifat Fareeya	99.42	184.12%	3,924.62
10	Al Hay El Rabee PS1	773.28	154.66%	23,611.70
11	Shouaifat Ra'esya	3,004.67	191.38%	96,419.28
12	Iskan Nekabat	429.59	63.18%	-
13	Mokawlon El Arab 1	4,893.72	139.82%	23,998.25
14	Mokawlon El Arab 2	6,089.22	151.10%	153,918.14
15	Manteka Sena'yea	730.48	155.42%	22,505.68
16	Imtedad Mostasmreen	21,400.28	270.55%	791,983.99
17	Gharb El Golf	347.61	40.89%	-

Table D-13: Pump Stations Evaluation for Wastewater Combined with 50-year scenario

No.	Name	Wastewater and 50-year Rainfall Discharge (l/s)	% Used of total pump capacity	Excess Water Amount (m <sup>3</sup> /d)
1	El Banafseg	708.05	75.32%	-
2	El Miraj	1,329.11	118.67%	18,067.32
3	El Yasmin	3,983.54	248.97%	205,937.79
4	West El Yasmin	1,214.42	552.01%	85,918.17
5	Ganoub El Academya Fareeya	730.95	332.25%	44,146.03
6	Ganoub El Academya Ra'esya	8,335.47	319.37%	158,679.01
7	Markaz Al Madena	12,902.37	305.02%	590,614.04



No.	Name	Wastewater and 50-year Rainfall Discharge (l/s)	% Used of total pump capacity	Excess Water Amount (m <sup>3</sup> /d)
8	Ganoub El Mostasmreen	14,928.66	277.48%	234,389.96
9	Shouaifat Fareeya	130.10	240.93%	6,575.26
10	Al Hay El Rabee PS1	1,016.64	203.33%	44,637.36
11	Shouaifat Ra'esya	3,923.73	249.92%	152,149.45
12	Iskan Nekabat	538.29	79.16%	-
13	Mokawlon El Arab 1	6,080.35	173.72%	70,793.00
14	Mokawlon El Arab 2	7,356.35	182.54%	216,603.99
15	Manteka Sena'yea	932.13	198.32%	39,927.79
16	Imtedad Mostasmreen	25,481.42	322.14%	1,027,249.29
17	Gharb El Golf	462.07	54.36%	-

Table D-14: Pump Stations Evaluation for Wastewater Combined with 100-year scenario

No.	Name	Wastewater and 50-year Rainfall Discharge (l/s)	% Used of total pump capacity	Excess Water Amount (m <sup>3</sup> /d)
1	El Banafseg	816.15	86.82%	-
2	El Miraj	1,555.06	138.84%	37,588.77
3	El Yasmin	4,681.13	292.57%	266,209.98
4	West El Yasmin	1,487.02	675.92%	109,470.41
5	Ganoub El Academya Fareeya	879.52	399.78%	56,982.55
6	Ganoub El Academya Ra'esya	9,729.80	372.79%	182,487.43
7	Markaz Al Madena	15,014.70	354.96%	749,310.64
8	Ganoub El Mostasmreen	17,143.20	318.65%	267,030.15
9	Shouaifat Fareeya	156.99	290.73%	8,898.67
10	Al Hay El Rabee PS1	1,229.95	245.99%	63,067.26
11	Shouaifat Ra'esya	4,729.32	301.23%	200,999.34
12	Iskan Nekabat	633.57	93.17%	-
13	Mokawlon El Arab 1	7,120.49	203.44%	111,810.62
14	Mokawlon El Arab 2	8,467.05	210.10%	271,550.83
15	Manteka Sena'yea	1,108.88	235.93%	55,199.02
16	Imtedad Mostasmreen	29,058.72	367.37%	1,233,469.49

No.	Name	Wastewater and 50-year Rainfall Discharge (l/s)	% Used of total pump capacity	Excess Water Amount (m <sup>3</sup> /d)
17	Gharb El Golf	562.40	66.17%	-

Table D-15: Pump Stations Evaluation for Wastewater with Maximum Projected Storm

No.	Name	Wastewater and 50-year Rainfall Discharge (l/s)	% Used of total pump capacity	Excess Water Amount (m <sup>3</sup> /d)
1	El Banafseg	1,173.95	124.89%	20,213.03
2	El Miraj	2,302.89	205.62%	102,202.04
3	El Yasmin	6,990.07	436.88%	465,702.44
4	West El Yasmin	2,389.27	1086.03%	187,425.01
5	Ganoub El Academya Fareeya	1,371.27	623.30%	99,469.61
6	Ganoub El Academya Ra'esya	14,344.80	549.61%	261,289.97
7	Markaz Al Madena	22,006.20	520.24%	1,274,574.03
8	Ganoub El Mostasmreen	24,473.04	454.89%	375,064.57
9	Shouaifat Fareeya	246.00	455.56%	16,588.81
10	Al Hay El Rabee PS1	1,935.97	387.19%	124,067.64
11	Shouaifat Ra'esya	7,395.72	471.06%	362,685.61
12	Iskan Nekabat	948.93	139.55%	23,235.16
13	Mokawlon El Arab 1	10,563.18	301.81%	224,338.00
14	Mokawlon El Arab 2	12,143.31	301.32%	476,652.32
15	Manteka Sena'yea	1,693.90	360.40%	105,744.63
16	Imtedad Mostasmreen	40,899.07	517.06%	1,892,794.14
17	Gharb El Golf	894.49	105.23%	3,843.93